




Applied Computational
Electromagnetics Society



Newsletter
Volume 18 – No. 1
ISSN 1056-9170



March 2003



**APPLIED COMPUTATIONAL ELECTROMAGNETICS SOCIETY
(ACES)**

NEWSLETTER

Vol. 18 No. 1

March 2003

TABLE OF CONTENTS

OFFICERS' REPORTS

President's Post – Osama A. Mohammed..... 5

COMMITTEE REPORTS

CEM News from Europe – Pat Foster 7

Publications Committee – Andrew Peterson..... 9

Financial Report – Allen Glisson 10

Membership Report – Bruce Archambeault 11

TECHNICAL FEATURE ARTICLE – “Using Joint Time-Frequency Analysis to Analyze Time-Domain Simulations of Shielding Structures”

Robert T. Johnk, Bruce Archambeault, and David R. Novotny..... 12

TUTORIAL ARTICLE – “Non-orthogonal FDTD Methods”

J. Alan Roden..... 42

EMC Application Notes – “Computational Electromagnetics and EMC – What's Next?” – Colin

Brench 61

ANNOUNCEMENTS:

The 20th Annual Review of Progress in Applied Computational Electromagnetics

-- Advance Program 63

-- Short Courses 79

-- Short Course Detail Descriptions 81

-- Naval Postgraduate School Map 91

APPLICATION for ACES Membership, Newsletter and Journal Subscription 92

ADVERTISING Rates..... 93

DEADLINE to Submission of Articles..... 93

PERMANENT STANDING COMMITTEES OF ACES, INC.

COMMITTEE	CHAIRMAN	ADDRESS
NOMINATIONS	Rene Allard	Penn State University PO Box 30 State College, PA 16804-0030
ELECTIONS	Rene Allard	Penn State University PO Box 30 State College, PA 16804-0030
FINANCE	Allen Glisson	EE Department Anderson Hall University of Mississippi University, MS 38677
PUBLICATIONS	Andrew Peterson	Georgia Institute of Technology School of ECE Atlanta, GA 30332-0250
CONFERENCE	Osama Mohammed	Florida International University ECE Department Miami, FL 33174
AWARDS	Pat Foster	MAAS 16 Peachfield Road Great Malvern, UK WR14 4AP

MEMBERSHIP ACTIVITY COMMITTEES OF ACES, INC.

COMMITTEE	CHAIRMAN	ADDRESS
SOFTWARE VALIDATION	Bruce Archambeault	IBM 158 Lin Tilley Road Durham, NC 27712
HISTORICAL	Robert Bevensee	BOMA Enterprises PO Box 812 Alamo, CA 94507-0812

ACES NEWSLETTER STAFF

EDITOR-IN-CHIEF, NEWSLETTER

Bruce Archambeault
IBM
3039 Cornwallis Road, PO Box 12195
Dept. 18DA B306
Research Triangle Park, NC 27709
Phone: 919-486-0120
email: barch@us.ibm.com

EDITOR-IN-CHIEF, PUBLICATIONS

Andrew Peterson
Georgia Institute of Technology, ECE
777 Atlantic Drive
Atlanta, GA 30332-0250
Phone: 404-894-4697
Fax: 404-894-5935
email: peterson@ee.gatech.edu

ASSOCIATE EDITOR-IN-CHIEF

Ray Perez
Martin Marietta Astronautics
MS 58700, PO Box 179
Denver, CO 80201
Phone: 303-977-5845
Fax: 303-971-4306
email: ray.j.perez@lmco.com

MANAGING EDITOR

Richard W. Adler
Naval Postgraduate School/ECE Dept.
Code ECAB, 833 Dyer Road, Room 437
Monterey, CA 93943-5121
Phone: 831-646-1111
Fax: 831-649-0300
email: rwa@attglobal.net

EDITORS

CEM NEWS FROM EUROPE

Pat R. Foster
Microwaves and Antenna Systems
16 Peachfield Road
Great Malvern, Worc. UK WR14 4AP
Phone: +44 1684 5744057
Fax: +44 1684 573509
email: prf@maasdesign.co.uk

TECHNICAL FEATURE ARTICLE

Andy Drozd
ANDRO Consulting Services
PO Box 543
Rome, NY 13442-0543
Phone: 315-337-4396
Fax: 314-337-4396
email: androl@aol.com

THE PRACTICAL CEMIST

W. Perry Wheless, Jr.
University of Alabama
PO Box 11134
Tuscaloosa, AL 35486-3008
Phone: 205-348-1757
Fax: 205-348-6959
Email: wwheless@ualvm.ua.edu

MODELER'S NOTES

Gerald Burke
Lawrence Livermore National Labs.
Box 5504/L-156
Livermore, CA 94550
Phone: 510-422-8414
Fax: 510-422-3013
email: burke2@llnl.gov

PERSPECTIVES IN CEM

Manos M. Tentzeris
Georgia Institute of Technology
ECE Dept.
Atlanta, GA 30332-0250
Phone: 404-385-0378
email: ementze@ece.gatech.edu

TUTORIAL

J. Alan Roden
IBM Microelectronics
Dept. OSXA
3039 Cornwallis Road
Research Triangle Park, NC 27709
Phone: 919-543-8645
email: jaroden@us.ibm.com

ACES JOURNAL

EDITOR IN CHIEF

Atef Elsherbeni
EE Department, Anderson Hall
University of Mississippi
University, MS 38677
Phone: 662-915-5382
email: atef@olemiss.edu

NEWSLETTER ARTICLES AND VOLUNTEERS WELCOME

The ACES Newsletter is always looking for articles, letters and short communications of interest to ACES members. All individuals are encouraged to write, suggest or solicit articles either on a one-time or continuing basis. Please contact a Newsletter Editor.

AUTHORSHIP AND BERNE COPYRIGHT CONVENTION

The opinions, statements and facts contained in this Newsletter are solely the opinions of the authors and/or sources identified with each article. Articles with no author can be attributed to the editors or to the committee head in the case of committee reports. The United States recently became part of the Berne Copyright Convention. Under the Berne Convention, the copyright for an article in this newsletter is legally held by the author(s) of the article since no explicit copyright notice appears in the newsletter.

BOARD OF DIRECTORS

EXECUTIVE COMMITTEE

Osama Mohammed, President
Bruce Archambeault, Vice President
Keith Lysiak, Secretary

Allen W. Glisson, Treasurer
Richard W. Adler, Executive Officer

DIRECTORS-AT-LARGE

Masanori Koshiba	2003	Bruce Archambeault	2004	Allen W. Glisson	2005
Osama Mohammed	2003	Andrzej Krawczyk	2004	Keith Lysiak	2005
Tapan Sarkar	2003	Ray Perez	2004	Eric Mechielssen	2005

ACES ELECTRONIC PUBLISHING GROUP

Atef Eisherbeni	Electronic Publication Managing Editor
Matthew J. Inman	Site Administrator
Jessica Drewrey	Assistant Administrator
Brad Baker	Contributing Staff
Imran Daker	Past Administrator
Chris Riley	Past Staff

Visit us on line at:
<http://aces.ee.olemiss.edu>

President Post

Osama Mohammed

After my first year at your service as ACES president, I am happy to report that our beloved society is on its way to being an important and influential institution in the field of applied computational electromagnetics. The conference is a highly influential outlet for promoting awareness of recent technical contributions to the advancement of computational electromagnetics. This year's annual conference in Monterey will be one of the best conferences we have had in some time, thanks to Dr. Atef El-Sherbeni for his leadership and efforts. The conference will feature new and original presentations, panel discussions as well as invited talks in a wide range of interest. We have noticed increased international participation and many long time ACES participants are coming back. With the new format of this annual review, the ACES participants will find more time for networking and discussions during the panel session, plenary sessions as well as in social functions and lunches.

Authors who submitted papers for the 2003 annual conference have the option of submitting an extended version of their accepted papers for peer review and possible publication in special issues of the ACES Journal.

In an effort to enhance the value of membership and increase membership services, the ACES Board of Directors restructured the membership fees as a direct consequence of the society's move to electronic publications and on-line access to these publications. Now the membership dues are quite reasonable and the complete fee schedule has been published in the November 2002 issue of the newsletter featuring the basic, moderate and expanded levels in addition to institutional memberships. The goal of this restructuring activity is to eventually convert all of our members to on-line access of services.

We have created the member communication committee. Under the leadership of our colleague Vince Rodriguez, monthly communications have been delivered to members via e-mail. This has increased the access for members to information and knowledge relating to society activities and has contributed to increased participation resulting in improving membership services. I expect this trend to continue and I have personally received a number of messages from ACES members around the world with offers of assistance and participation in activities. In the near future the member communication committee will be charged with the creation of an effort to increase the membership numbers, keep membership statistics and identify additional membership services. The creation of ACES Chapters overseas will also be discussed and acted upon.

The ACES web site has become an important tool in delivering membership services and publication. My sincere congratulations to Dr. Atef El-Sherbeni for his leadership, dedication and innovative contributions in getting the web site to a highly professional level with various levels of access and data tracking. Now the web site is used for conferences, the newsletters and the ACES journal in addition to comprehensive member services. In the near future, the ACES web site will be the main source for delivering almost all of the membership services as well as conferences, publications and administrative activities.

The conference committee is working hard to identify sites and groups who will agree to organize the conference for the next five years. Since our annual conference is the main source of funding, this long-range plan is very important to ensure the long-term viability of the society's finances.

Dr. Rene Allard, our nomination and election committee chairman announced the results of Board of Directors elections, which include Dr. L. Kampel and the re-election of Drs. T. Sarkar and O. Mohammed for three-year terms starting March 2003. Our sincere thanks and appreciation go to Dr. Allard for his valuable efforts in this process.

The Annual conference in Monterey will have several social functions including a reception, wine and cheese, all lunches and the Awards Banquet. Awards represent a major part of ACES operations and are a way to thank those who have done so much for our society. The Awards Banquet will feature many awards for deserving ACES members who have helped the society for years and for those who have contributed to the success of the annual conference. I encourage all participants to attend the Banquet to congratulate our colleagues and to spend a nice evening with the ACES family.

As I promised you in my first message in July 2002, I will continue to promote ACES on all fronts and will work hard on getting our society to be valuable for its members and a financially viable organization for our future. On behalf of the ACES Board of Directors, I invite all members to participate in achieving these goals.

O. Mohammed
ACES President

CEM News From Europe

Pat Foster

The United Kingdom branch of ACES, ACES(UK), held its annual one-day meeting on December 16th, 2002. The highlight was a half-day short course from Professor Ron Marhefka of Ohio State University who addressed us on 'Application of Asymptotic Methods to Large Practical Electromagnetic Prediction and Design Problems'. After a short introduction on the contents of the NEC-Basic Scattering Code, he concentrated on the latest developments to the code and discussed some detailed applications. For example, multilayer radomes can now be modeled and hybrid methods based on the importation of antenna or element data from elsewhere have been implemented and extensively used. He emphasized that NEC-BSC has a limit on the number of structure-ray interactions because the code is dealing with exterior problems.

The algorithm treatment of dielectric including wedge diffraction was discussed as was coupling between antenna elements on a curved impedance surface. These are important developments which have not yet been published in full. Extensions to coupling theory on a curved surface give better agreement than previously.

Examples given included

- 1) An example of a GPS antenna on the International Space Station
- 2) An antenna array mounted on a box and the box mounted on an aircraft. This was modeled by first modeling the array on a box in NEC-BSC and then feeding the radiation patterns back into NEC-BSC as a point source. This was measured on a scale model and the agreement was excellent down to very low signal levels of -50dB below peak gain.

The course extended into the afternoon due to the number of questions from the audience on the course and there was an animated discussion of validation and how to determine numerically the error in predictions. This course was much appreciated by the audience (24 people).

The rest of the day was taken up by four papers presented by members.

Chris Emson of Vector Fields described an FDTD program, CONCERTO, which has a number of useful features apart from the comprehensive GUI which Vector Fields always supplies. The code can deal with curved surfaces and thus avoids the problems of staircasing. The program, of course, includes dielectrics and the results I have seen presented (here and elsewhere) are very impressive.

Pat Foster described recent work on a hybrid method which imports PO currents into a GTD/UTD program, ALDAS. The examples discussed were all of high gain reflectors, particularly earth-watch reflectors on spacecraft where the local structure of the spacecraft may influence the radiation patterns.

Wayne Arter of Culham discussed INSTANTE which is a GTD/UTD program using Shoot-and-bounce ray tracing and a structure geometry based on NURBS. Most of

the paper was devoted to the computation of coupling between antennas and results compared favourably with the standard measurements made by Bull and Smithers. Agreement is to +/-5 db at the -70 dB level.

Colin Sillence of Sowerby Research Centre, BAE Systems, Filton discussed Fast Multipole Methods in Method of Moments code as applied to the NASA almond. Good agreement with other codes was achieved for a dimension of 40 wavelengths. FMM allows the extension of the geometry to a 60 wavelength NASA almond which is very impressive. There was a lengthy discussion of agreement between various computational methods for the NASA almond.

One interesting thread running through the day's presentation, and this includes the short course, is that the dimensions of the problems tackled have risen rapidly over the past few years and that much better agreement with measurement is expected and achieved.

Publications Report for March 2003

As my three-year term as Publications Chair comes to a close, I would like to thank all the ACES members who support our publications, especially our hard-working editors Atef (Journal) and Bruce (Newsletter), and our managing editor (Dick Adler). ("Hard-working" somehow doesn't do justice to Dick's efforts on behalf of ACES.)

I also continue to encourage our readers to submit noteworthy articles to these publications. At the present time, our primary means of publication is changing from print media to electronic media, and none of us are quit sure how that transition will be accepted!

I also encourage any of you out there with ideas for special issues to share them with the editors. I believe that one of the best ways that ACES can maintain momentum and continue to carve out a niche for our publications is to aggressively seek out timely topics for special issues.

My impression at the present time is that ACES publications are strong and are meeting the needs of our members. The editors, officers, and board members of ACES are all receptive to suggestions, so keep them coming!

Andrew F. Peterson
School of ECE
Georgia Institute of Technology
Atlanta, GA 30332-0150
404-894-4697
peterson@ee.gatech.edu

2002 FINANCIAL REPORT

ASSETS

BANK ACCOUNTS	1 JAN 2002	31 DEC 2002
MAIN CHECKING	13,943	9,431
EDITOR CHECKING	3,316	3,325
SECRETARY CHECKING	2,156	6,458
SAVINGS	111	111
HIGH RATE SAVINGS	51,383	37,320
CREDIT CARD	12,193	1,587
CD #1	13,642	14,088
CD #2	13,468	13,968
CD #3	13,353	14,071
CD #4	<u>13,415</u>	<u>13,982</u>
TOTAL ASSETS	\$136,979	\$114,342

LIABILITIES: \$0

NET WORTH 31 December 2002: \$114,342

INCOME

Conference	35,419
Short Courses	7,485
Publications	1,201
Membership	12,725
Interest & misc.	<u>3,427</u>
TOTAL	\$60,257

EXPENSE

Conference	48,743
Short Courses	3,390
Publications	10,073
Services (Legal, Taxes)	1,526
Postage	2,868
Supplies & misc.	9,000
Website & Electronic Publishing	<u>7,294</u>
TOTAL	\$82,894

NET DECREASE for 2002 was \$22,637

In 2001, the net operating loss was \$11,594. In 2002 our net operating loss was \$22,637. Our current net worth, \$114,342, has decreased by 17% from last year.

Allen Glisson
Treasurer

THE APPLIED COMPUTATIONAL ELECTROMAGNETICS SOCIETY, INC.

NOTICE OF THE ANNUAL BUSINESS MEETING

Notice is hereby given that the annual business meeting of the Applied Computational Electromagnetics Society, Inc. will be held on Monday 24 March 2003, in 102 Glasgow Hall at the Naval Postgraduate School, Monterey, CA. The meeting is scheduled to begin at 7:55 AM PST for purposes of:

1. Receiving the Financial Statement and Treasurer's Report for the time period ending 31 December 2002.
2. Announcement of the Ballot Election of the Board of Directors.

By order of the Board of Directors
Bruce Archambeault, Secretary

ANNUAL REPORT 2002

As required in the Bylaws of the Applied Computational Electromagnetics Society, Inc. a California Nonprofit Public Benefit Corporation, this report is provided to the members. Additional information will be presented at the Annual Meeting and that same information will be included in the July Newsletter for the benefit of members who could not attend the Annual Meeting.

MEMBERSHIP REPORT

As of 31 December 2002, the paid-up membership totaled 272, with approximately 34 % of those from non-U.S. countries. There were 23 full time student, unemployed and retired members; 62 industrial (organizational) members; and 187 regular members. The total membership has decreased by 17 % since 1 Jan 2002, with non-U.S. membership decreasing by 21%.

Bruce Archambeault, Secretary

Using Joint Time-Frequency Analysis to Analyze Time-Domain Simulations of Shielding Structures

Robert T. Johnk, Bruce Archambeault, and David R. Novotny

Introduction

Simulation of real-world EMC effects has recently become popular. These simulations can be performed in either the frequency-domain (typically, Method of Moments (MoM) and Finite Element Method (FEM)) or in the time-domain (typically, Finite-Difference Time-Domain (FDTD), Transmission Line Matrix method (TLM), or Partial Element Equivalent Circuit (PEEC) method). Simulation in each domain has its advantages and disadvantages. However, time domain simulation is a commonly used EMC tool, mostly due the ease of use of FDTD simulators and the ability to model transient and wideband effects.

Time domain simulation tools are extremely powerful. However, if a structure is resonant with a high Q-factor, the simulations can require long computational times. Classic examples of this effect are encountered in highly resonant structures, such as shielded enclosures and in the decoupling of power/ground planes in printed circuit boards. FDTD is especially useful for modeling these. In the shielded enclosure case, slots and apertures are easily included in the model. In the decoupling example, FDTD easily allows dielectric materials to be included. The main disadvantage of modeling these types of structures with a conventional FDTD analysis (or any other time domain simulation tool) is the long run time required.

Joint Time Frequency Analysis (JTFA) is a powerful tool that is used to post process waveforms obtained from time-domain numerical simulations. JTFA is applied directly to a numerically generated time-domain record, and useful parameters can be extracted using an efficient data processing sequence. The main advantage of JTFA lies in the ability to extract useful parameters using shorter time records. This allows for numerical codes to be run for a shorter length of time, and the final results extrapolated to obtain useful estimates of shielding parameters. This allows more cases to be analyzed and optimal usage of resources by minimizing run-times.

This paper describes the implementation and use of JTFA in conjunction with FDTD simulations of the shielding of slots and enclosures. Several detailed examples are given that highlight the use and application of JTFA.

Joint Time-Frequency Analysis

Joint Time-Frequency Analysis (JTFA) was developed in the 1940's [1,2]. It has reached a high degree of mathematical sophistication and the number of applications continues to grow. Some applications where JTFA has been effectively applied are: processing of speech signals, seismic data processing, image

processing, analysis of musical instruments, and architectural acoustics [3-7]. In the domain of electromagnetics, it has been applied to the analysis of cavities, waveguiding structures, scattering objects, and antennas [8,9]. JTFA also has potential for the investigation of a number of problems in Electromagnetic Compatibility (EMC). One EMC application where JTFA shows much promise is the analysis of time-domain numerical simulations of electromagnetic shielding structures, such as metal plates with resonant coupling apertures and metal enclosures with embedded apertures. When these shielding structures are simulated numerically, long run times are often required to compute parameters such as quality factor (Q) and shielding. JTFA provides a nice way to avoid long run times by enabling us, under certain conditions, to extrapolate decay and shielding characteristics beyond the maximum computed time step of a time-domain EM simulation. This allows the engineer to run many more models while varying parameters such as aperture size, etc. We can also use JTFA to gain more insight and information than can be obtained from only a time-domain waveform or its frequency-domain counterpart.

To better understand the JTFA, we start with the traditional Fourier transform defined as [10]:

$$H(f) = \int_{-\infty}^{\infty} h(t) e^{-j2\pi ft} dt \quad (1)$$

where f is the frequency (Hz), $h(t)$ is the time-domain waveform to be analyzed, and $H(f)$ is the complex frequency spectrum (magnitude & phase). In practice, we process discrete waveforms generated by time-domain electromagnetic codes. The outputs are finite-duration data sequences $h(t_i)$ of length N , where $i = 1, 2, 3, \dots, N$. We can efficiently analyze the frequency content by applying a Fast-Fourier transform (FFT) to obtain a discrete frequency spectrum $H(f_i)$. The Fourier transform analyzes a signal and provides information about its magnitude and phase across frequency. It does not tell us anything about the time at which a particular frequency component appears in a signal. This is one drawback of the Fourier transform, it does not have any ability to provide resolution in time—the time information is embedded in the phase of the signal and is distributed throughout all of the frequencies. One way to overcome this difficulty is through a multiplication of the signal in (1) by a windowing function to yield:

$$G(f, \tau) = \int_{-\infty}^{\infty} g(t) w(t - \tau) e^{-j2\pi ft} dt \quad (2)$$

where $G(f, \tau)$ is the short-time Fourier transform (STFT) [2], $w(t)$ is a specified windowing function over the time interval, $0 \leq t \leq W$, and is zero elsewhere. The parameter τ is the amount by which the window is shifted in time to analyze a selected section of the waveform $h(t)$. The short-time Fourier transform is a function of two variables, time (τ) and frequency (f), and hence term “Joint Time-Frequency Analysis.” With JTFA we now analyze both the frequency content of a waveform and the time interval during which a frequency component is generated. The process of performing a JTFA analysis is one of sliding a window over a time-domain signal and Fourier analyzing it at a succession of window positions. Smaller window widths provide better resolution in time, and wider windows less resolution in time. There is a tradeoff, however. The ability to resolve signals

simultaneously in both the time and frequency domains can be precisely stated in terms of the so-called uncertainty relation [11]:

$$\Delta t \Delta f \geq \frac{1}{2\pi} \quad (3)$$

where Δt is the time resolution (sec) and Δf is the frequency resolution Hz. Thus our ability to resolve simultaneously in both time and frequency is limited. If we desire high resolution in frequency, we must accept less in the time domain. Conversely, if we desire more resolution in time we must accept less in the frequency domain.

Table 1. Some commonly used windows suitable for short-time Fourier analysis.

Window Type	Functional Form ($i=0,1,\dots,N-1$)
Rectangular	$w(i)=1$
Hanning	$w(i) = 0.5 - 0.5 \cos(2\pi i/N)$
Blackman	$w(i)=0.42-0.5 \cos(2\pi i/N)-0.08 \cos(4\pi i/N)$
Hamming	$w(i) = 0.54 - 0.46 \cos(2\pi i/N)$
Kaiser-Bessel	$w(i)=I_0(\beta[1.0-a^2])/I_0(\beta)$ where I_0 is the zero-order modified Bessel function, $a=(i-k)/k$, $k=(N-1)/2$

Windowing

Windowing is simply a process of isolating a desired section of a waveform and deleting the rest. There are a number of ways the data within the window can be treated. One approach is to leave the data unaltered using a rectangular window. An example of a rectangular window is illustrated in Figure 1 in which a 40ns wide window is applied to a waveform. Alternatively, we can taper the signal using a number of possible window types. Some well-known tapered windows are: Hanning, Hamming, Blackman, and Kaiser-Bessel, summarized in Table 1. A more extensive summary of available window types and mathematical properties is provided in [12]. Again, there are trade-offs when deciding which window function to use. Figure 2a depicts the time- and frequency-domain properties of several commonly used windows. In the case of the rectangular window, an abrupt truncation in the time-domain leads to a frequency-domain amplitude spectrum that has a narrow main lobe characteristic; first and second sidelobe levels at -13 dB and -17 dB respectively. When the Hanning taper of Figure 2b is applied, the width of the main lobe is nearly twice that of a rectangular window, however the first sidelobe level drops down to -37 dB. In general, tapering increases the width of the main lobe and reduces the level of the sidelobes, which increases the dynamic range of the frequency domain result. An extremely useful window for this type of analysis is the Kaiser-Bessel window. This window function has a variable index β which allows for a wide range of taper characteristics. This feature makes the Kaiser-Bessel window ideal for JTFA. Figures 2c and 2d depict

Kaiser Bessel window characteristics for indices of 1.0 and 1.6 respectively. For $\beta=1.0$, the main lobe is only somewhat wider than that of the rectangular window, and it has lower sidelobe levels—a significant improvement over the rectangular window. Setting $\beta=1.6$ obtains characteristics that are slightly better than those of the Hanning window.

In order to understand the impact of windowing in JTFA, consider the following complex waveform consisting of a number of sinusoids damped by differing amounts:

$$s(t) = 0.1\sin(2\pi f_1 t) + \text{Exp}[-d_1 t]\sin(2\pi f_2 t) + \text{Exp}[-d_2 t]\sin(2\pi f_3 t) + \text{Exp}[-d_3 t]\sin(2\pi f_4 t) \quad (4)$$

where f_i ($i=1,2,3,4$) are the frequencies of the sinusoidal waveforms, and d_i ($i=1,2,3$) are exponential decay rates. One possible waveform is plotted in Figures 3a, along with the frequency-domain amplitude spectrum in Figure 3b. This waveform has frequency components at 200, 500, 800, and 1100 MHz, with decay rates $d_1=5 \times 10^6$, $d_2=15 \times 10^6$, and $d_3=50 \times 10^6$. The waveform has a very complex structure and resembles those encountered in time domain shielding simulations. The simple FFT frequency-domain plot clearly separates the four components with progressively lower Q-factors as the frequency increases. Neither the time- nor the frequency-domain plots clearly highlight the decay rates.

The power of JTFA can be applied to this waveform. Figure 4 shows the results of a JTFA analysis using three different 100ns duration window types. We now have a 3-dimensional graph with spectrum amplitude plotted as a function of time and frequency. The frequency components appear as ridges which are parallel to the τ , or time, axis. The amount of definition (dynamic range) achieved depends on the window used. A rectangular window is used in Figure 4a, and the “valleys” between the ridges are filled in by high sidelobe levels. Application of a Hanning window improves the dynamic range and produces much better definition as is seen in Figure 4b. This is particularly the case with the 1100 MHz component which is barely visible in the rectangular window analysis, and becomes well defined upon application of a tapered window. Better results were obtained with a Kaiser-Bessel window (index $\beta=3.0$) and is shown in Figure 4c. Not only are the frequency components visible with deep “valleys” in between, but the varying rates of decay are clearly visible. The decay rates are proportional to the downward rates of descent of the ridge peaks. The capability to display and analyze decay rates directly is a powerful feature of JTFA in the analysis of shielding problems.

JTFA of a Resonant Slot in a Metal Sheet – a Canonical Example

We now consider the analysis of a resonant slot embedded in an infinite metal sheet using the Finite-Difference Time-Domain (FDTD) technique [13]. The geometry is shown in Figure 5a, and consists of a pulsed current source, a perfectly-conducting metal sheet that extends out to the edge of the computational domain (simulating a sheet of infinite extent), a 30.0 cm x 0.1cm slot, and an ideal

field monitor point, located 6.0 m from the slot center provides information on the three electric-field components. The source is an impressed electric current density that is rapidly switched on and off, generating a pulsed electromagnetic wave traveling outward in all directions at the speed of light. The source approximates a short radiating dipole (1.0 cm long) having broad directional coverage. A portion of the wavefront penetrates to the other side of the sheet. A monitor point, located at a specified location on the other side of the sheet, measures the component fields 6.0 m away from the center of the slot. One way to quantify the amount of slot penetration is to compare the results with the free-space geometry of Figure 5b, where the metal sheet/slot combination has been removed. The free-space configuration provides a reference for comparison and allows the results to be normalized to the free-space case. Typical reference and slot waveforms obtained from a FDTD code are shown in Figures 6a and 6b respectively. The reference FDTD waveform has a short temporal extent of approximately 2 ns, and has useable spectrum extending from 100 MHz to approximately 3 GHz. The slot waveform has reduced peak amplitudes, and has an extended time domain response. It has a more complex structure with harmonically-related sinusoidal components that decay exponentially. These components are visible as sharp peaks in the amplitude spectrum at 483, 1483, and 2445 MHz.

The results can be displayed either as “shielding” or “penetration”. High penetration implies low shielding, and conversely, low penetration corresponds to high shielding levels. As we shall see, using penetration instead of shielding generates useful graphical displays. Figure 7 shows the penetration through the slot. The slot exhibits resonant peaks in penetration at a fundamental frequency of 483 MHz and at the third and fifth harmonics of 1483 MHz, and 2445 MHz. A maximum penetration of -9.7 dB (9.7 dB of shielding) occurs at the fundamental slot resonance of 483 MHz at which the slot length is close to one-half wavelength.

If we perform a JTFA analysis on the slot-penetration, time-domain waveform and normalize the results with the amplitude-spectrum of the free-space reference, we effectively remove the frequency dependence of the source. The result is a function of frequency and the window parameters (delay, length, and type), and is more complex. JTFA results obtained for different window lengths are shown in Figures 8a-c. In Figure 8a, a 20ns duration Kaiser-Bessel window ($\beta=3.0$) is used. The three resonances are visible as prominent ridges running parallel to the time (τ) axis. The impact of reducing the window length by factors of 2 and 4, (leaving the other parameters unchanged) is shown in Figures 8b and 8c respectively. As the window length decreases, the ridges become broader in frequency. This is a result of the uncertainty principle of time and frequency stated earlier in (3).

We can derive additional information from the JTFA analysis that was not available in the original frequency domain analysis. The amplitudes of the ridges decrease in time (τ), and this is caused by decaying slot resonances. We can extract this decay from the JTFA plot of Figure 8b and obtain the results of Figure 9. The linear characteristic (on a dB scale) indicates an exponential decay. The dashed lines on the plot are the result of a least-squares fit to a straight line. This

procedure directly yields the decay slopes. The fundamental mode exhibits the slowest decay rate, while increasing rates of decay are noted for the third and fifth harmonics. These decay rates can be directly related to the quality factor (Q) through the relation [8]

$$Q = 2\pi \cdot 10^{-9} f t_{decay} \tag{5}$$

where f is the frequency (Hz) and t_{decay} is the decay time (ns) of a selected resonance. The decay time is the time it takes for the signal energy to decay to $1/e$ (-4.3 dB) of its original value. Once the slope of the decay is known, the decay time is computed from the formula

$$t_{decay} = \frac{-4.3}{a} \tag{6}$$

Table 2. Q-factors obtained from a JTFA analysis of normalized penetration data. The selected frequencies correspond to slot resonant peaks.

Frequency (MHz)	t_{decay} (ns)	Q-Factor
483	2.90	8.80
1483	1.82	16.95
2445	1.56	23.97

where a is the slope (dB/s) determined by a least-squares fit, and t_{decay} is the decay time (ns). Table 2 below summarizes the Q-factor results obtained directly from the JTFA analysis.

JTFA of a Box with an Embedded Slot Aperture – a Real-World Example

While the analysis of a simple (infinite) metal plate with an aperture is instructive, a complex, real-world analysis is performed on a structure used to study the penetration of electromagnetic signals into aircraft structures, and to develop practical and efficient test procedures to assess aircraft shielding [14]. A shielded enclosure with the previously studied aperture is analyzed. Once a shielded enclosure is added, we would expect to find many more resonant frequencies due to the physical dimensions of the enclosure. Figure 10 shows such a structure. It consists of the same 30 cm x 0.1cm slot embedded in the face of a rectangular metal box with dimensions 1.03 m x 0.93 m x 73 m. The interior of the box contains a metal paddle to function as a diffuser and to maximize excitation of available cavity modes inside the box, and can well simulate obstructions in the box such as a card in a PC or a bulkhead in an aircraft. Two of the box walls are covered with 1cm-thick, lossy dielectric (non-magnetic) walls with the parameters $\epsilon_r=1.0$, and conductivity, σ , which can be selected to control the rate of decay of the generated waveform. The same pulsed source is located inside the box, and an ideal monitor point is located 6.0 m from the geometric center of the slot. The resulting electric field waveform and the associated penetration spectrum, computed using the same reference waveform as in Figure 6, are shown in Figure 11 with slab conductivities set at $\sigma = 250$ S/m. Due to the addition of the box, the

resulting waveform is much more complex, and has a much longer temporal extent than encountered with the slot alone. The penetration spectrum now exhibits a highly complex noise-like spectrum that exhibits large and rapid variations as a function of frequency. Peaks in the penetration spectrum are seen in the vicinity of the slot resonances. This complex structure is due to the modal structure in the box that changes rapidly with frequency, and thereby randomizes the field structure. This is in stark contrast to the isolated slot, for which the variations are better behaved.

If a JTFA is now performed on the box waveform, we obtain the results of Figure 12a. Additional complexity occurs in the multitude of ridges that are caused by the box cavity modes. While the penetration decays with increasing τ , the decay is not distinctly exponential—the behavior is quite erratic. The slot resonances are somewhat visible as broad ridges in the vicinity of the three resonant frequencies. The decay characteristics of several frequency components near the slot resonance peaks are shown in Figure 12b. The decay of the third and fifth overtones is quite erratic, and is clearly not exponential. A complex modulation is imposed, which is caused by interference from additional box modes that are close to the selected frequencies. A similar modulation effect is encountered in the evaluation of the sound properties of rooms in architectural acoustics [7]. We are now dealing with a two-fold complexity in both frequency and time.

In order to obtain meaningful data from this simulation, statistical averaging of the data was performed to smooth out the rapid variations. An efficient way to accomplish this is to frequency average the penetration data over a specified bandwidth [14]. This is implemented by averaging signal energy to obtain a specified bandwidth to obtain the mean penetration

$$\langle P(f_n) \rangle = \frac{1}{2N+1} \sqrt{\sum_{i=n-N}^{i=n+N} |P(f_i)|^2} \quad (7)$$

where the index n is the center frequency of the averaging window, N is the number of discrete FFT frequencies above and below the center frequency of the window, and $P(f)$ is the penetration at a selected frequency. Equation (7) is equivalent to a rectangular sliding window of width $2N+1$ that performs a smoothing operation by averaging out random variations in the data. The impact of this can be seen in Figures 13a-c where the averaging bandwidth are 10, 50, and 200 MHz respectively. Larger frequency bandwidths produce a higher degree of smoothing. As bandwidth increases, the rapid and random variations caused by the box modes are suppressed, highlighting the systematic effects of the slot.

We can use this averaging process in conjunction JTFA results in which we now apply (7) at each window position. The averaged JTFA results are shown in Figure 14 for averaging bandwidths of 50, 100, and 200 MHz. As the averaging bandwidth is progressively increased, the randomizing effects of the box cavity modes are suppressed, and the slot resonances become distinctly visible.

Extracting the decay rate at the three resonant peaks, results in Figure 15a-c. As the averaging bandwidth increases, the decay approaches a single-exponential characteristic (a straight line in dB), and the modulation effect is mitigated. We can now, as earlier, perform a least-squares fit at the three frequencies to obtain the decay characteristics. The results of the fitting process are plotted as dashed lines in the plots. Rapid convergence in decay times occurs with increasing bandwidth, with maximum change of less than 4% in slope noted as bandwidth increases from 100 to 200 MHz. Using equation (5) and (6), we can use the curve fits to estimate Q-factors at the three frequencies, summarized in Table 3. The addition of the box increases the resulting Q-factors by two orders of magnitude. Also, the box/slot interaction shifts the peak resonant frequencies somewhat from those of an isolated slot.

A Proposed Method for Estimating Total Penetration

An FDTD simulation was performed on the box structure of Figure 16 with the same dimensions, ideal monitor point, and the same excitation source as analyzed in the last section. The lossy slabs are no longer present, and each of the six faces has five randomly placed 4 cm x 4 cm square apertures, which do not exhibit any resonant behavior in the 200-3000 MHz frequency range for which the analysis is conducted. Moreover, since the box walls are perfect electric conductors, coupling through the apertures provides the only loss mechanism. The electric field waveform is shown in Figure 17. Ten days on a 1.8 GHz Pentium processor were required to run this simulation for 950ns, and no apparent decay is visible! Clearly, the sub-resonant apertures do not provide much loading! In order to accurately estimate shielding, a much longer run time would be required to achieve a suitable amount of decay in the waveform—this is not a viable option.

Table 3. Energy decay times and associated Q-factors obtained from a JTFA analysis of the box/slot combination of figure. The selected frequencies correspond to slot resonances. The conductance of the dielectric slabs is $\sigma=250$ S/m

Frequency (MHz)	t_{decay} (ns)	Q-Factor
502	100	315
1485	115	1,069
2431	149	2,271

Table 4. Energy decay times and associated Q-factors at selected frequencies obtained from a JTFA analysis of the box/slot combination of figure 15. Note how the Q-factors decrease rapidly with increasing frequency.

Frequency (MHz)	t_{decay} (ns)	Q-Factor
1000	3,159	19,850
2000	1,098	13,802
2500	341	5,353
3000	210	3,966

A JTFA analysis using a 200ns Kaiser-Bessel window ($\beta=2.0$) on the box waveform and 200 MHz of frequency averaging is shown in Figure 18. Results are shown for several frequencies for which higher rates of decay occur as the frequency is increased. This is a direct consequence of the frequency dependence of the aperture radiated power. Once again, JTFA reveals physical effects that are not visible in the time domain alone. The least-squares fits are shown as dashed lines, and the decay rates are approximately exponential. The resulting Q-factors are summarized in Table 4 below, with considerably higher values than those encountered in the loaded box cases.

The high Q-factors and associated slow decay rates pose a challenge in estimating the penetration. A promising approach that is currently being investigated is first to invoke the assumption of single exponential decay and then extrapolate beyond the computed time range. The process is illustrated in Figure 19. We start with the least-squares fit obtained from a combination of joint time-frequency analysis and frequency averaging. The penetration line is sampled at an interval of W , corresponding to the window width used in the JTFA. The samples give us information about signal energies at sequential and non-overlapping window positions. We can now sum these components to obtain the total penetration. Although there are an infinite number of samples, the assumption of exponential decay results in a simple geometric progression that is readily summed in closed form [15]. Some results obtained, using this method for the configuration of Figure 16 are summarized on Table 5. The penetration increases rapidly above 1000 MHz due to the increasing electrical size of the rectangular apertures. The influences of window function and duration on the structure penetration are currently being investigated. In addition, our research is focusing on the development of guidelines for optimal window parameter selection. The application of this technique to shielding structures is work in progress, and more research is currently being conducted to bring it to maturity.

Conclusions

Table 5. Box penetration computed from a combination of joint time-frequency analysis and a 200 MHz averaging bandwidth

Frequency (MHz)	Penetration (dB) Kaiser-Bessel Window $\beta=2.0, W=200\text{ns}$
1000	-17.8
2000	-5.1
2500	-6.2
3000	-4.9

Joint time-frequency analysis is a potentially powerful tool for the analysis of EMC shielding problems using time-domain numerical codes. It permits us to use shorter run times, and extract useful parameters such as a Q-factor, and under certain conditions, shielding. The application of this technique to other types of shielding structures is work in progress, and other potential applications of this method are currently being investigated.

Acknowledgements

First and foremost, the authors are deeply indebted to Arthur Ondrejka (NIST Emeritus) for his pioneering work and mentorship in joint time-frequency analysis. We are also indebted to Dave Walen, Tony Wilson, and John Dimtroff of the FAA for their generous support in the development of this powerful tool during 2001-2003. The authors are also indebted to Mike Hatfield of the Naval Surface Warfare Center for his support of the genesis of this technique during 1993-1994. We are also indebted to Perry Wilson and Dennis Friday of the NIST RF Technology division for their generous support.

References

- [1] D. Gabor, "Theory of communication," J. IEE (London), vol. 93, pp. 429-457, 1946.
- [2] L. Cohen, "Time-frequency distributions-a review," Proc. IEEE, vol. 77, no. 7, July 1989
- [3] T.F. Quatieri, *Discrete-Time Speech Signal Processing*, Upper Saddle River N.J.: Prentice-Hall, 2002.

- [4] B. B. Hubbard, *The World According to Wavelets*, Natick, MA: A. K. Peters Ltd., 1998.
- [5] S. Qian and D. Chen, *Joint Time-Frequency Analysis*, Upper Saddle River N.J.: Prentice-Hall, 1996.
- [6] J.F. Alm and J.S. Walker, "Time-frequency analysis of musical instruments," *SIAM Review*, vol. 44, pp. 457-476, August, 2002.
- [7] F. A. Everest, *Master Handbook of Acoustics*, New York, NY: McGraw Hill, 2001.
- [8] J..M. Ladbury, R.T. Johnk, A.R. Ondrejka, "Rapid evaluation of mode-stirred chambers using impulsive waveforms, NIST Technical Note 1381, June 1996.
- [9] L. Carin and L.B. Felsen, "Wave-oriented data processing for frequency- and time-domain scattering by nonuniform truncated arrays. *IEEE Antennas Propagation Magazine*, 36: pp. 29-43, 1994.
- [10] R. N. Bracewell, *The Fourier Transform and its Applications*, New York, NY: McGraw-Hill, 1978.
- [11] L. Cohen, *Time-Frequency Analysis*, Upper Saddle River N.J.: Prentice-Hall, 1995.
- [12] A. D. Poularikas, *Handbook of Formulas and Tables for Signal Processing*, Boca Raton, FL: CRC Press, 1999.
- [13] A. Taflove and S. Hagness, *Computational Electrodynamics: The Finite-Difference Time-Domain Method*, Boston MA: Artech House, 2000.
- [14] C. A. Grosvenor, R. T. Johnk, D. R. Novotny, N. Canales, C. .M. Weil, J. Veneman, *A Two-Phase Airframe Shielding Performance Study Using Ultra-wideband Measurement Systems*, NIST IR, *to be published*.
- [15] H. B. Dwight, *Tables of Integrals and Other Mathematical Data*, New York, NY: MacMillan, 1961.

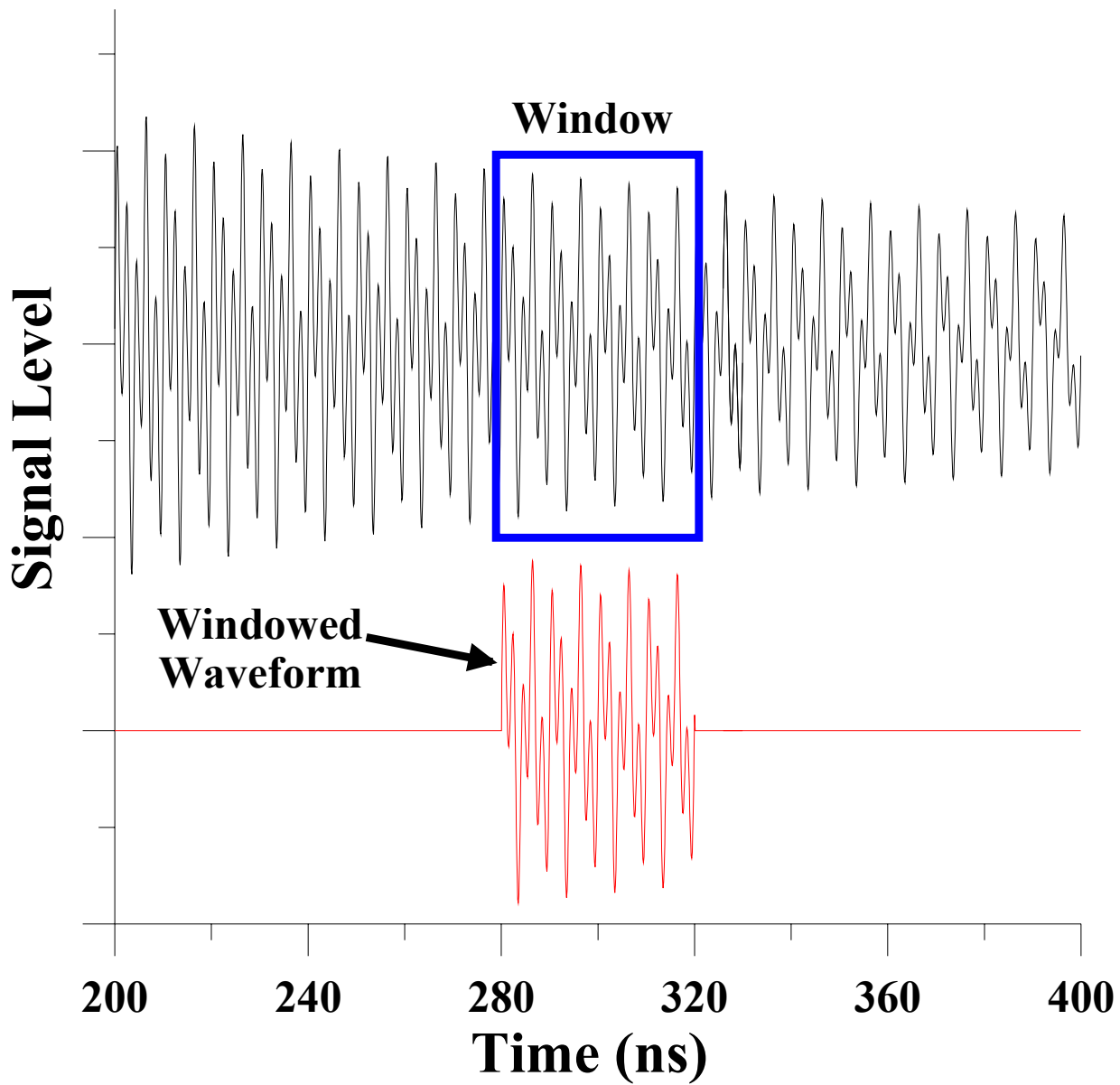


Figure 1. The most basic form of time windowing (rectangular window). The selected section of the top waveform remains unmodified, while the remaining section is deleted.

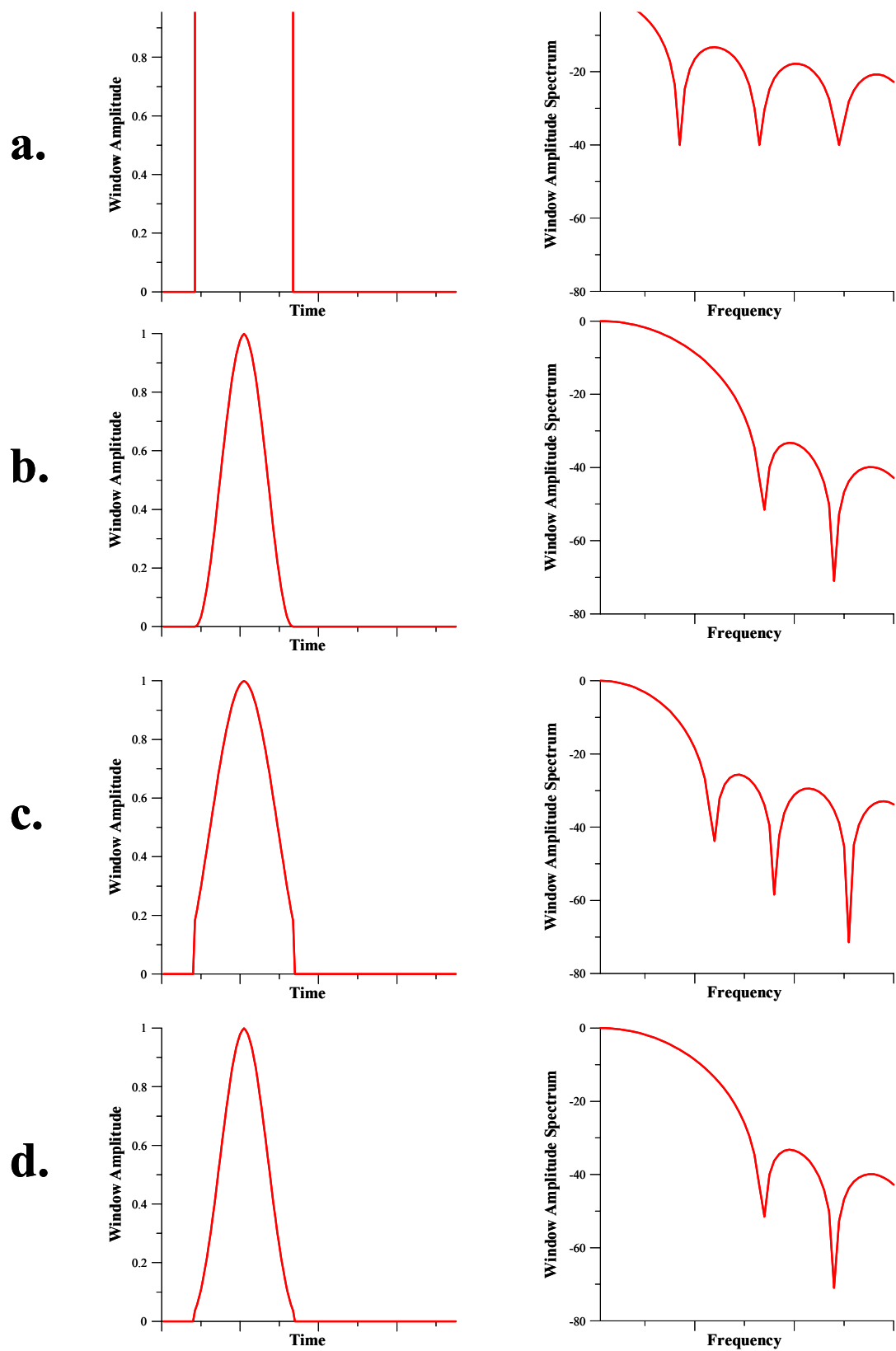
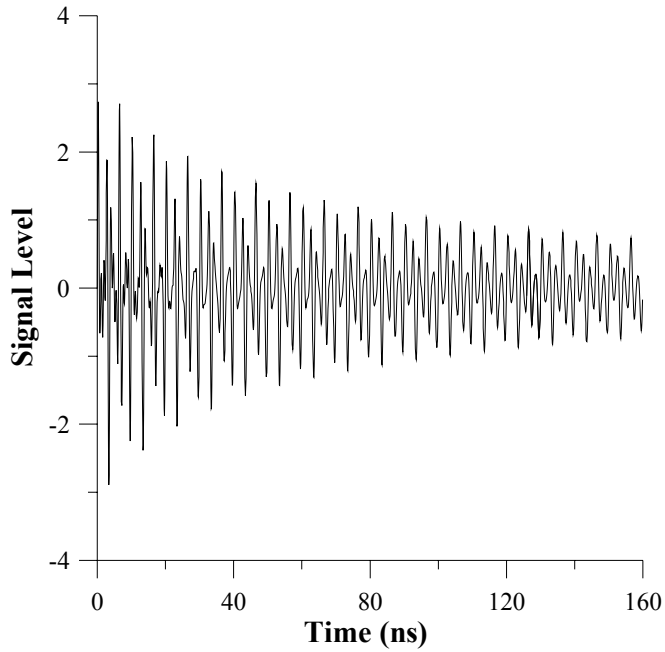
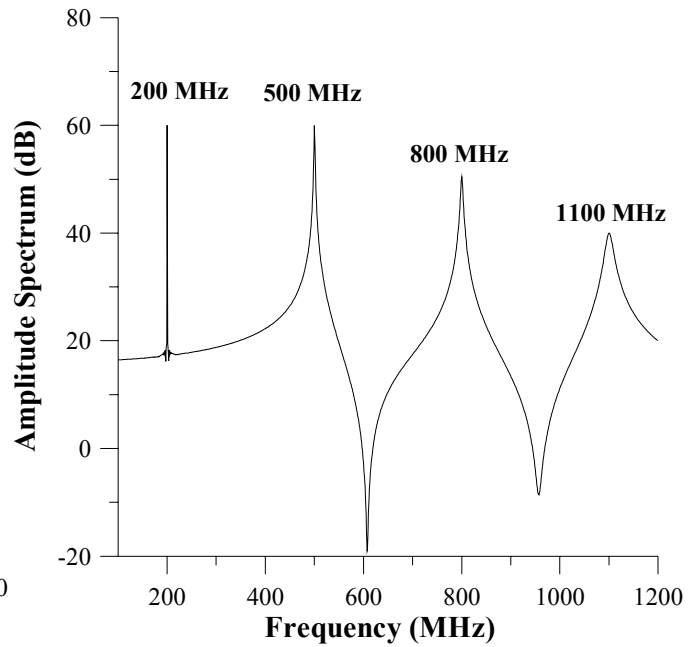


Figure 2. The time and frequency characteristics of four different time windows: **a.** rectangular window, **b.** Hanning window, **c.** Kaiser-Bessel window with index $\beta=1.0$, **d.** Kaiser-Bessel window with $\beta=1.6$. Note the tradeoffs in the time- and frequency-domains.



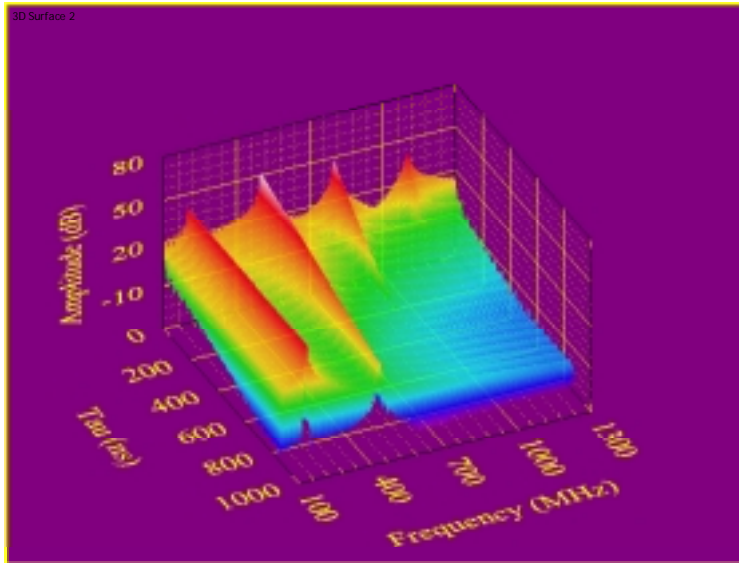
a.



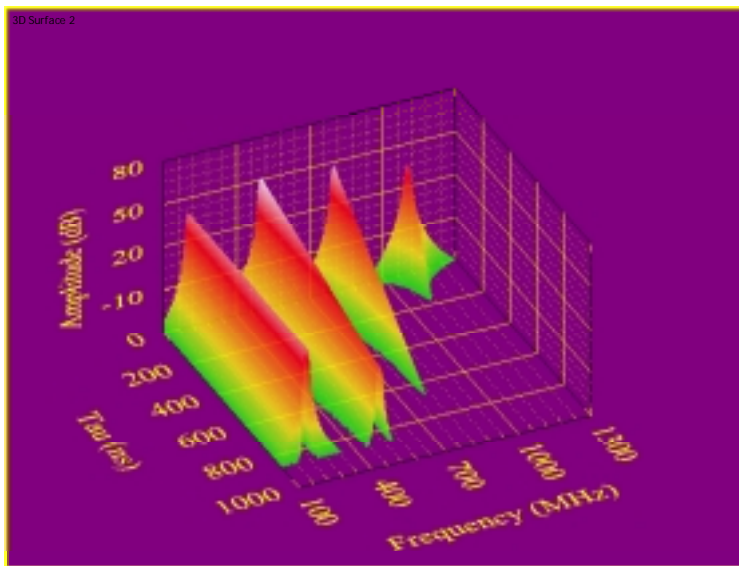
b.

Figure 3 **a.** Waveform obtained from (3) with $f_1=200\text{ MHz}$, $f_2=500\text{ MHz}$, $f_3=800\text{ MHz}$, $f_4=1,100\text{ MHz}$, $d_1=5.0 \times 10^6$, $d_2=5.0 \times 10^6$, and $d_3=1.5 \times 10^6$, **b.** Associated amplitude spectrum (the narrow spike at 200 MHz is a result of no decay).

a.



b.



c.

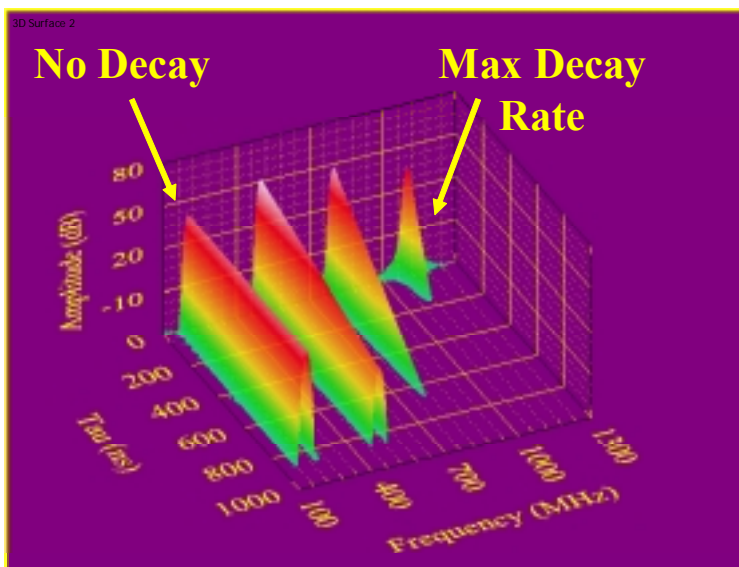


Figure 4. Joint time-frequency analysis of the waveform of (4) using a 100 ns window: **a.** rectangular window, **b.** Hanning window, **c.** Kaiser-Bessel window with $\beta=3.0$. Note that the frequency component at 200 MHz does not decay, while increasing decay rates along the time (τ) axis are noted at the higher frequencies.

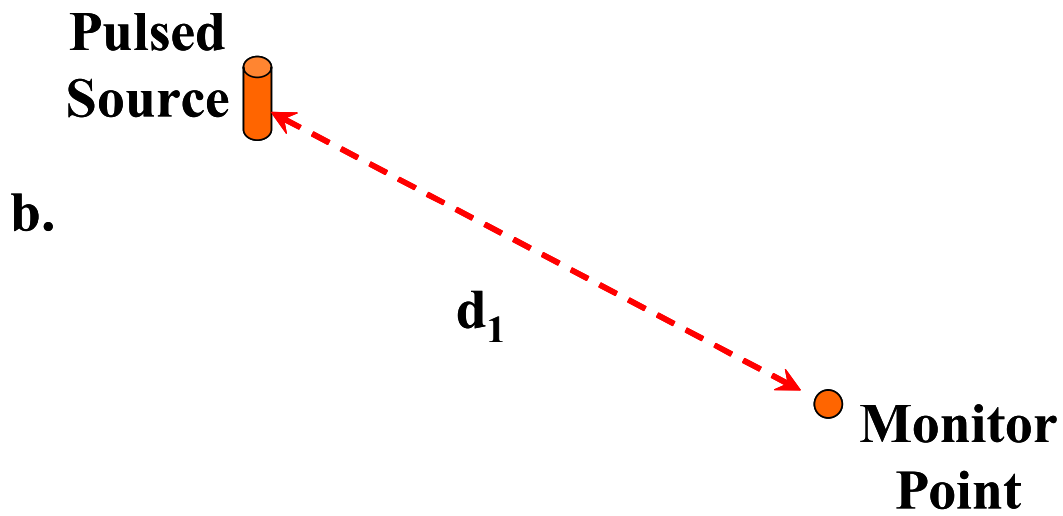
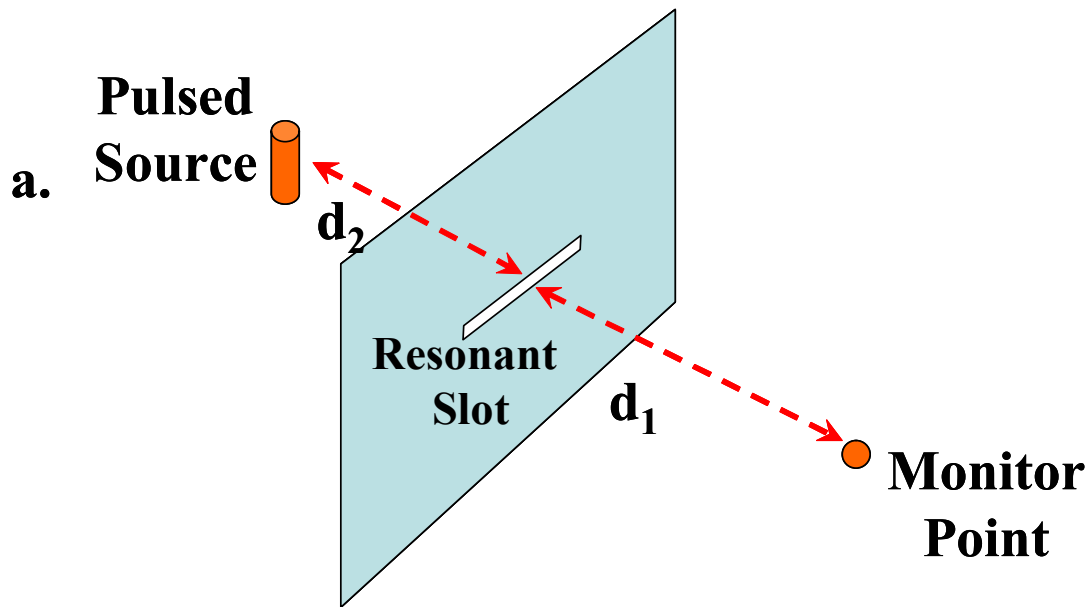
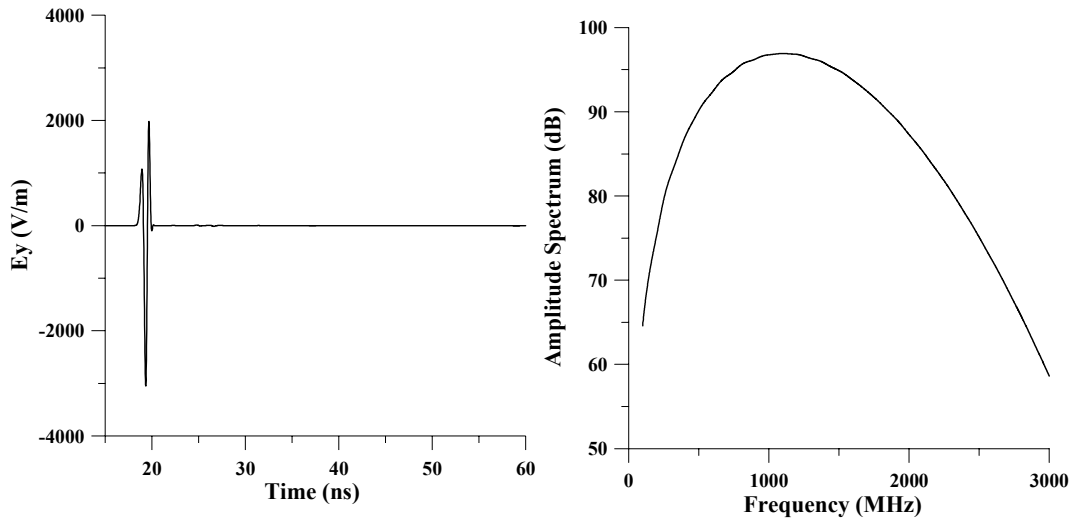
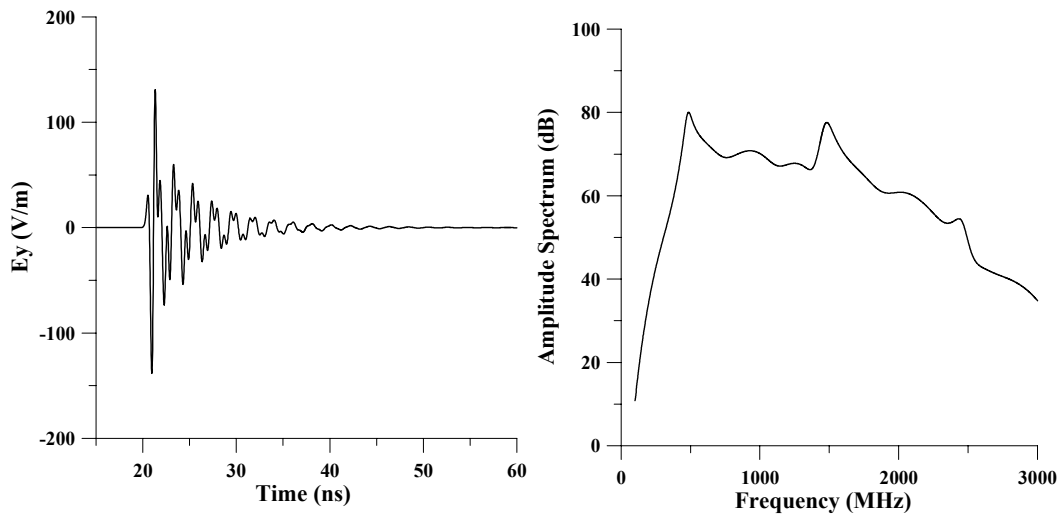


Figure 5 **a.** FDTD model of resonant slot (30.0 cm x 0.1 cm) embedded in a perfectly conducting plane of infinite extent, **b.** FDTD model of free-space reference. $d_1=6.0$ m and $d_2=0.5$ m.



a.



b.

Figure 6 **a.** FDTD generated reference waveform and associated amplitude spectrum, **b.** Waveform and corresponding amplitude spectrum obtained with a 30 cm x 0.1 cm resonant slot embedded in an infinite ground plane. Note the resonant peaks the neighborhood of 500, 1500, and 2500 MHz.

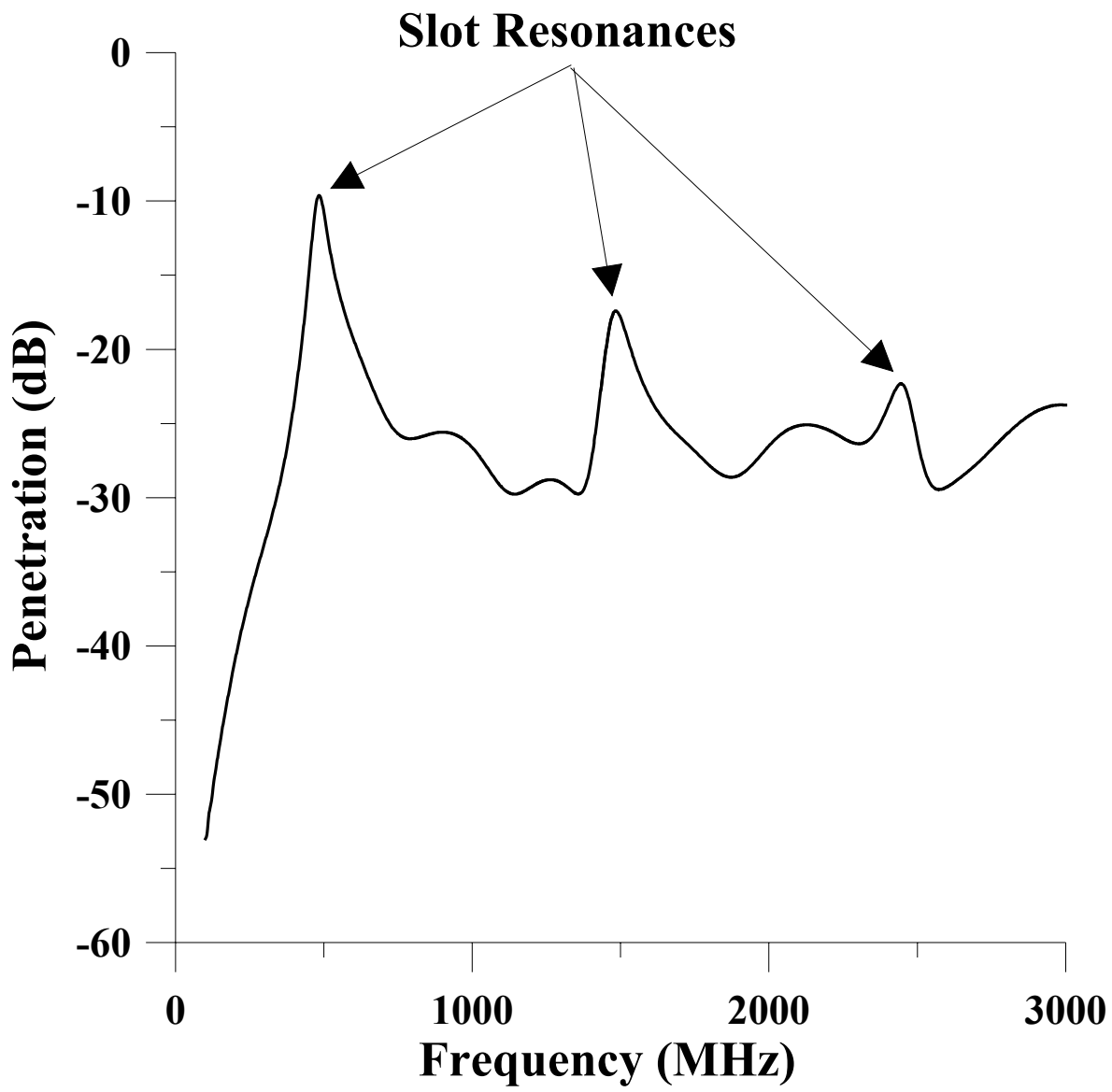


Figure 7. Normalized penetration for a 30 cm x 0.1 cm slot embedded in a perfectly conducting ground plane.

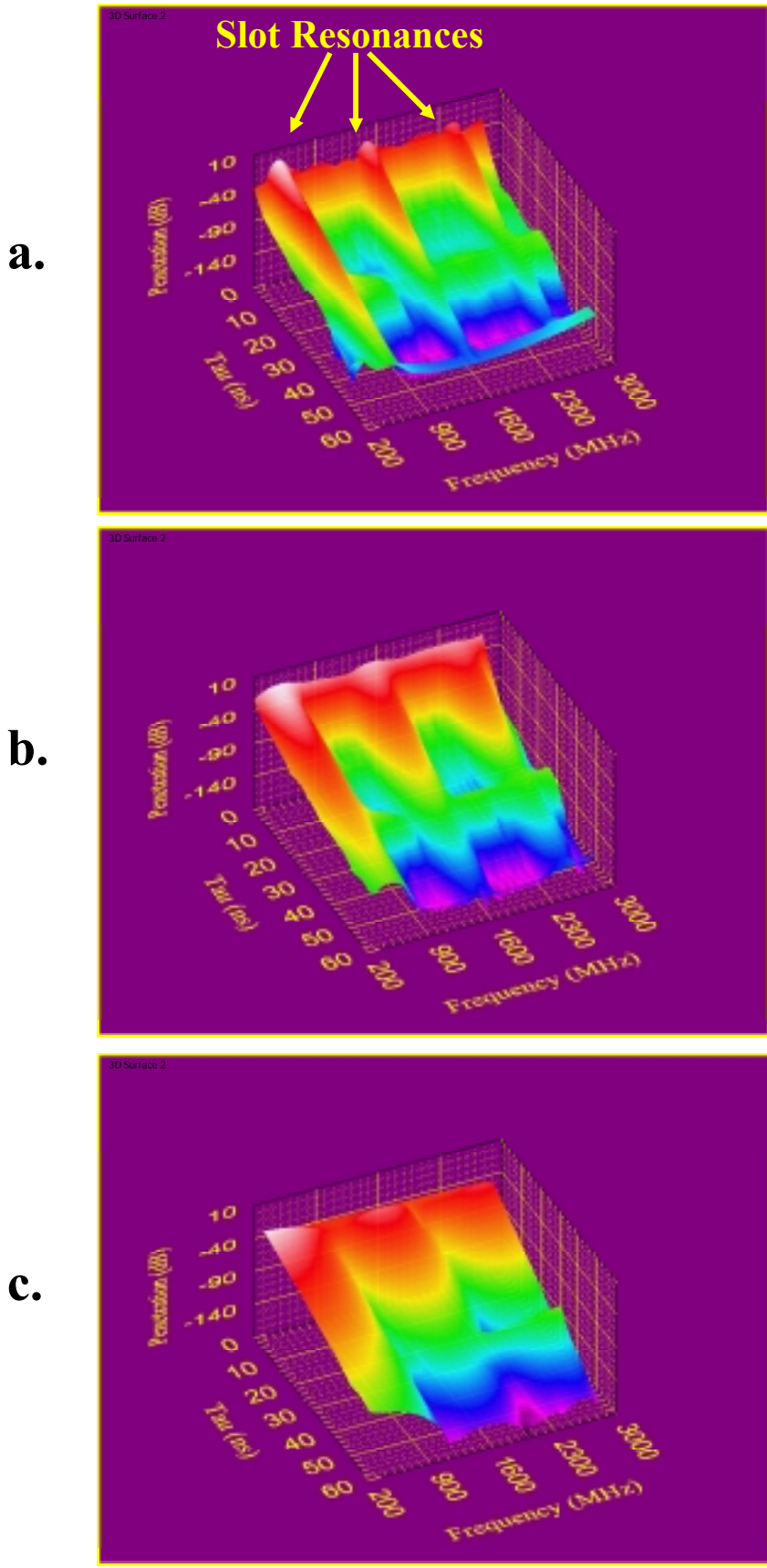


Figure 8. JTF analysis of the slot waveforms, **a.** 20 ns duration Kaiser-Bessel window with $\beta=3.0$, **b.** 10 ns duration Kaiser-Bessel window with $\beta=3.0$, **c.** 5 ns duration Kaiser-Bessel window with $\beta=3.0$.

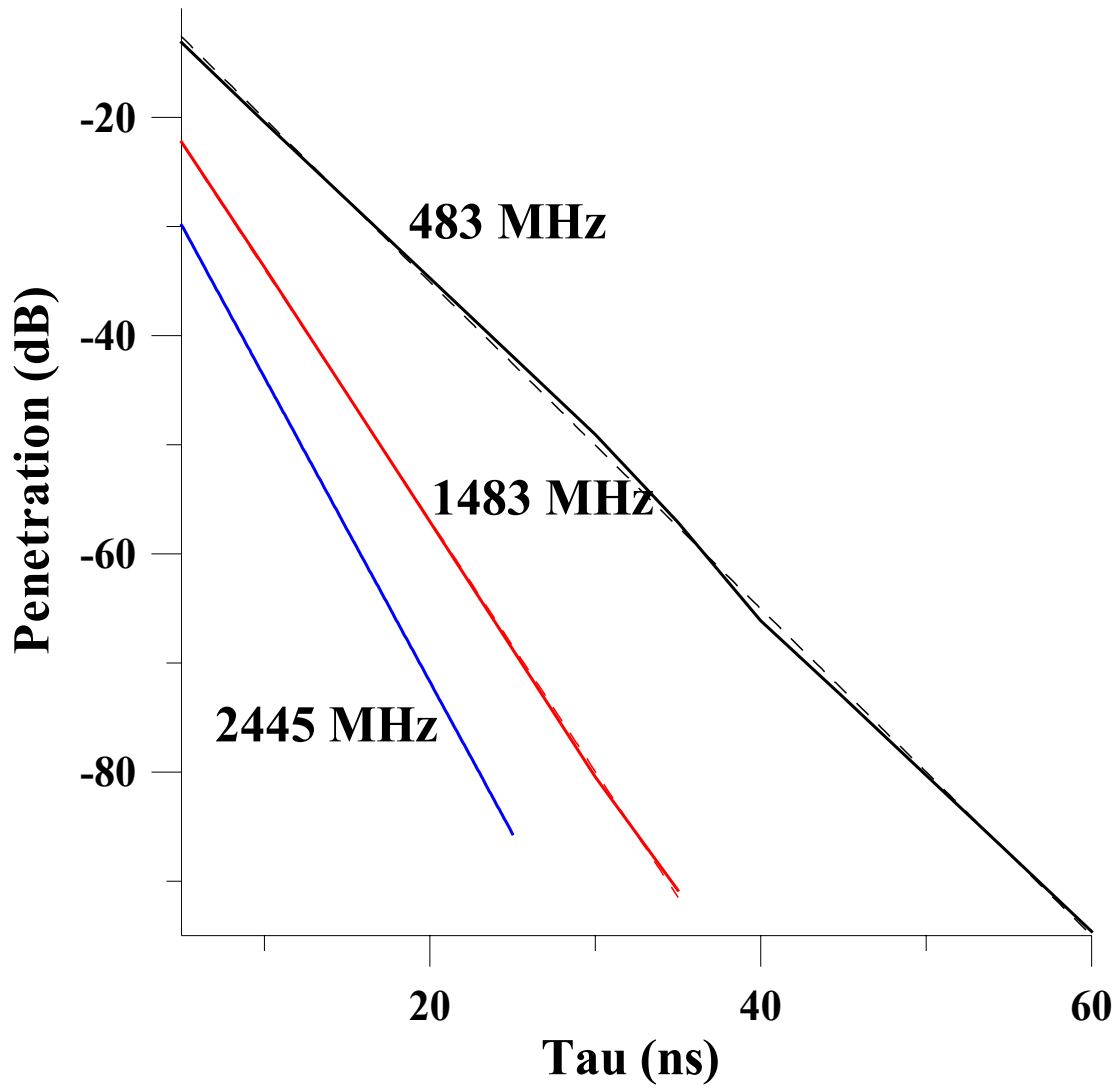


Figure 9. Slot decay characteristics obtained at the resonant peaks using a 10 ns duration Kaiser-Bessel window with $\beta=3.0$.

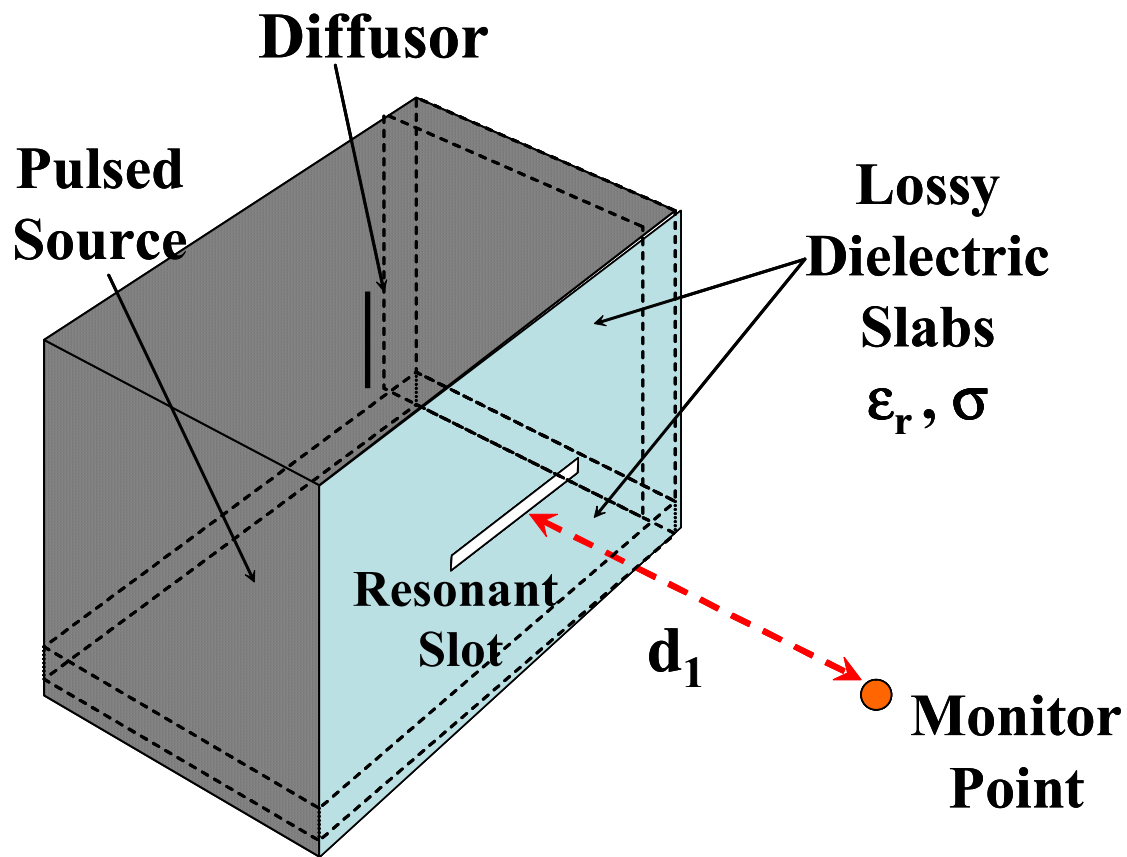


Figure 10. A 1.03 m x 0.93 m x 73 m metal box with a 0.3 m x 0.001 m resonant slot embedded in the face. Two interior box walls are loaded with lossy dielectric slabs with a variable conductance σ and $\epsilon_r=1.0$. The monitor point is positioned $d_1=6.0$ m from the center of the slot.

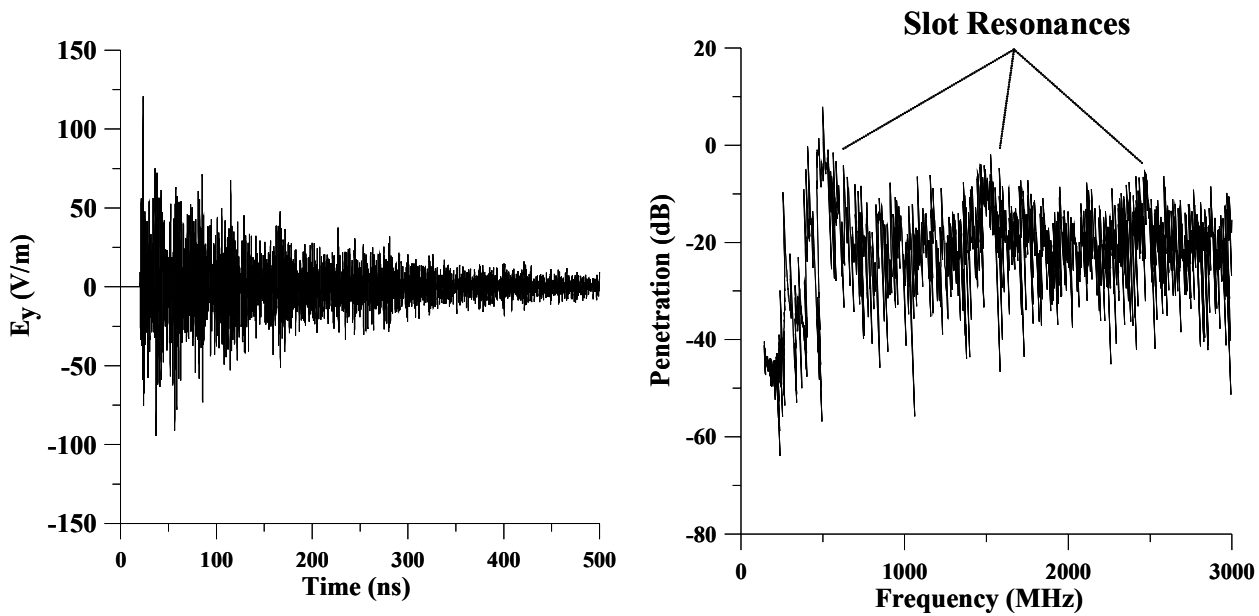
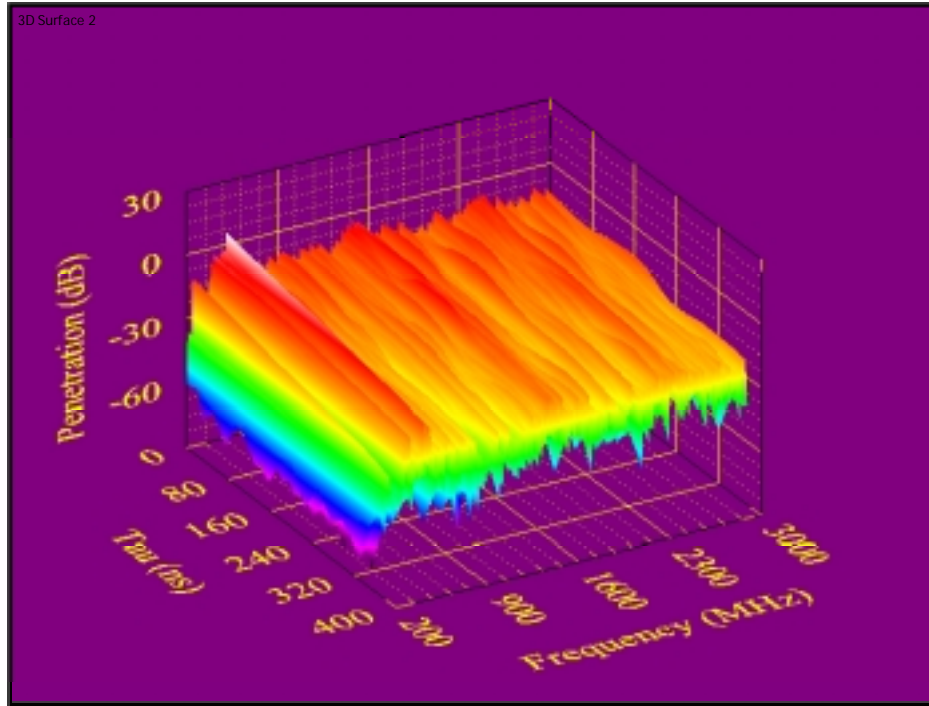


Figure 11. Time domain box electric field waveform and associated penetration spectrum obtained at a monitor point 6.0 m from the center of a 30 cm x 0.1 cm slot embedded in a highly conducting metal box. The lossy slabs each have a conductance $\sigma = 250$ S/m. Note the peaks in the penetration in the neighborhood of the slot resonances.

a.



b.

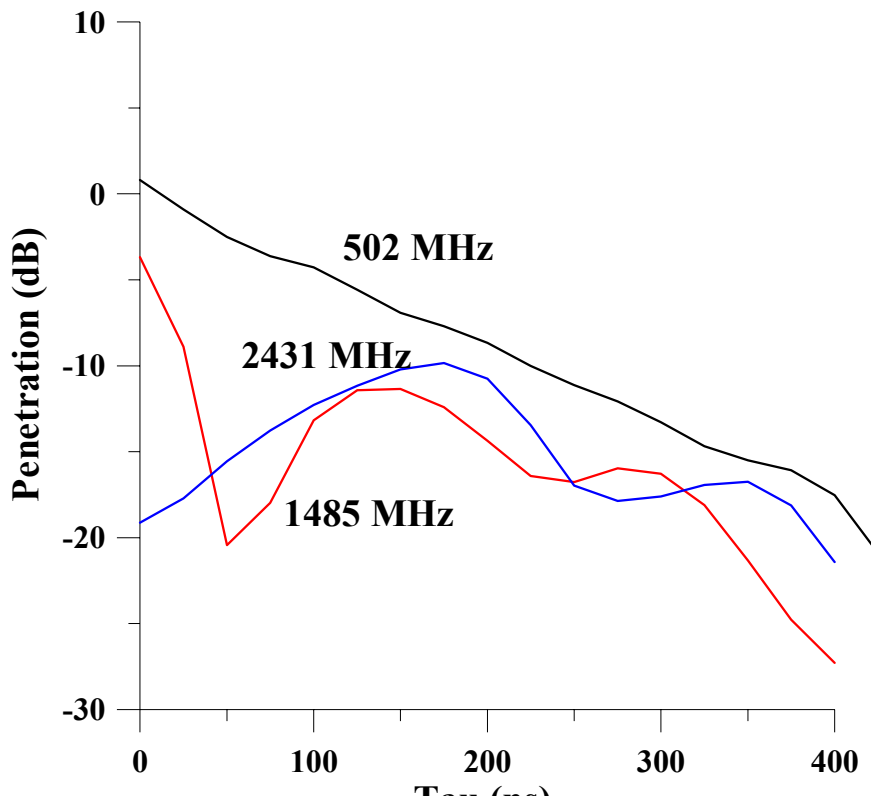


Figure 12 **a.** Joint time-frequency analysis of the box/slot combination with $\sigma = 250$ S/m. A 200ns wide Kaiser-Bessel window ($\beta=2.0$) is used. Note the complex structure of the penetration spectrum due to the box cavity modes, **b.** selected spectral decay components—note the erratic decay caused by interference between closely spaced box cavity modes.

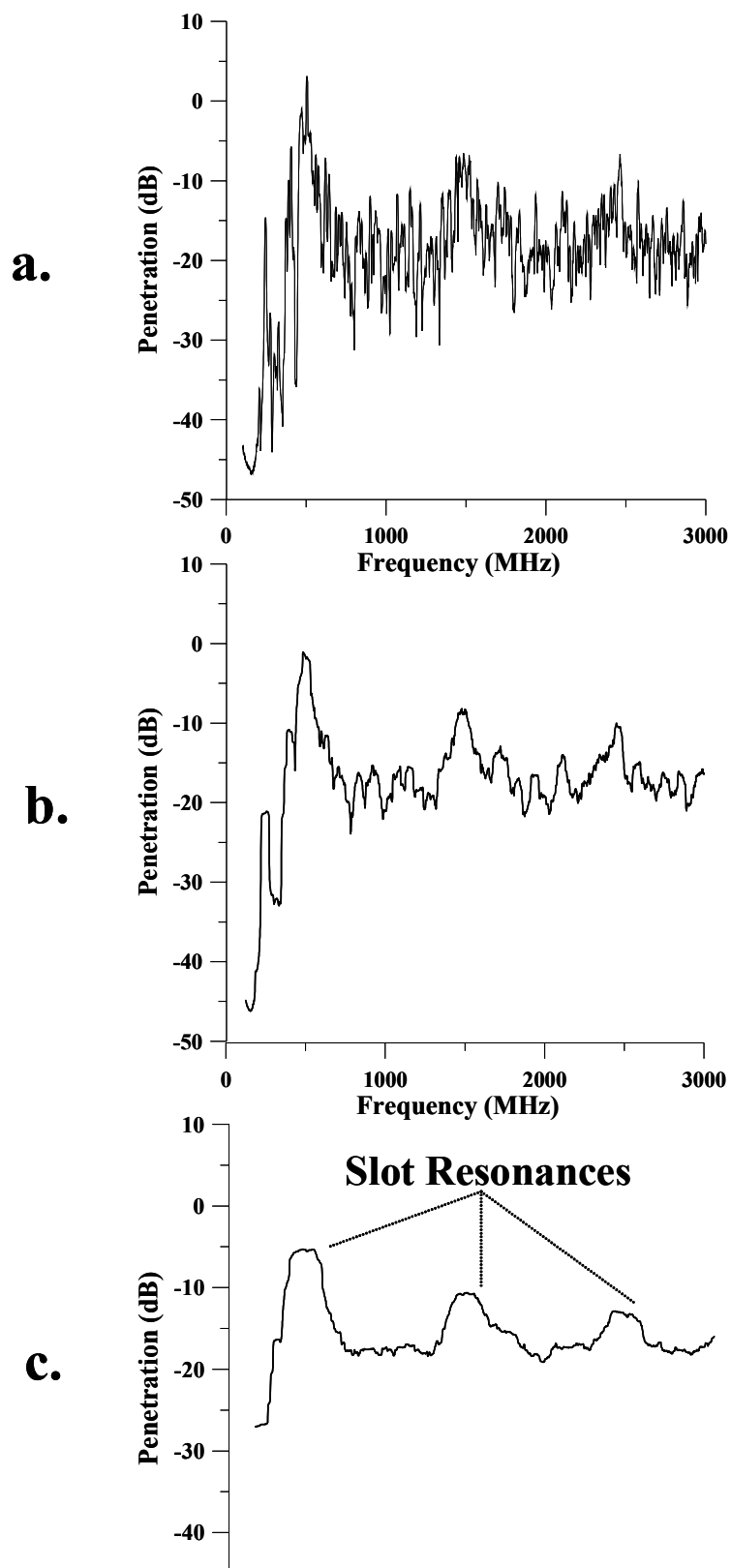
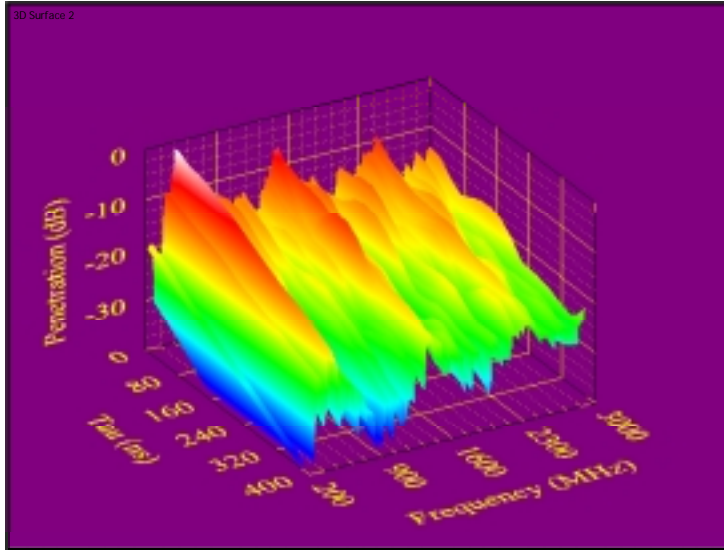
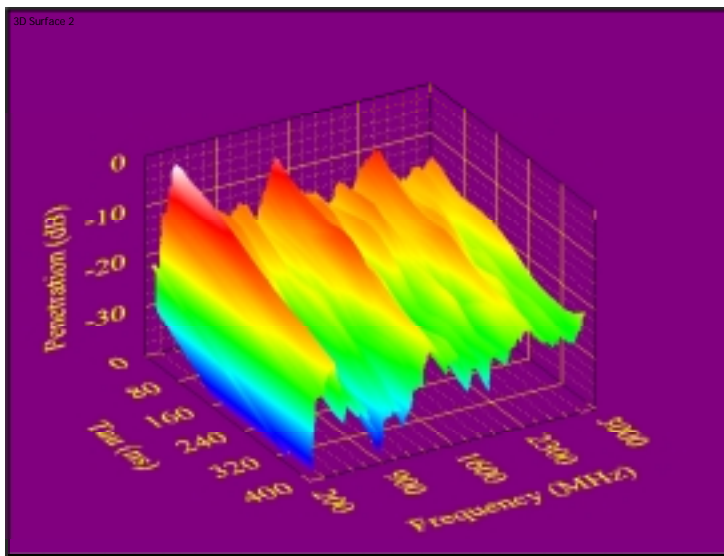


Figure 13. Impact of frequency averaging on the of box/slot structure penetration amplitude spectrum using a 200ns wide Kaiser-Bessel window ($\beta=2.0$), **a.** 50 MHz averaging bandwidth, **b.** 100 MHz averaging bandwidth, **c.** 200 MHz averaging bandwidth. Note how the slot resonances become more visible as the averaging bandwidth is increased.

a.



b.



c.

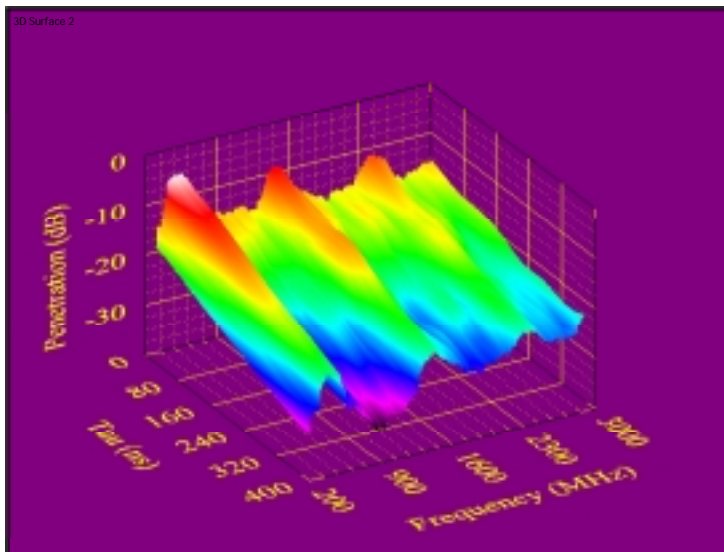


Figure 14. Impact of frequency averaging on the JTFA of box/slot structure penetration, **a.** 50 MHz, **b.** 100 MHz, **c.** 200 MHz. 200ns wide Kaiser-Bessel window ($\beta=2.0$) is used. Note how the slot resonances become more visible as the averaging bandwidth is increased.

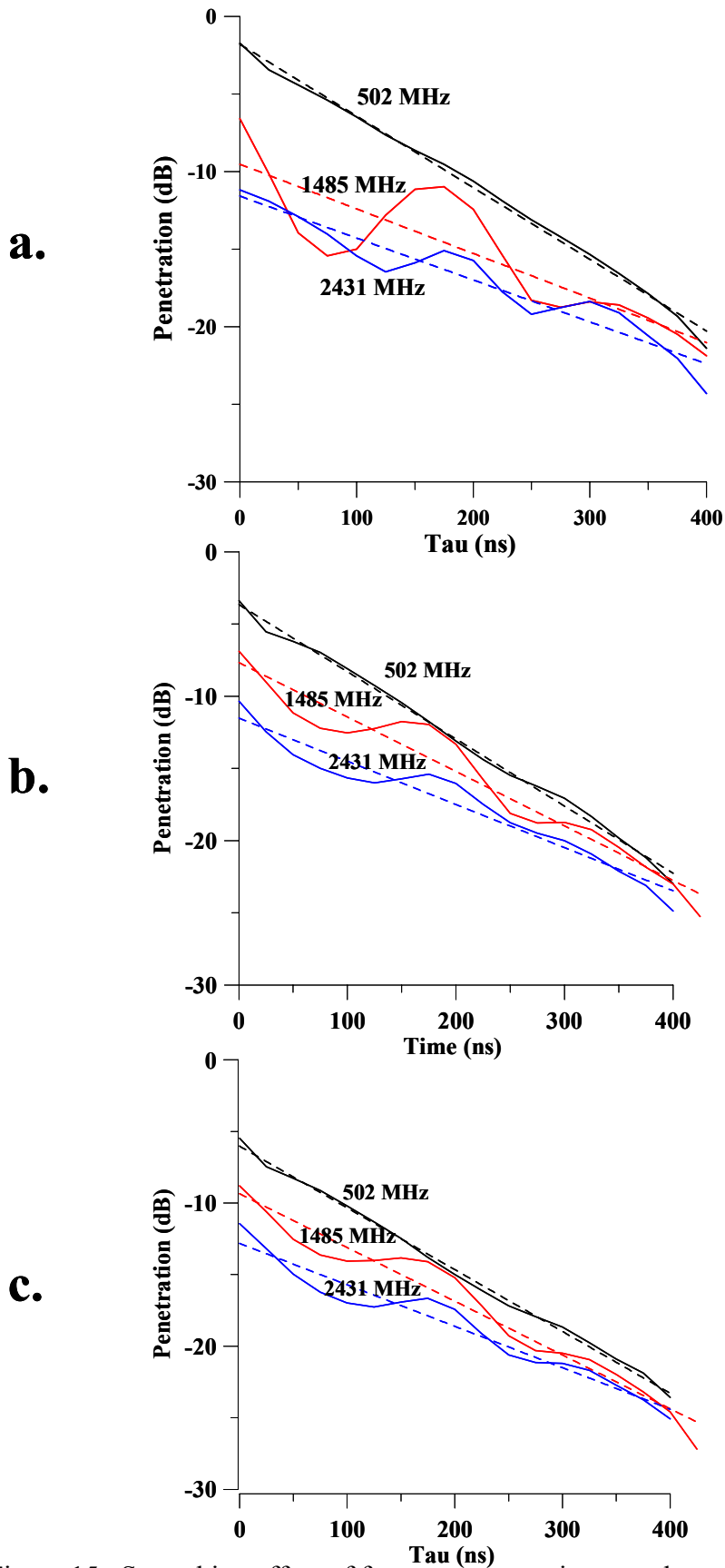


Figure 15. Smoothing effect of frequency averaging on selected frequency components, **a.** 50 MHz averaging bandwidth, **b.** 100 MHz averaging bandwidth, **c.** 200 MHz averaging bandwidth. Note how increased bandwidths reduces interferences effects between adjacent modes and accentuates the exponential decay with only minor variations in the slope of the extracted decay.

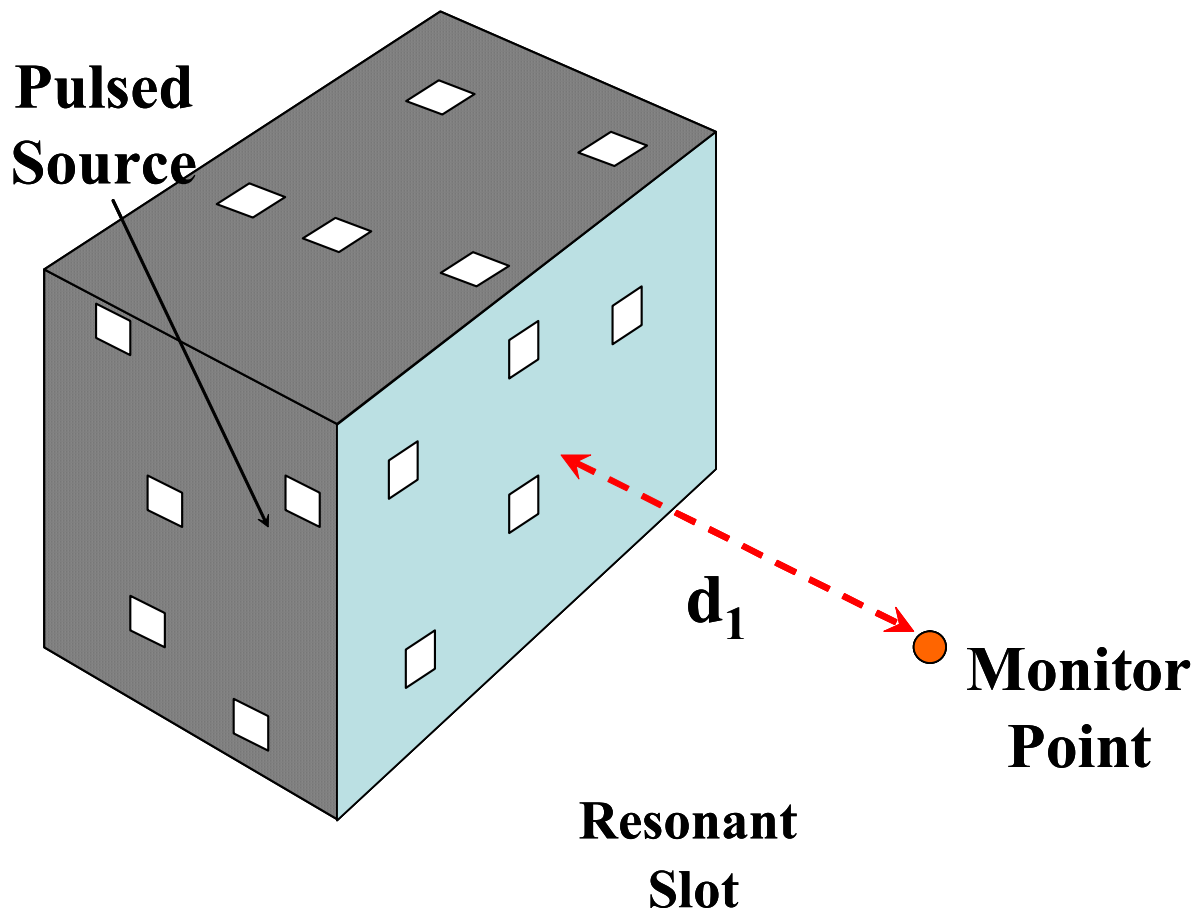


Figure 16. A 1.03 m x 0.93 m x 73 m metal box with five 4 cm x 4 cm apertures embedded in each face. The monitor point is positioned $d_1=6.0$ m from the center of the front face. The interior of the box is unloaded, and the only loss is due to radiation from the apertures.

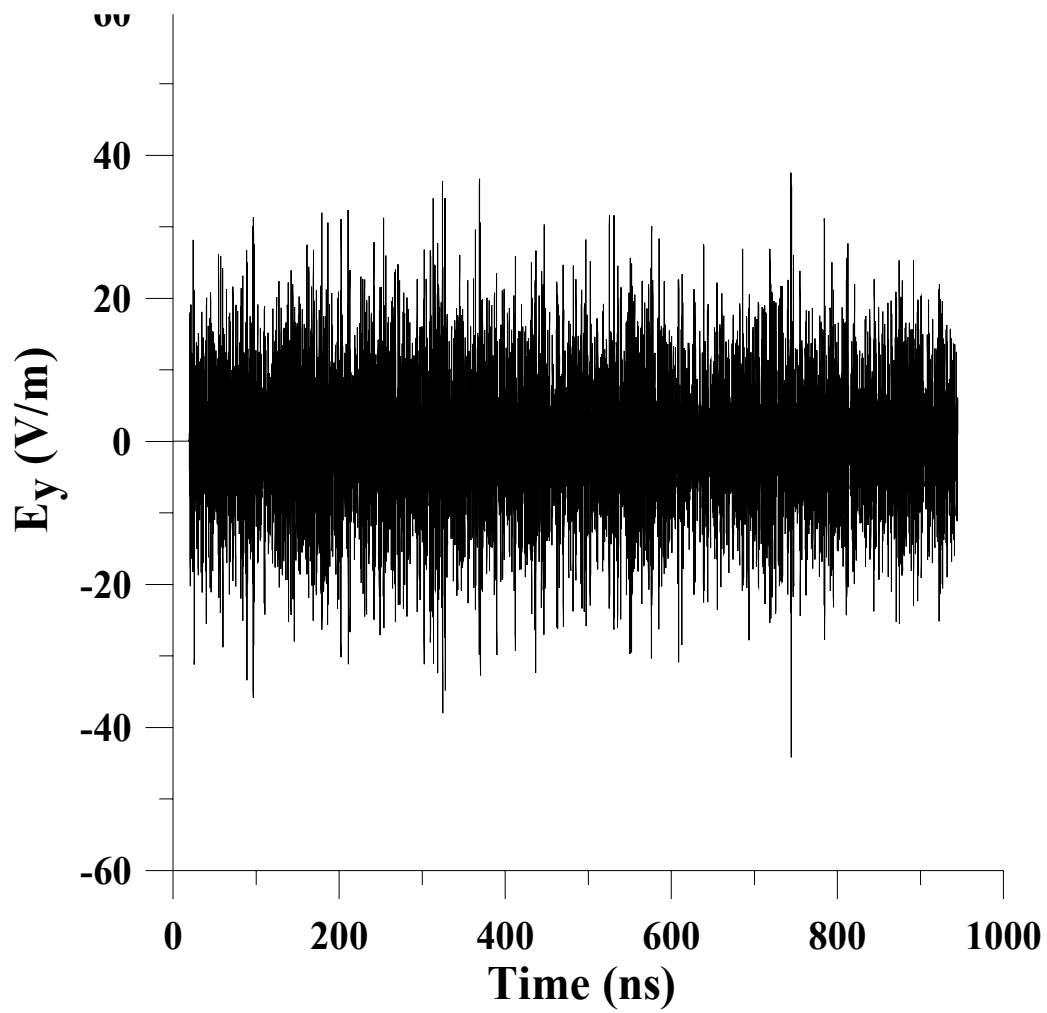


Figure 17. Time domain box waveform obtained at the monitor point. Note that there is no appreciable decay due to small aperture radiation efficiency.

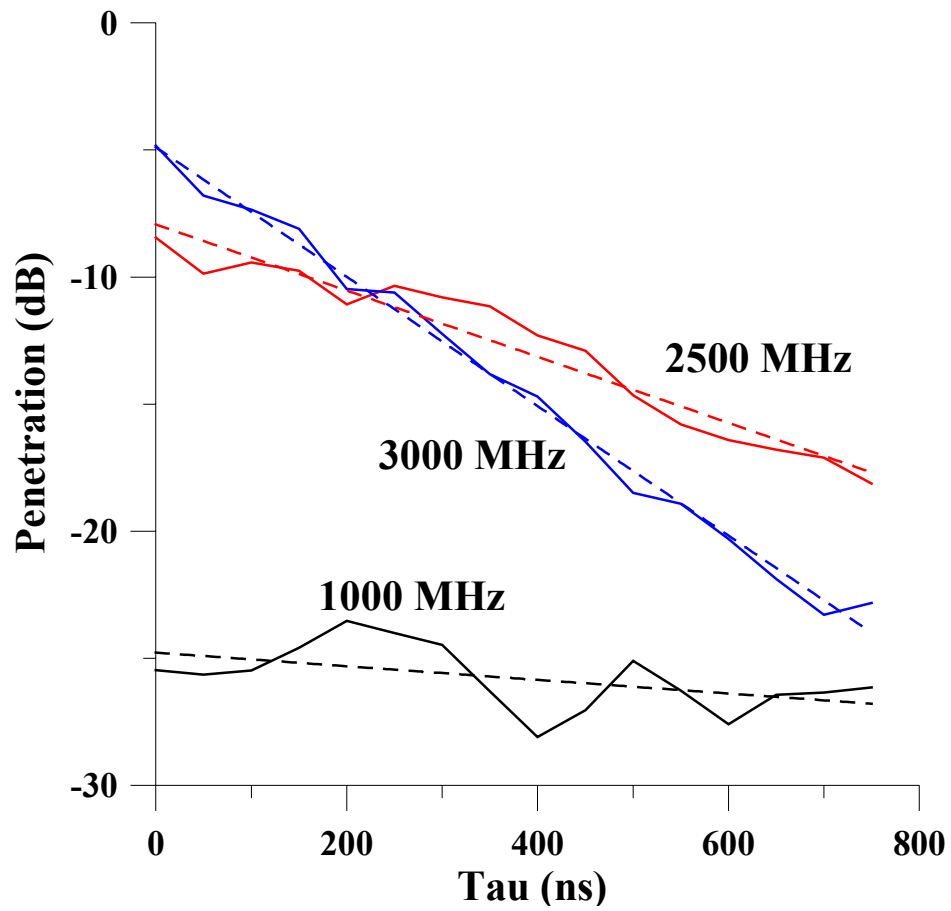


Figure 18. JTFA analysis of the box loaded with thirty 4 cm x 4 cm slots. Note the increased decay rates at the higher frequencies due to increased radiation efficiency.

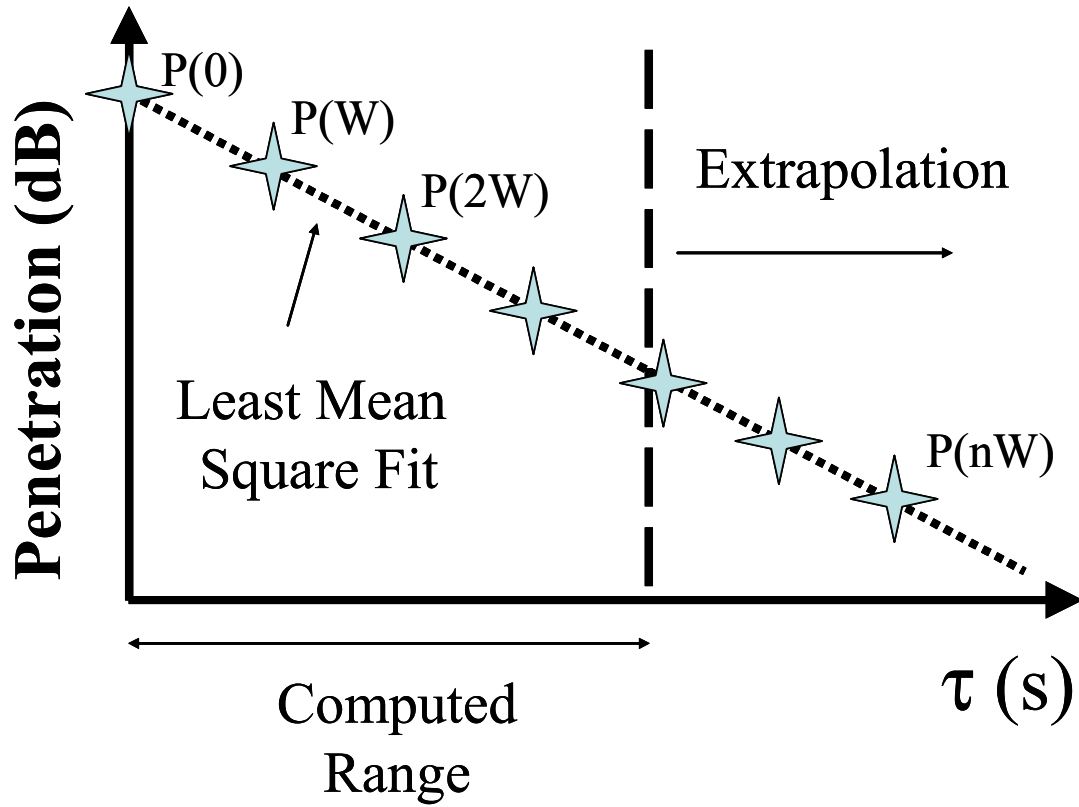


Figure 19. Computing total penetration from a least-squares fit. Samples are taken at an equal interval W , corresponding to the window width selected for the original JTFA analysis. The samples are then summed to obtain total penetration.

Non-orthogonal FDTD Methods

J. Alan Roden, Aerospace Corporation

I. ABSTRACT

This paper presents an in-depth tutorial on the non-orthogonal Finite-Difference Time-domain Method (NFDTD). The mathematical formulation as well as the details of implementation are presented in detail. A variety of examples are presented along with discussion of some of the common problems associated with the method.

II. INTRODUCTION

The Finite-Difference Time-Domain technique has captured much attention since the conception of the Yee [1] cell in the 1960's. It is easily applied in an orthogonal coordinate system. Here the derivatives which are present in the curl operations of Maxwell's equations are naturally applied to the fields which lie on the underlying orthogonal grid. Unfortunately, when curved bodies requiring high accuracy are modeled, an orthogonal implementation of the FDTD technique can lead to a forbidding computational task. While increasingly finer discretization will diminish dispersion related errors, accomplishing a true representation of the geometry features can be impractical.

To overcome this problem, it is desirable that the underlying coordinate system naturally conform to the contours of the physical boundaries of the problem geometry. In the early work of Stratton [2] and later Holland [3], it was demonstrated that if a geometry may be represented by a global curvilinear coordinate system, the FDTD algorithm may be efficiently applied leading to a second order accurate solution in both time and space. This is accomplished by expressing and solving Maxwell's curl equations in the general curvilinear space. This methodology will be referred to as the globally non-orthogonal finite-difference time-domain or GNFDTD method in this work. Later, it was found that the GNFDTD technique can also be efficiently applied on a local basis [5] in those cases where a global curvilinear coordinate system was not practical. This technique is called the NFDTD technique. These methods both rely on a structured grid which is either regular or irregular in nature.

Additionally, Madsen [6], Gedney [7] and others have introduced a DSI (Discrete Surface Integral) method which supports an unstructured grid and can be much more effective in modeling arbitrarily shaped contours with a much more robust grid. This family of solutions generally requires a complementary gridding package such as IDEAS. Other techniques have also been introduced based on local grid deformation such as the contour path (CP-FDTD [9]) and the conformal (CFDTD [10]) techniques. These techniques tend to be less general in nature.

Each of these methods conforms to curved bodies with differing complexities, differing stability criteria, and differing accuracies. The mathematical form of these techniques is described in the previous citations as well as in [8]. In this work, a detailed analysis of the NFDTD and GNFDTD methods are given and the proper implementation of the underlying constructs is illustrated. Furthermore, discussion of their applicability and shortcomings will be presented.

III. THE FDTD TECHNIQUE IN GLOBAL CURVILINEAR COORDINATES

In problems where the geometry conforms to a globally defined curvature, the globally non-orthogonal FDTD technique (GNFDTD) may be applied. In such cases, a set of global curvilinear coordinates ($\vec{u}^1, \vec{u}^2, \vec{u}^3$) may be defined such that each position in the orthogonal space is given by a position vector of the form

$$\vec{r}(x, y, z) = \vec{r}(u^1, u^2, u^3). \quad (1)$$

For a given point $P(u^1, u^2, u^3)$ a set of vectors is defined by [2]

$$\vec{a}_1 = \frac{\partial \vec{r}}{\partial u^1} \quad \vec{a}_2 = \frac{\partial \vec{r}}{\partial u^2} \quad \vec{a}_3 = \frac{\partial \vec{r}}{\partial u^3}. \quad (2)$$

These vectors are referred to as the unitary vectors for the point P and they define the unitary axes of the general curvilinear space. These vectors are typically not of unit length. An alternate set of vectors called the contravariant vectors are denoted by superscripts and are the reciprocals of these vectors. These vectors are defined through the relation

$$\begin{aligned} \vec{a}^1 &= \frac{\vec{a}_2 \times \vec{a}_3}{\sqrt{g}} \\ \vec{a}^2 &= \frac{\vec{a}_3 \times \vec{a}_1}{\sqrt{g}} \\ \vec{a}^3 &= \frac{\vec{a}_1 \times \vec{a}_2}{\sqrt{g}} \end{aligned} \quad (3)$$

where g is the determinant of the metric tensor $[g]$ defined by

$$g_{i,j} = \vec{a}_i \cdot \vec{a}_j \quad (4)$$

or alternately

$$\sqrt{g} = \vec{a}_i \cdot (\vec{a}_{(i+1) \bmod 3} \times \vec{a}_{(i+2) \bmod 3}). \quad (5)$$

The coordinate system defined by these two sets of vectors is illustrated in Figure 1. Due to their reciprocal relation, it can be shown that

$$\vec{a}_i \cdot \vec{a}^j = \delta_{i,j} \quad (6)$$

where $\delta_{i,j}$ is the Kronecker delta function. This identity can easily be shown by using the definition of the contravariant vectors given in (3). For example

$$\vec{a}_1 \cdot \vec{a}^1 = \frac{\vec{a}_1 \cdot (\vec{a}_2 \times \vec{a}_3)}{\sqrt{g}} = 1 \quad (7)$$

$$\vec{a}_2 \cdot \vec{a}^1 = \frac{\vec{a}_2 \cdot (\vec{a}_2 \times \vec{a}_3)}{\sqrt{g}} = 0. \quad (8)$$

As was shown by Stratton, the vector fields in the orthogonal space are related to vector fields of the general curvilinear space through the relation

$$\vec{F} = \sum_{i=1}^3 f^i \vec{a}_i \quad (9)$$

where f^i is the contravariant field vector whose vector direction is defined by the unitary vectors \vec{a}_j , $\vec{a}_k \neq \vec{a}_i$ and \vec{F} represents the vector fields of an orthogonal space. Also, because contravariant and covariant vectors are a reciprocal set the reciprocal relation exists of

$$\vec{F} = \sum_{i=1}^3 f_i \vec{a}^i. \quad (10)$$

A set of metrics may also be defined for the contravariant vectors \vec{a}^i as

$$g^{i,j} = \vec{a}^i \cdot \vec{a}^j \quad (11)$$

using these metrics the vector field components in the general curvilinear space may also be related as

$$\begin{aligned} f_i &= \sum_{j=1}^3 g_{i,j} f^j \\ f^i &= \sum_{j=1}^3 g^{i,j} f_j. \end{aligned} \quad (12)$$

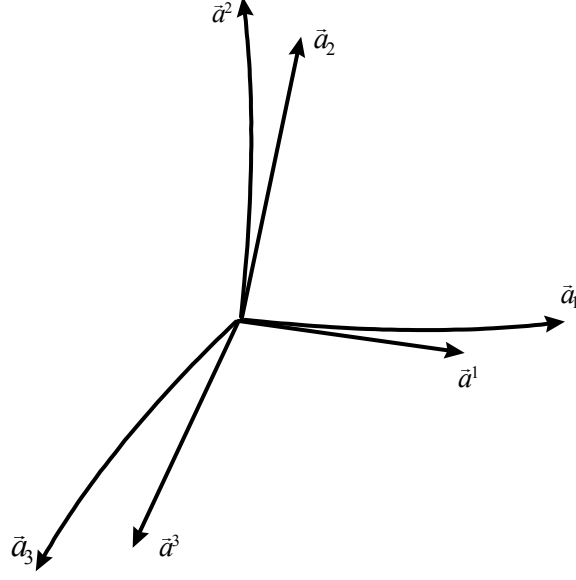


Figure 1 – Unitary and reciprocal vectors.

Using (6), (9) and (11) it can easily be shown that the covariant and contravariant field components are related to those in the orthogonal space by the relations

$$f_i = \vec{a}_i \cdot \vec{F} \quad (13)$$

and

$$f^i = \vec{a}^i \cdot \vec{F}. \quad (14)$$

The fields in the general curvilinear space are of geometry dependent units. To obtain these field values in geometry independent units the normalization of

$$\bar{F}_i = \frac{F_i}{\sqrt{g_{ii}}} \quad (15)$$

and

$$\bar{F}^i = \frac{F^i}{\sqrt{g^{ii}}} \quad (16)$$

may be applied.

Maxwell's curl equations may be constructed using the concepts outlined above. To this end, the formulation of the \hat{a}^1 component of the curl operation is examined in the general curvilinear space. The right hand side of this component may be approximated as

$$\nabla \times \vec{F} \cdot \hat{a}^1 = \lim_{C \rightarrow 0} \frac{1}{A} \oint_C \vec{F} \cdot d\vec{l} \quad (17)$$

where A is the area of the surface bounded by the covariant vectors u_2 and u_3 as illustrated in Figure 2. The discretized line integral around the contour C is given in terms of the covariant field values as

$$\oint \vec{F} \cdot d\vec{l} = \left\{ (F_3 du^3)_{u^2+du^2} - (F_3 du^3)_{u^2} - (F_2 du^2)_{u^3+du^3} + (F_2 du^2)_{u^3} \right\} \quad (18)$$

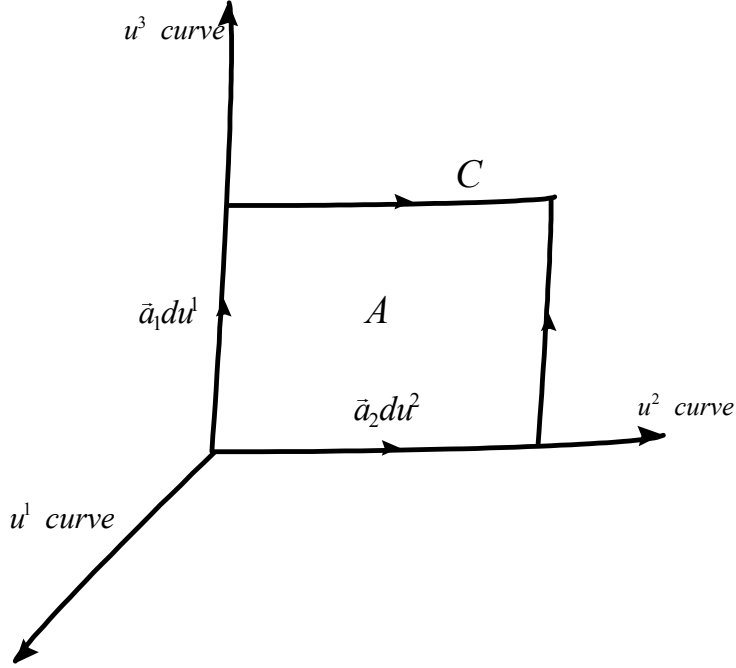


Figure 2 – Illustration of the curl operation in general curvilinear coordinates.

and approximating these differences by the first terms of the Taylor series expansion we may write

$$\oint \vec{F} \cdot d\vec{l} = \left\{ \frac{\partial F_3}{\partial u^2} - \frac{\partial F_2}{\partial u^3} \right\} du^2 du^3. \quad (19)$$

The area of the surface bounded by C is given by

$$\begin{aligned} A &= \sqrt{\vec{a}_2 \times \vec{a}_3 \cdot \vec{a}_2 \times \vec{a}_3} du^2 du^3 \\ &= |\vec{a}^1| \sqrt{g} du^2 du^3 \end{aligned} \quad (20)$$

and the unit normal in the direction of \vec{a}^1 is given by

$$\frac{\vec{a}^1}{\sqrt{\vec{a}^1 \cdot \vec{a}^1}} \quad (21)$$

so

$$\nabla \times \vec{F} \cdot \hat{a}^1 = \frac{1}{\sqrt{g}} \left\{ \frac{\partial F_3}{\partial u^2} - \frac{\partial F_2}{\partial u^3} \right\}. \quad (22)$$

The discretization of the other components of the curl operation in a similar way, leads to Maxwell's equations for a sourceless media in the general curvilinear space which are

$$j\omega\mu H^1 = -\frac{1}{\sqrt{g}} \left\{ \frac{\partial E_3}{\partial u^2} - \frac{\partial E_2}{\partial u^3} \right\} \quad (23)$$

$$j\omega\mu H^2 = -\frac{1}{\sqrt{g}} \left\{ \frac{\partial E_1}{\partial u^3} - \frac{\partial E_3}{\partial u^1} \right\} \quad (24)$$

$$j\omega\mu H^3 = -\frac{1}{\sqrt{g}} \left\{ \frac{\partial E_2}{\partial u^1} - \frac{\partial E_1}{\partial u^2} \right\} \quad (25)$$

$$j\omega\epsilon_0\epsilon_r E^1 + \sigma E^1 = \frac{1}{\sqrt{g}} \left\{ \frac{\partial H_3}{\partial u^2} - \frac{\partial H_2}{\partial u^3} \right\} \quad (26)$$

$$j\omega\epsilon_0\epsilon_r E^2 + \sigma E^2 = \frac{1}{\sqrt{g}} \left\{ \frac{\partial H_1}{\partial u^3} - \frac{\partial H_3}{\partial u^1} \right\} \quad (27)$$

$$j\omega\epsilon_0\epsilon_r E^3 + \sigma E^3 = \frac{1}{\sqrt{g}} \left\{ \frac{\partial H_2}{\partial u^1} - \frac{\partial H_1}{\partial u^2} \right\}. \quad (28)$$

A. Efficient Implementation

The efficient implementation of (23) through (28) in the general curvilinear space is now illustrated. It is noted that these equations have a form which images the standard orthogonal FDTD technique. Therefore, the discretization of these equations is accomplished in a similar way. Specifically, a central difference approximation is applied both in space and time to the differential operators embodied in (23) through (28). To enhance the computational efficiency of this method the following substitutions are made

$$\begin{aligned} \vec{h}_i &= H_i \sqrt{\eta_0} \Delta_i \\ \vec{e}_i &= \frac{E_i}{\sqrt{\eta_0}} \Delta_i \end{aligned} \quad (29)$$

so that the update equations are now written as

$$e_{i,j,k}^{1^{n+1}} = a_{i,j,k}^e e_{i,j,k}^{1^n} + b_{i,j,k}^{e1} \left(h_{3i,j,k}^{n+\frac{1}{2}} - h_{3i,j-1,k}^{n+\frac{1}{2}} - h_{2i,j,k}^{n+\frac{1}{2}} + h_{2i,j,k-1}^{n+\frac{1}{2}} \right) \quad (30)$$

$$e_{i,j,k}^{2^{n+1}} = a_{i,j,k}^e e_{m,n,p}^{2^n} + b_{i,j,k}^{e2} \left(h_{1i,j,k}^{n+\frac{1}{2}} - h_{1i,j,k-1}^{n+\frac{1}{2}} - h_{3i,j,k}^{n+\frac{1}{2}} + h_{3i-1,j,k}^{n+\frac{1}{2}} \right) \quad (31)$$

$$e_{i,j,k}^{3^{n+1}} = a_{i,j,k}^e e_{i,j,k}^{3^n} + b_{i,j,k}^{e3} \left(h_{2i,j,k}^{n+\frac{1}{2}} - h_{2i-1,j,k}^{n+\frac{1}{2}} - h_{1i,j,k}^{n+\frac{1}{2}} + h_{1i,j-1,k}^{n+\frac{1}{2}} \right) \quad (32)$$

$$h_{i,j,k}^{1^{n+\frac{1}{2}}} = h_{i,j,k}^{1^{n-\frac{1}{2}}} - b_{i,j,k}^{h1} \left(e_{3i,j+1,k}^n - e_{3i,j,k}^n - e_{2i,j,k+1}^n + e_{2i,j,k}^n \right) \quad (33)$$

$$h_{i,j,k}^{2^{n+\frac{1}{2}}} = h_{i,j,k}^{2^{n-\frac{1}{2}}} - b_{i,j,k}^{h2} \left(e_{1i,j,k+1}^n - e_{1i,j,k}^n - e_{3i+1,j,k}^n + e_{3i,j,k}^n \right) \quad (34)$$

$$h_{i,j,k}^{3^{n+\frac{1}{2}}} = h_{i,j,k}^{3^{n-\frac{1}{2}}} - b_{i,j,k}^{h3} \left(e_{2i+1,j,k}^n - e_{2i,j,k}^n - e_{1i,j+1,k}^n + e_{1i,j,k}^n \right) \quad (35)$$

where

$$a_{i,j,k}^e = \frac{2 - c_0 \Delta_t \sigma \eta_0}{2 + \sigma \eta_0 c_0 \Delta_t} \quad (36)$$

$$b_{i,j,k}^{e1} = \frac{2c_0 \Delta_t \Delta_{u^1}}{(2 + \sigma \eta_0 c_0 \Delta_t) \epsilon_{r_{i,j,k}} \sqrt{g} \Delta_{u^2} \Delta_{u^3}}, \quad b_{i,j,k}^{e2} = \frac{2c_0 \Delta_t \Delta_{u^2}}{(2 + \sigma \eta_0 c_0 \Delta_t) \epsilon_{r_{i,j,k}} \sqrt{g} \Delta_{u^1} \Delta_{u^3}} \quad (37)$$

$$b_{i,j,k}^{e3} = \frac{2c_0 \Delta_t \Delta_{u^3}}{(2 + \sigma \eta_0 c_0 \Delta_t) \epsilon_{r_{i,j,k}} \sqrt{g} \Delta_{u^1} \Delta_{u^2}} \quad (38)$$

$$b_{i,j,k}^{h1} = \frac{c_0 \Delta_t \Delta_{u^1}}{\sqrt{g} \Delta_{u^2} \Delta_{u^3}}, \quad b_{i,j,k}^{h2} = \frac{c_0 \Delta_t \Delta_{u^2}}{\sqrt{g} \Delta_{u^1} \Delta_{u^3}}, \quad b_{i,j,k}^{h3} = \frac{c_0 \Delta_t \Delta_{u^3}}{\sqrt{g} \Delta_{u^1} \Delta_{u^2}}. \quad (39)$$

Each of these coefficients may be precomputed to enhance the computational efficiency of the updates.

The update expressions of (30) through (35) are updated explicitly based on prior computed covariant field values. Since only contravariant fields are known explicitly from the update equations, a set of auxiliary expressions must be introduced which relates the covariant fields to the contravariant fields computed by (30) through (35). This is accomplished through the relation expressed in (12). Equation (12) requires that all three field components be known at the same position in space. However, due to the staggered nature of the grid the computed fields are not collocated. Therefore, to achieve spatial alignment the fields values which share the endpoints of desired covariant field value f_i are averaged to give a second order accurate approximation of the covariant fields. The resultant projections are given by

$$E_{1i,j,k} = g_{11}E_{i,j,k}^1 + \frac{g_{12}}{4}(E_{i,j,k}^2 + E_{i+1,j,k}^2 + E_{i,j-1,k}^2 + E_{i+1,j-1,k}^2) + \frac{g_{13}}{4}(E_{i,j,k}^3 + E_{i+1,j,k}^3 + E_{i,j,k-1}^3 + E_{i+1,j,k-1}^3) \quad (40)$$

$$E_{2i,j,k} = g_{22}E_{i,j,k}^2 + \frac{g_{21}}{4}(E_{i,j,k}^1 + E_{i,j+1,k}^1 + E_{i-1,j,k}^1 + E_{i-1,j+1,k}^1) + \frac{g_{23}}{4}(E_{i,j,k}^3 + E_{i,j+1,k}^3 + E_{i,j,k-1}^3 + E_{i,j+1,k-1}^3) \quad (41)$$

$$E_{3i,j,k} = g_{33}E_{i,j,k}^3 + \frac{g_{31}}{4}(E_{i,j,k}^1 + E_{i-1,j,k}^1 + E_{i,j,k+1}^1 + E_{i-1,j,k+1}^1) + \frac{g_{32}}{4}(E_{i,j,k}^2 + E_{i,j-1,k}^2 + E_{i,j,k+1}^2 + E_{i,j-1,k+1}^2) \quad (42)$$

for the electric field and for the magnetic field

$$H_{1i,j,k} = g_{11}H_{i,j,k}^1 + \frac{g_{12}}{4}(H_{i,j,k}^2 + H_{i-1,j,k}^2 + H_{i,j+1,k}^2 + H_{i-1,j+1,k}^2) + \frac{g_{13}}{4}(H_{i,j,k}^3 + H_{i-1,j,k}^3 + H_{i,j,k+1}^3 + H_{i-1,j,k+1}^3) \quad (43)$$

$$H_{2i,j,k} = g_{22}H_{i,j,k}^2 + \frac{g_{21}}{4}(H_{i,j,k}^1 + H_{i,j-1,k}^1 + H_{i+1,j,k}^1 + H_{i+1,j-1,k}^1) + \frac{g_{23}}{4}(H_{i,j,k}^3 + H_{i,j-1,k}^3 + H_{i,j,k+1}^3 + H_{i,j-1,k+1}^3) \quad (44)$$

$$H_{3i,j,k} = g_{33}H_{i,j,k}^3 + \frac{g_{31}}{4}(H_{i,j,k}^1 + H_{i+1,j,k}^1 + H_{i,j,p-1}^1 + H_{i+1,j,p-1}^1) + \frac{g_{32}}{4}(H_{i,j,k}^2 + H_{i,j+1,k}^2 + H_{i,j,k-1}^2 + H_{i,j+1,k-1}^2). \quad (45)$$

The stability relation for non-orthogonal grids takes a similar form to that for orthogonal grids[5]. It is derived by assuming a plane wave propagation of the form

$$\vec{E}(u^1, u^2, u^3, t) = \vec{E}_0 e^{-j(k_1 u^1 + k_2 u^2 + k_3 u^3)} \quad (46)$$

in the general curvilinear space where

$$k_i = \hat{a}_i \cdot \vec{k}. \quad (47)$$

Subsequently, the wave equation is formulated in the curvilinear space and the growth factor constrained as

$$|\alpha| = \left| \frac{\vec{E}^{n+1}}{\vec{E}^n} \right| \leq 1.0. \quad (48)$$

This leads to a stability relation of

$$\Delta t \leq \frac{1}{c \sqrt{\sum_{j=1}^3 \sum_{i=1}^3 \frac{|g^{i,j}|}{\Delta u^i \Delta u^j}}} \quad (49)$$

for the FDTD in globally curvilinear coordinates. A complete proof is found in [8], [5].

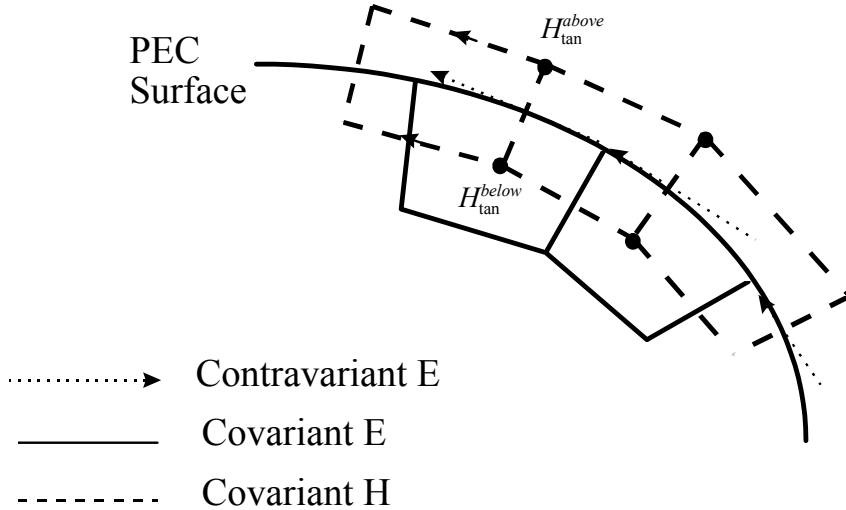


Figure 3 – Orientation of contravariant and covariant E field vectors on a perfectly conducting surface.

B. Boundary Conditions

Physical boundary conditions are present in any problem geometry and are essential for grid termination. These physical boundary conditions include the perfect electric conductor (PEC) and the perfect magnetic conductor (PMC). While these boundaries are easily implemented in an orthogonal space, a bit more consideration is required in the non-orthogonal space. This is due to the fact there are two sets of fields at each boundary which must be terminated: the contravariant and covariant fields. Consider the case of the PEC boundary condition for a curved metal surface in the general curvilinear space. This is illustrated in Figure 3. It is clear from this illustration that the covariant \vec{E} fields which are tangential at the surface must be set to zero as in the orthogonal FDTD case. There is no basis for setting the contravariant fields to zero at the surface, however. In order to update the contravariant electric fields along the surface of the conductor, the covariant magnetic fields which surround the field location must be known. The proper implementation of the PEC boundary condition requires that these fields be defined such that in the limit as the grid becomes orthogonal, the boundary conditions of the conductor are satisfied. A proper update strategy for these fields is accomplished through imaging of the tangential covariant magnetic fields from just above the conductor surface as

$$H_{tan_{below}} = H_{tan_{above}}.$$

The contravariant magnetic field values interior to the conductor are explicitly set to zero. As a result, the only contributing term to the line integral in the update for the contravariant electric field at the surface comes from the covariant magnetic field which passes through the surface of the conductor, which should be the case.

The PMC boundary condition is implemented in an analogous manner to the orthogonal case. For consistency, both the contravariant and covariant field components are imaged.

C. GNFDTD Results

A non-orthogonal general curvilinear space is applicable to a limited set of problems. Two examples of such a space are given by a globally skewed grid and a globally twisted grid. While the globally skewed grid is not of great value, it does serve to demonstrate some of the qualities of a globally nonorthogonal implementation

A globally skewed grid might find application in some waveguide systems. As an illustration of the application of the FDTD technique in a globally skewed grid, a microstrip planar microstrip transmission

line is analyzed. The transmission line consists of conductor of width 2.413 mm placed at a height of 0.795 mm above a perfectly conducting ground plane. The two conductors are separated by a dielectric substrate with a relative permittivity of $\epsilon_r = 2.2$. In order to compare the merits of the orthogonal FDTD and the GNFDTD methods, the problem is analyzed in three different manners: Using orthogonal grids and with the conductor aligned along the x axis, using a globally nonorthogonal grid (GNFDTD) where the y axis is skewed at 45 degrees with respect to the x axis, and using an orthogonal grid with a 45 degree skewed microstrip where stairstepping is used. The formulation of the GNFDTD coordinate system is presented in the following section followed by the three results. For the orthogonal grid analysis a discretization of $\Delta_x = \Delta_y = 0.3447 \text{ mm}$, $\Delta_z = 0.265 \text{ mm}$ was used. The grid is terminated using a uniaxial PML implementation which is documented in [15].

The position vector for a global curvilinear coordinate system which naturally conforms to this geometry is given by

$$\vec{r}(u^1, u^2, u^3) = \hat{x}u^1 + \hat{y}(u^2 + u^1 \tan \theta) + \hat{z}u^3 \quad (50)$$

from which the unitary vectors are given as

$$\begin{aligned} \vec{a}_1 &= \hat{x} + \hat{y} \tan \theta \\ \vec{a}_2 &= \hat{y} \\ \vec{a}_3 &= \hat{z} \end{aligned} \quad (51)$$

where θ is the angle of the skew with respect to the x axis. The g matrix for this grid is independent of position and is given by

$$g_{i,j} = \begin{bmatrix} 1 + \tan^2 \theta & \tan \theta & 0 \\ \tan \theta & 1 & 0 \\ 0 & 0 & 1 \end{bmatrix} \quad (52)$$

and $\sqrt{g} = 1.0$.

The orientation of the skewed microstrip line in the GNFDTD grid which corresponds to (3) is illustrated in Figure 4 while the orthogonal grid which uses stairstepping approximation of the geometry is illustrated in Figure 5.

The bend in the orthogonal grid model is due to the absorbing boundary. For a conductor terminating normally into the PML absorbing boundary the energy is absorbed optimally and negligible reflection error is produced. The termination is much less than ideal for an arbitrary angular termination. For this reason, the microstrip is turned 5 cells before the absorbing boundary such that it enters the boundary orthogonally. A second cost associated with the orthogonal implementation of this geometry occurs because the problem does not naturally align with the rectangular coordinate axes. As a result, the width of the numerical space must be increased linearly as the length of the line increases. This leads to greater computational costs.

In contrast to the orthogonal FDTD grid of Figure 5, the GNFDTD modeled microstrip terminates directly into the end wall boundary. This leads to an excellent impedance match across the frequency band studied. Also, the microstrip line is aligned naturally to the grid so that increasing line length does not increase the transverse dimensions of the problem. The proper design of the absorbing boundary in non-orthogonal coordinates is discussed further in Chapter 4.

The results of the skewed microstrip analysis are demonstrated in Figure 6 for the GNFDTD method and the orthogonal FDTD method. The two results are compared to the non-skewed line to demonstrate the error introduced by the skew. It is observed that at lower frequencies the orthogonal staircasing approximation is slightly more accurate than the GNFDTD. At higher frequencies, however, the dispersion is considerably higher for the orthogonal FDTD solution leading to significant error. This can be attributed to both increased sensitivity to the discontinuities caused by staircasing and the bend which is implemented to achieve better absorbing boundary performance. It should be noted that much worse performance was observed when the microstrip line did not enter the absorbing boundary orthogonally. The computation grid of the orthogonal FDTD was $70 \times 110 \times 20$ while that of the GNFDTD was $70 \times 47 \times 20$. The GNFDTD implementation required roughly twice the computation time of the orthogonal FDTD implementation. It should be noted, however, that the accuracy of the physical representation of the geometry is highly dependent on both the transverse and longitudinal discretization for the orthogonal model of the 45 degree

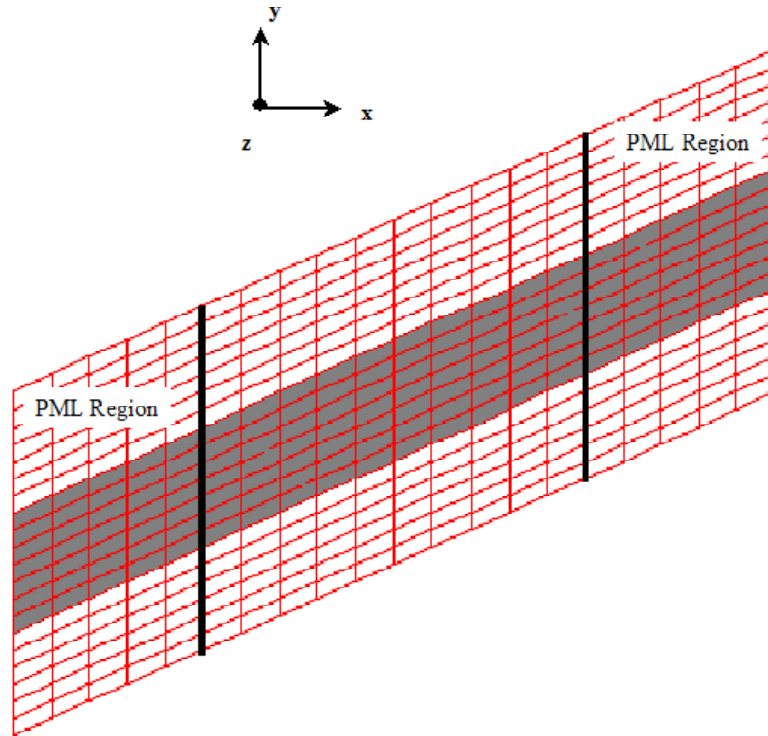


Figure 4 – Overhead view (-Z viewing direction) of a 45 degree skewed microstrip as represented by a globally nonorthogonal skewed grid.

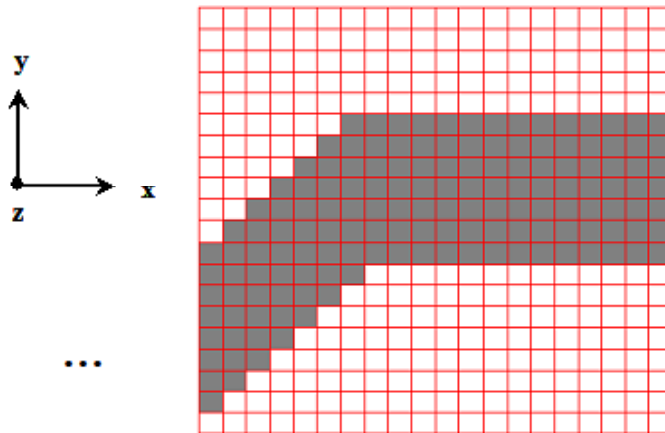


Figure 5 – Illustration of termination region discretization of skewed microstrip transmission line on an orthogonal grid.

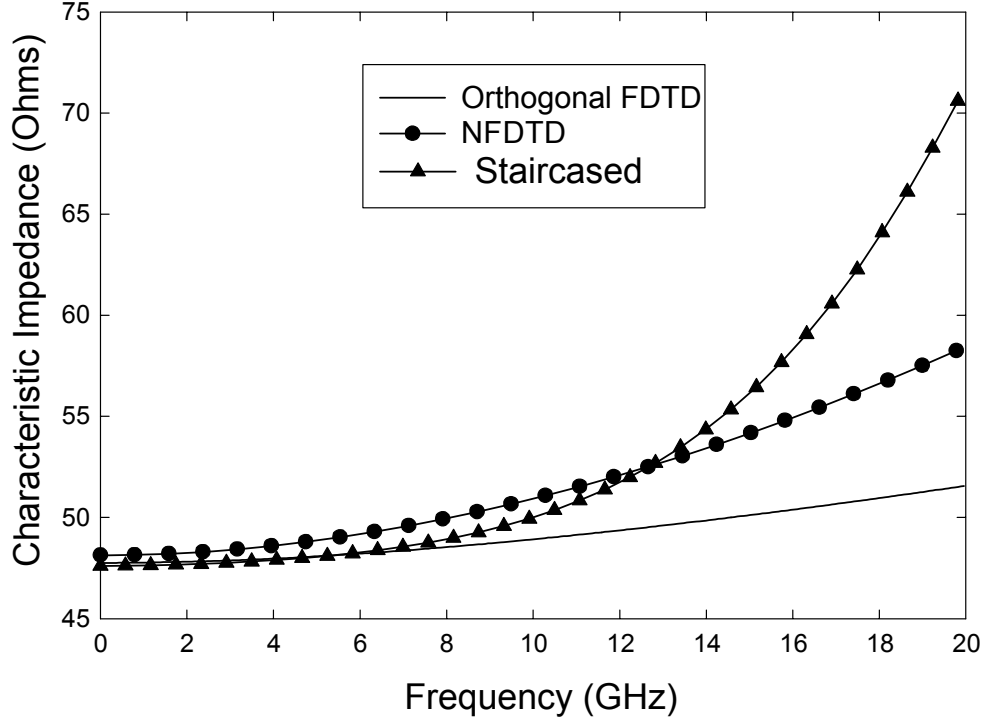


Figure 6 – Analysis of microstrip transmission line with 45 degree skew using orthogonal and non-orthogonal FDTD.

line. For the nonorthogonal implementation, the longitudinal discretization is only driven by the desired frequency range of the simulation, thus a much coarser grid can likely be used.

As a second illustration of the application of a globally non-orthogonal grid in a general curvilinear coordinate system, a twisted pair round wire transmission line is analyzed. The geometry consists of two round wires, whose cross-section is approximated by staircasing here, with a twist applied such that the waveguide undergoes a rotation of approximately 360 degrees over the length of the transmission line. Some clear advantages may be gained by using the proper coordinate system for analyzing complex geometries such as a waveguide or an antenna which have a helical twist. Certainly, accuracy is enhanced by properly conforming to the geometry. Equally important, greater solution efficiency may be achieved by taking advantages of the problem symmetries which are present in the conformal space. Such is the case for a pair of round wires which are twisted along the longitudinal direction (twisted pair line). The application of a twisted global curvilinear coordinate system as described in the following paragraphs allows the modeling of the twisted geometry using the same odd/even symmetric boundaries as were used for the straight wire case. Specifically, PMC and PEC planes are implemented to effectively reduce the problem size to twenty-five percent of the original geometry.

In a twisted coordinate system defined by

$$\vec{r}(u^1, u^2, u^3) = \hat{x}(u^1 \cos \theta - u^2 \sin \theta) + \hat{y}(u^1 \sin \theta + u^2 \cos \theta) + \hat{z}u^3 \quad (53)$$

where $\theta = pz$ and p is the pitch density of the line, the u^1, u^2 coordinate axes rotate by an angle θ as the u^3 dimension is increased. The unitary vectors for this space are given by

$$\begin{aligned} \vec{a}_1 &= \hat{x} \cos \theta + \hat{y} \sin \theta \\ \vec{a}_2 &= -\hat{x} \sin \theta + \hat{y} \cos \theta \\ \vec{a}_{3\Box} &= \Box -\hat{x}p(u^1 \sin \theta + u^2 \cos \theta) + \Box \hat{y}p(u^1 \cos \theta - u^2 \sin \theta) + \hat{z} \end{aligned}$$

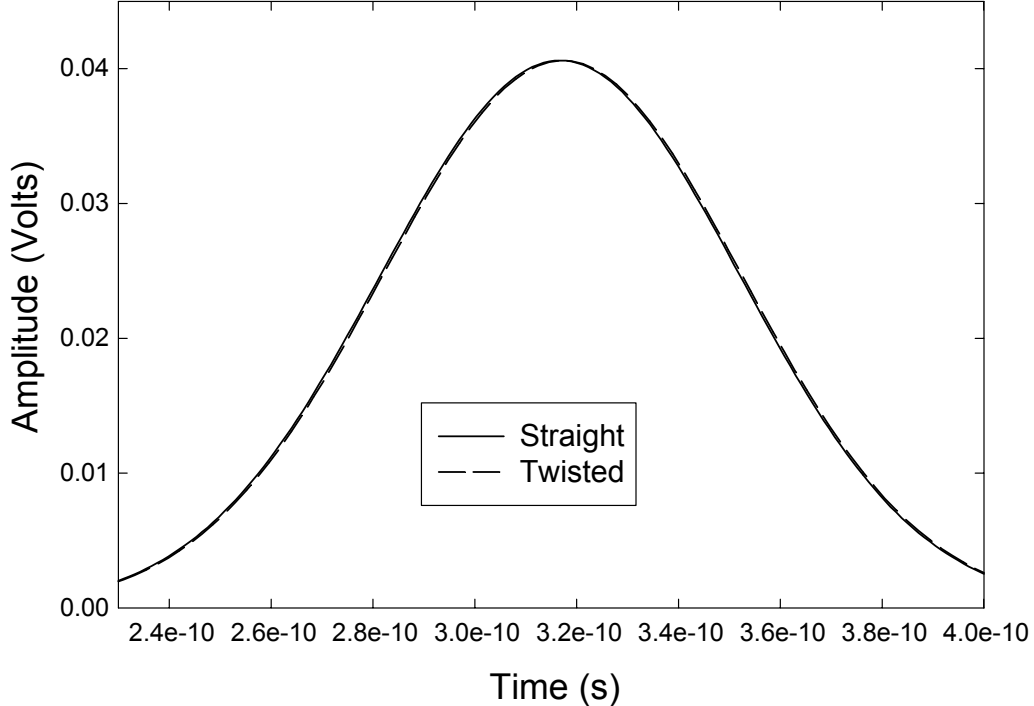


Figure 7 – Time-Domain results of twisted and untwisted transmission line excited by a Gaussian source.

and the metric coefficient matrix is

$$g_{i,j}(u^1, u^2) = \begin{bmatrix} 1 & 0 & -u^2 p \\ 0 & 1 & u^1 p \\ -u^1 p & u^1 p & 1 + p^2 (u^{1^2} + u^{2^2}) \end{bmatrix} \quad (54)$$

where $\theta = pz$ and p is the pitch density in radians/meter, also $\sqrt{g} = 1.0$.

Presently, no analytic expression exists for the impedance of the twisted-pair transmission line studied here. One expects that if the twist is gradual a quasi-TEM mode will be supported and the field pattern will be close to that of the parallel line. Figure 7 compares the time-domain waveform which results from launching a gaussian pulse along the twisted line with $p = 315.0$ r/m. This twist rate is typical of a twisted pair transmission line. The voltage between the two conductors is measured at two points separated by fifty cells. The time-domain results are compared to same geometry but with zero pitch.

These results show that a slight time delay is introduced for the twisted case due to the additional length traversed by the signal as a result of the twist. The length scale factor is given by $l_3 = \sqrt{g_{33}}$ and concurs with the time delay displayed.

IV. THE FDTD TECHNIQUE IN LOCAL CURVILINEAR COORDINATES (NFDTD)

In the previous sections it was demonstrated that for regular geometries where the position vector for a point $P(u^1, u^2, u^3)$ could be analytically defined that general curvilinear coordinate system concepts may be employed and consequently the FDTD method is easily implemented. For many practical problems such as the round wire geometry, such a global coordinate system is not applicable. In cases such as this, general curvilinear coordinate system concepts may be introduced on a local basis [5], [3].

To this end, a structured grid is first designed to conform to the problem geometry, typically using a CAD package or similar. This grid may be chosen to align with either the electric field or magnetic field components depending on where the boundary conditions of the physical geometry are to be enforced. For

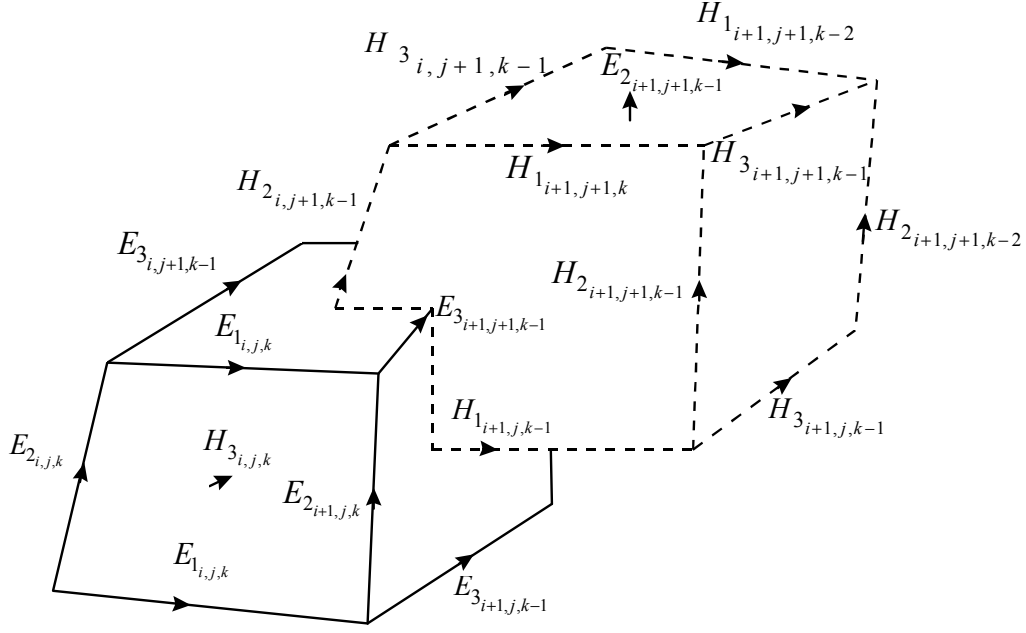


Figure 8 – Primary/Dual grid configuration for irregular grids.

this work, a primary grid is generated using a computer code such that the grid conforms to boundaries where the electrical properties may be described. A secondary grid is then generated by connecting the barycenters of the primary grid for cells which share a common face. Such a grid is illustrated in Figure 8. For a geometry which is described by an irregular grid such as Figure 8 the covariant vectors are directly defined by the grid edges of the secondary and primary grid, for example

$$\vec{A}_1 = \hat{x} (u_a^1 - u_b^1) + \hat{y} (u_a^2 - u_b^2) + \hat{z} (u_a^3 - u_b^3) \quad (55)$$

where the two points a and b are the endpoints of the edge which defines \vec{A}_1 . Each covariant vector is therefore scaled by edge length and is a linear line segment. These covariant vectors constitute the unitary vectors of the general curvilinear coordinate system. Both the NFDTD and the GNFDTD method are based on curvilinear coordinate concepts. Therefore, the identities given in (3) through (16) are still applicable. The two methods differ in manner in which the curvilinear coordinate system constructs are defined. Specifically, in the NFDTD method, the vectors about each cell face define a unique local curvilinear coordinate system. The formulation of the NFDTD method is demonstrated in the following sections.

In an irregular non-orthogonal space, Maxwell's equations are most naturally applied in their integral form. To this end, the integral form of Maxwell's equations are applied at each cell face of both the secondary and primary grid. The integral form of Maxwell's equations are given by

$$\int \int \frac{\partial \mu \vec{H}}{\partial t} \cdot d\hat{s} = - \oint_C \vec{E} \cdot d\vec{l} \quad (56)$$

$$\int \int \left(\frac{\partial \epsilon \vec{E}}{\partial t} + \sigma \vec{E} \right) \cdot d\hat{s} = \oint_C \vec{H} \cdot d\vec{l} \quad (57)$$

The field components of the line integral on the right hand side are naturally written in terms of the covariant fields of the general curvilinear space since these field components flow around each cell face and are scaled by the length of their respective edges. The contravariant field values have a vector direction which is normal to each cell face and therefore are the natural choice for the left hand sides of (56) and (57). Each

curvilinear component of these equations is extracted by taking the dot product of each side with the unit vector \widehat{A}^i . In the discretized general curvilinear space the surface integral on the left hand side of (57) is then approximated for each face as

$$\begin{aligned} \int \int \frac{\partial \mu \vec{F}}{\partial t} \cdot d\widehat{s}_i &= \frac{\partial \mu F^i}{\partial t \left| \vec{A}^i \right|} ds_i \\ &= \frac{\partial \mu F^i}{\partial t} V \end{aligned} \quad (58)$$

where V is the volume of the local coordinate system and is given by

$$V = \vec{A}_i \cdot \left(\vec{A}_{(i+1) \bmod 3} \times \vec{A}_{(i+2) \bmod 3} \right).$$

The six update equations for both the electric and magnetic field may now be written directly in the discrete space as

$$E_{i,j,k}^{1^{n+1}} = a_{i,j,k}^e E_{i,j,k}^{1^n} + b_{i,j,k}^{e1} \left(H_{3i,j,k}^{n+\frac{1}{2}} - H_{3i,j-1,k}^{n+\frac{1}{2}} - H_{2i,j,k}^{n+\frac{1}{2}} + H_{2i,j,k-1}^{n+\frac{1}{2}} \right) \quad (59)$$

$$E_{i,j,k}^{2^{n+1}} = a_{i,j,k}^e E_{m,n,p}^{2^n} + b_{i,j,k}^{e2} \left(H_{1i,j,k}^{n+\frac{1}{2}} - H_{1i,j,k-1}^{n+\frac{1}{2}} - H_{3i,j,k}^{n+\frac{1}{2}} + H_{3i-1,j,k}^{n+\frac{1}{2}} \right) \quad (60)$$

$$E_{i,j,k}^{3^{n+1}} = a_{i,j,k}^e E_{i,j,k}^{3^n} + b_{i,j,k}^{e3} \left(H_{2i,j,k}^{n+\frac{1}{2}} - H_{2i-1,j,k}^{n+\frac{1}{2}} - H_{1i,j,k}^{n+\frac{1}{2}} + H_{1i,j-1,k}^{n+\frac{1}{2}} \right) \quad (61)$$

$$H_{i,j,k}^{1^{n+\frac{1}{2}}} = H_{i,j,k}^{1^{n-\frac{1}{2}}} - b_{i,j,k}^{h1} \left(E_{3i,j+1,k}^n - E_{3m,n,p}^n - E_{2i,j,k+1}^n + E_{2i,j,k}^n \right) \quad (62)$$

$$H_{i,j,k}^{2^{n+\frac{1}{2}}} = H_{i,j,k}^{2^{n-\frac{1}{2}}} - b_{i,j,k}^{h2} \left(E_{1i,j,k+1}^n - E_{1m,n,p}^n - E_{3i+1,j,k}^n + E_{3i,j,k}^n \right) \quad (63)$$

$$H_{i,j,k}^{3^{n+\frac{1}{2}}} = H_{i,j,k}^{3^{n-\frac{1}{2}}} - b_{i,j,k}^{h3} \left(E_{2i+1,j,k}^n - E_{2i,j,k}^n - E_{1i,j+1,k}^n + E_{1i,j,k}^n \right) \quad (64)$$

where

$$a_{i,j,k}^e = \frac{2 - \Delta_t \sigma}{2 + \sigma \Delta_t} \quad (65)$$

$$b_{i,j,k}^{e1} = \frac{2\Delta_t}{(2 + \sigma \Delta_t) \epsilon_0 \epsilon_{r_{i,j,k}} V_{i,j,k_e}^1}, \quad b_{i,j,k}^{e2} = \frac{2\Delta_t}{(2 + \sigma \Delta_t) \epsilon_0 \epsilon_{r_{i,j,k}} V_{i,j,k_e}^2} \quad (66)$$

$$b_{i,j,k}^{e3} = \frac{2\Delta_t \Delta_u^3}{(2 + \sigma \Delta_t) \epsilon_0 \epsilon_{r_{i,j,k}} V_{i,j,k_e}^3} \quad (67)$$

$$b_{i,j,k}^{h1} = \frac{\Delta_t}{\mu_0 V_{i,j,k_h}^1}, \quad b_{i,j,k}^{h2} = \frac{\Delta_t}{\mu_0 V_{i,j,k_h}^2}, \quad b_{i,j,k}^{h3} = \frac{\Delta_t}{\mu_0 V_{i,j,k_h}^3} \quad (68)$$

and

$$V_{i,j,k_e}^1 = \frac{\vec{A}_{1i,j,k}^e \cdot \left(\left(\vec{A}_{2i,j,k}^h + \vec{A}_{2i,j,k-1}^h \right) \times \left(\vec{A}_{3i,j,k}^h + \vec{A}_{3i,j-1,k}^h \right) \right)}{4} \quad (69)$$

$$V_{i,j,k_h}^1 = \frac{\vec{A}_{1i,j,k}^h \cdot \left(\left(\vec{A}_{2i,j,k}^e + \vec{A}_{2i,j,k+1}^e \right) \times \left(\vec{A}_{3i,j,k}^e + \vec{A}_{3i,j+1,k}^e \right) \right)}{4}$$

$$V_{i,j,k_e}^2 = \frac{\vec{A}_{2i,j,k}^e \cdot \left(\left(\vec{A}_{3i,j,k}^h + \vec{A}_{3i-1,j,k}^h \right) \times \left(\vec{A}_{1i,j,k}^h + \vec{A}_{1i,j,k-1}^h \right) \right)}{4} \quad (70)$$

$$V_{i,j,k_h}^2 = \frac{\vec{A}_{2i,j,k}^h \cdot \left(\left(\vec{A}_{3i,j,k}^e + \vec{A}_{3i+1,j,k}^e \right) \times \left(\vec{A}_{1i,j,k}^e + \vec{A}_{1i,j,k+1}^e \right) \right)}{4} \quad (71)$$

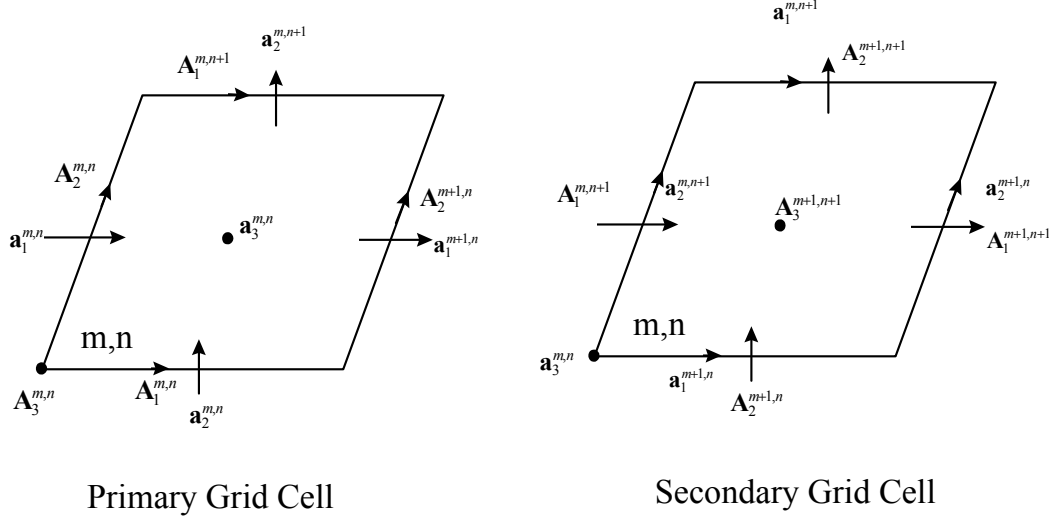


Figure 9 – Vector relations for a primary and secondary grid face.

$$V_{i,j,k_e}^3 = \frac{\vec{A}_{3i,j,k}^e \cdot \left((\vec{A}_{1i,j,k}^h + \vec{A}_{1i,j-1,k}^h) \times (\vec{A}_{2i,j,k}^h + \vec{A}_{2i-1,j,k}^h) \right)}{4} \quad (72)$$

$$V_{i,j,k_h}^3 = \frac{\vec{A}_{3i,j,k}^h \cdot \left((\vec{A}_{1i,j,k}^e + \vec{A}_{1i,j+1,k}^e) \times (\vec{A}_{2i,j,k}^e + \vec{A}_{2i+1,j,k}^e) \right)}{4}. \quad (73)$$

Here the computed contravariant field values are normalized by *length* and the covariant field values are scaled by *length*. Figure 9 illustrates the indexing structure for the dual grid for primary grid vectors \vec{A}_i and secondary grid vectors \vec{a}_i . Note that all variables denoted by a superscript(subscript) of h pertain to secondary grid field quantities while those with an e pertain to the primary grid.

The contravariant field updates of (59) through (64) are executed in a time-marching manner with each field value on the right-hand-side known, albeit indirectly, from previous computations. For non-orthogonal grids, the contravariant vectors and the covariant vectors are not aligned. Therefore, these contravariant field values must be projected onto each covariant edge using the relation

$$f_i = \sum_{j=1}^3 g_{i,j} f^j \quad (74)$$

to render the field values which are required on the right hand side of the field updates. For a regular grid each of the terms in (74) are unambiguously defined.

If an irregular grid is used the correct choice of the unitary vectors which define each $g_{i,j}$ is somewhat ambiguous. Both field and vectorial averaging must be applied to accomplish (74). This leads to error as each component f^i which contributes to (74) is computed from a unique local coordinate system defined by the face through which the field component f^i passes.

There are several reasonable manners by which each $g_{i,j}$ may be constructed. In general these are defined by

$$g_{i,j} = \vec{A}_i \cdot \vec{A}_j \quad (75)$$

where the \vec{A}_i is the vector along which the desired covariant field F_i is located and ideally \vec{A}_j is one of the remaining two covariant vectors of the local coordinate system to which \vec{A}_i belongs and it belongs to the

local coordinate system to which F^j belongs. Clearly the second vector can not be uniquely chosen for a staggered grid where no vector triple is collocated. The vector integrity of one of the two coordinate systems in an individual component projection may be respected, but not both.

The first approach investigated respects the vector integrity of local coordinate system of the face to which the field value F_i belongs. To accomplish this, the vectors $\vec{A}_{j=(i+1) \bmod 3}$, $\vec{A}_{j=(i+2) \bmod 3}$ are chosen from the local face through which F_i passes. Note that these vectors are defined by the *dual* grid from that of \vec{A}_i . These vectors are defined from the average value of each of the opposing sets of edges which define the face penetrated by edge i . The self term of the projection is defined by $\vec{A}_{j=i} = \vec{A}_i$. In this manner, a unique set of $g_{i,j}$ exist for each edge in both the secondary and primary grids. This projection method is referred to as G^{avg} .

The second approach favors the integrity of the coordinate system to which the projected field value F^j and corresponding unitary vector \vec{A}_j belongs. For this method \vec{A}_j is defined by the edge vector which is spatially aligned with F^j and in the *same* grid. This projection method requires a separate projection for each of the four components which contribute to F_i and thus is more computationally expensive than the G^{avg} approach. This method is referred to as the G^4 approach.

A final technique recognizes that the vector length of the second term of the projections of G^{avg} could be inconsistent with that of the projected field F^j . To correct this, the projection technique of G^{avg} is applied with length normalization and scaling in an attempt to minimize error. Again four separate projections are required for this technique. This projection technique is referred to as G^{scaled} .

Mathematically, the projections G^{avg} and G^{scaled} require a projection of the form

$$f_i = g_{i,i}f^i + \sum_{j=i+1}^{(i+2) \bmod 3} \sum_{m=1}^4 g_{i,j}f^j \quad (76)$$

where each field value for $i \neq j$ are one of the four averaged field components in (40) through (45).

A global stability criterion can not be formulated for this method due to the irregularness of the grid. A stability relation may be formulated on a cell by cell basis however using the curvilinear coordinate system composed of the unitary vectors of each face. Using a similar method as was described in the previous section, the stability is given as

$$\Delta_t \leq \frac{1}{c \sup \sqrt{\sum_{j=1}^3 \sum_{i=1}^3 |g^{i,j}|}} \quad (77)$$

where the sup operator denotes the maximum value throughout the entire space on both the primary and secondary grids.

A. NFDTD Results

The round wire transmission line is a challenging geometry for studying the effects of proper contour modeling[16]. This geometry is studied here with an irregular grid applied to the wire cross-section. The discretization is illustrated in Figure 10. In this illustration a PMC is placed at the center of the two wires to utilize even symmetry which exists, while a PEC plane is placed between the two wires to capitalize on the odd symmetry of this dimension. The geometry is 70 cells in the longitudinal direction with a discretization of $\Delta_{u_3} = 0.5 \text{ mm}$. The geometry is terminated with a 10 cell PML absorbing boundary at the $+u_1$, $+u_2$, and $\pm u_3$ extents. The convergence characteristics of the characteristic impedance are studied to determine the effectiveness of the NFDTD. It is noted that the grid is gradually transitioned to an orthogonal grid toward the outer extents of the grid. This allows for a more simplistic and accurate implementation of the absorbing boundary. Care should be taken to accomplish the tapering slowly as to prevent grid size relate discontinuities. As a good practice, one should attempt to keep all element sizes on the same order in each dimension. Large cell size changes can lead to local first order error. For each discretization chosen the distance to the side-wall absorbing boundaries is kept constant. The radius of each wire is $a = 0.25 \text{ mm}$ and the distance between the two wires is $d = 0.9 \text{ mm}$.

The results of this study are illustrated in Figures 11 through 13. It is clear from these illustrations that the projection method denoted as G^{avg} is slightly more accurate for this geometry than the other methods

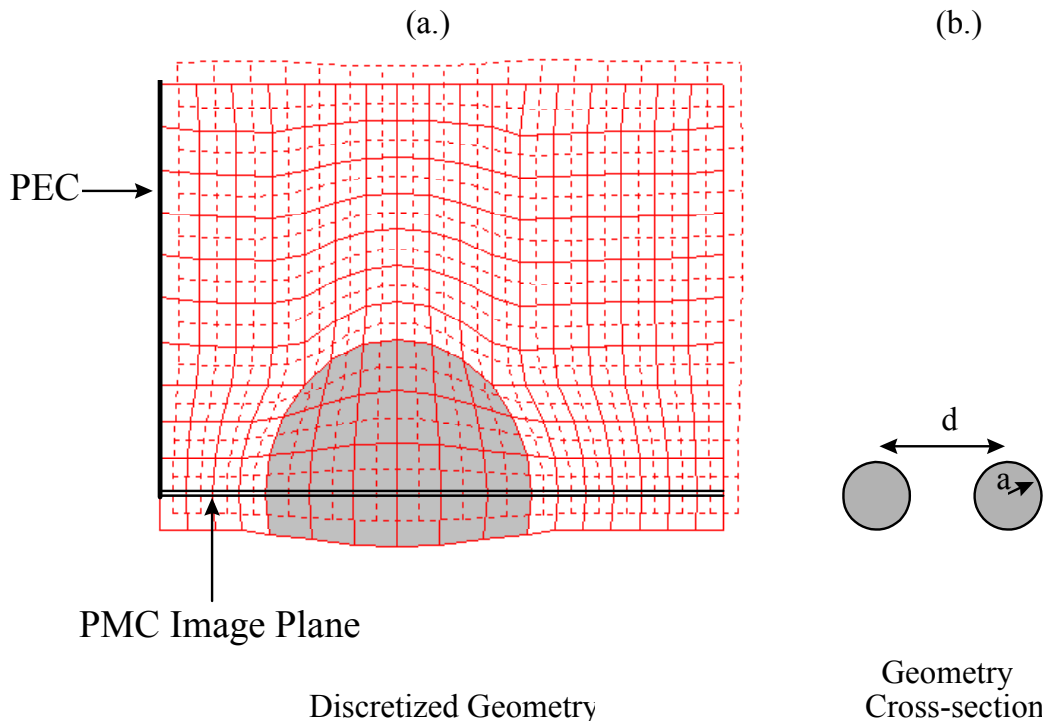


Figure 10 – Illustration of the discretization of one quadrant a round wire transmission line including secondary and primary grids. PEC and PMC planes are introduced to reflect odd and even symmetry about the x and y planes respectively.

implemented. For either of these projection methods, the results are much more accurate than is achievable using the orthogonal FDTD and as many as *forty* cells across the conductor.

V. LATE-TIME INSTABILITY

It has been demonstrated by Gedney, Roden[17] that the stability relations given in 49, 77 are necessary yet not sufficient conditions for stability within non-orthogonal FDTD methods. For most problems, these constraints on the time step are sufficient such that over the period of time required to obtain necessary simulation data no instability is encountered. In the extreme late-time, however, instabilities can occur with *any* of the projection methods illustrated in this text as well as those which define the GenYee family of non-orthogonal methods. While the details will not be repeated here, the basic finding was that the update matrix formed by the curl operator combined with the projection operations must be symmetric in order for the system to possess long term stability. In other words we must have that $G_{ij} = G_{ji}$. Since the G^4 method accomplishes this symmetry, it is the most stable of all the projection methods demonstrated in this work. In addition to symmetry, the quality of the quality of the grid also impacts late-time stability. The grid characteristic which tends to cause instability is the degree of nonorthogonality present at each vertices. Specifically, if the angles between adjoining vectors are very small (less than 45 degrees) or very large (greater than 135 degrees) late-time stability can occur. As a result, the associated vectors are not sufficiently orthogonal to render an independent basis. For structured grids such as those in the NFDTD or GNFDTD methods, poor quality grids are very common. It has been found that a much more robust set of edge vectors may be generated using unstructured grids. Therefore, methods such as GenYee can render a more stable solution method. This issue is the subject of further research.

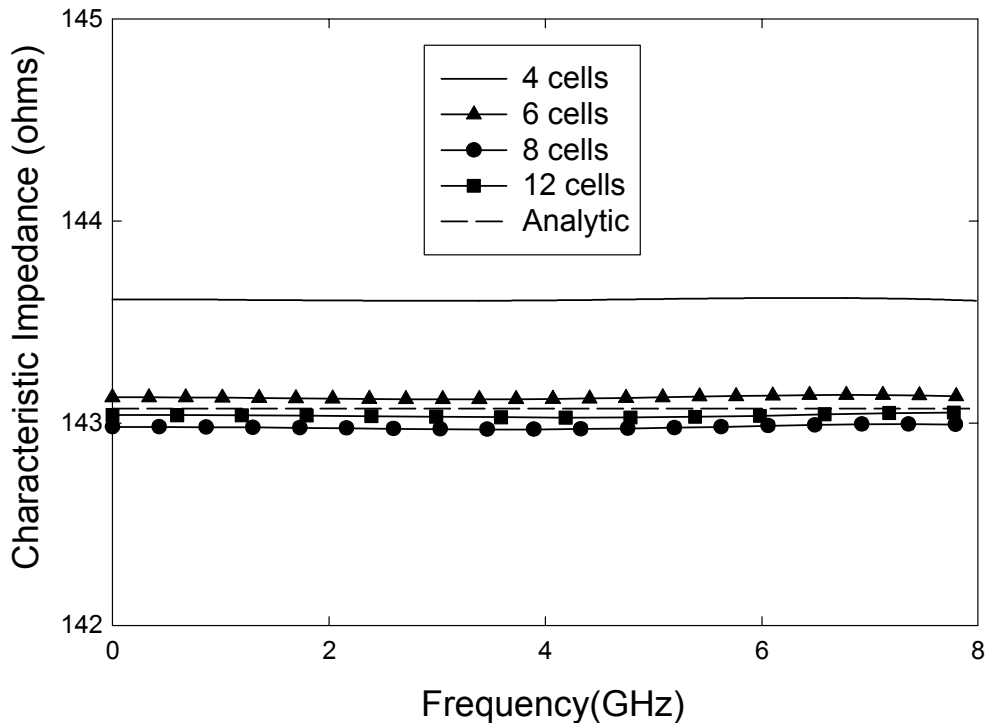


Figure 11 – Convergence of characteristic impedance of a round wire transmission line for the G^{avg} projection method.

VI. CONCLUSION

The non-orthogonal FDTD method provides a robust solution to full wave electromagnetic analysis in the presence of oblique or curved geometries. Two methods were examined for the analysis of complex geometries with curved boundaries. The GNFDTD method is applicable for geometries where curvature exists throughout the grid. It is accomplished by defining a global curvilinear coordinate system which conforms to the geometry and then solving Maxwell's equation in general curvilinear coordinates. The method can provide more accuracy than the orthogonal FDTD method as well as lower numerical dispersion. This method requires about three times the computations of the orthogonal FDTD method. For some problems, accurate gridding of a structure using the orthogonal FDTD technique may not be feasible and therefore the added computational burden of the GNFDTD method is acceptable.

The NFDTD is a more general approach to modeling irregular geometries. To accomplish this method, general curvilinear coordinate systems are introduced for each cell face in the grid and projections are constructed on a local basis. This method proved very robust in the analysis of round wire transmission lines. Late time instabilities were observed which could limit the application of this method for some highly resonant problems. It was found that a simple projection scheme using averaged projection values provided the most accurate solution. The most stable solution, however, was rendered by using a slightly less accurate approach which computed projections separately for each of the four fields projected. The additional cost of this projection method can certainly be justified for some problem sets.

REFERENCES

- [1] K. S. Yee, "Numerical Solution of Initial Boundary Value Problems Involving Maxwell's Equations in

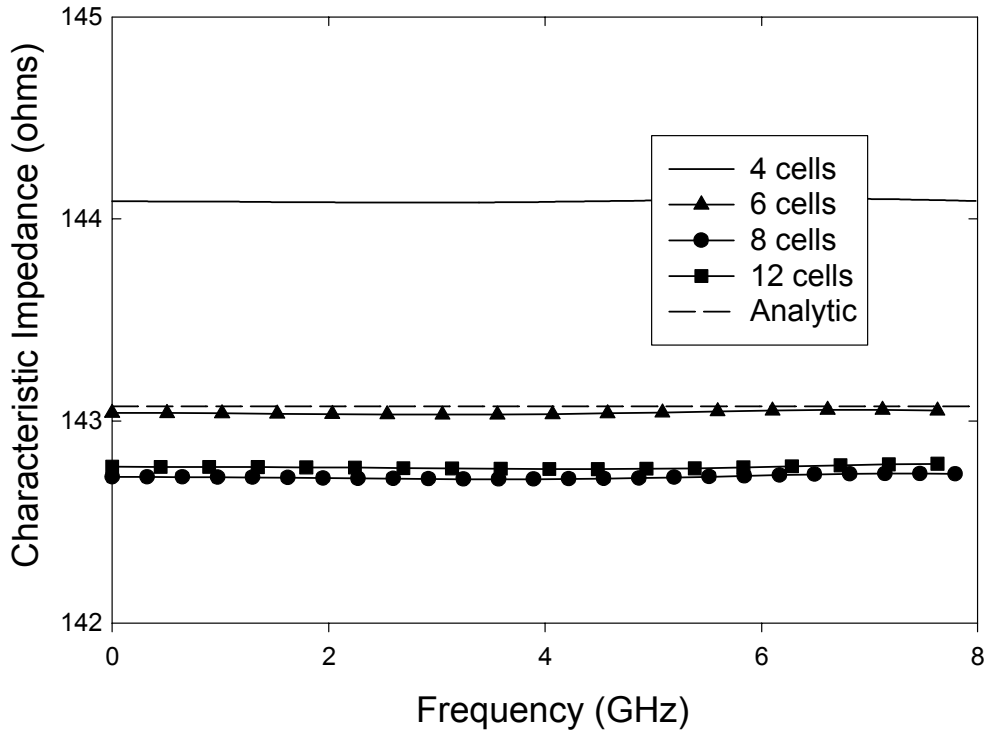


Figure 12 – Convergence of characteristic impedance of a round wire transmission line for the G^4 projection method.

Isotropic Media”, *IEEE Trans. Antennas and Propagation*, vol. AP-14, no. 5, pp. 302-307, May 1966.

[2] J. A. Stratton, *Electromagnetic Theory*, New York, McGraw-Hill, 1941, pp. 38-47.

[3] R. Holland, “Finite-Difference Solution of Maxwell’s Equations in Generalized Non-orthogonal Coordinates”, *IEEE Trans. on Nuclear Science*, vol. NS-30, No. 6, December 1983.

[4] M. Fusco, “FDTD Algorithm in Curvilinear Coordinates”, *IEEE Trans. on Antennas and Propagation*, vol. 38, no. 1, pp. 302-307, January 1990.

[5] J.-F. Lee, “Modeling Three-Dimensional Discontinuities in Waveguides Using Non-orthogonal FDTD Algorithm”, *IEEE Transactions on Microwave Theory and Techniques*, vol. 40, no. 2, Feb. 1992.

[6] N. Madsen and R. Ziolkowski, “Divergence preserving discrete surface integral methods for Maxwell’s equations using nonorthogonal unstructured grids”, *Journal of Computational Physics*, vol. 119, no. 1, p. 34-35, January, 1995.

[7] S. D. Gedney and F. Lansing, “Full wave analysis of printed microstrip devices using a generalized-Yee algorithm”, 1993 IEEE Symposium on Antennas and Propagation Proceedings, Ann Arbor, MI, June 27-July 2, 1993.

[8] A. Taflov, *Computational Electrodynamics: The Finite Difference Time Domain Method*, Boston, Artech House, 1995.

[9] C. Railton, “Stabilised CPFDTD algorithm for the analysis of arbitrary 3D PEC structures”, *IEE Proceedings - Microwaves, Antennas and Propagation*, vol.143, no.5, p. 367-72.

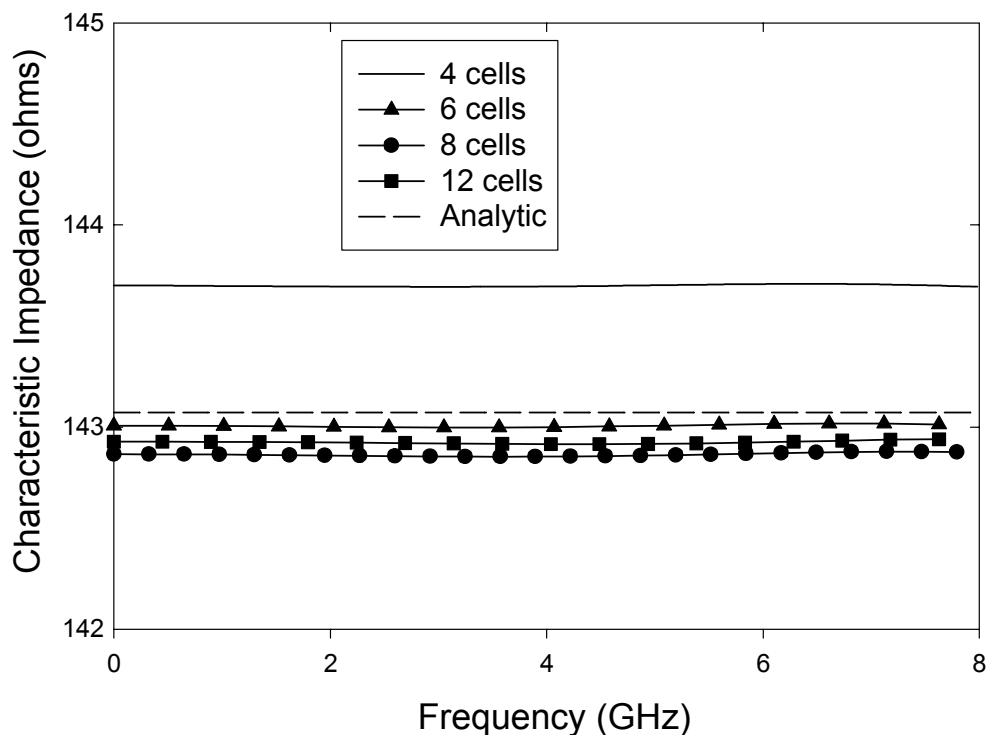


Figure 13 – Convergence of the characteristic impedance of a round wire transmission line using the G^{scale} projection method.

- [10] Wenhua Yu, Raj Mittra, "Accurate modelling of planar microwave circuits using conformal FDTD algorithm", *Electronics Letters*, March, 2000.
- [11] Jiayuan Fang and Danwei Xeu, "Numerical Errors in the Computation of Impedances by FDTD Method and Ways to Eliminate Them", *IEEE Microwave and Guided Letters*, vol. 5., No. 1 Jan. 1995.
- [12] E.A. Navarro, C. Wu, P.Y. Chung and J. Litva, "Application of PML Superabsorbing Boundary Condition to Non-orthogonal FDTD Method", *Electronic Letters*, vol. 30, no.20, p. 1654-1656, 1994.
- [13] J. W. Gibbs, *Vector Analysis*, Yale University Press, New Haven, Conn, 1941.
- [14] S. Ramo, J. R. Whinnery, T. V. Duzer, *Fields and Waves in Communications Electronics*, Second Edition, p 252, John Wiley and Sons, New York. 1965.
- [15] J. A. Roden, S. D. Gedney, "Efficient Implementation of the Uniaxial Based PML Media in Three-Dimensional Non-orthogonal Coordinates Using the FDTD Technique", in press *Microwave and Optical Tech. Let.* February 26, 1997.
- [16] J. Alan Roden, *Broadband Electromagnetic Analysis of Complex Structures using the FDTD Technique in General Curvilinear Coordinates*, Ph.D. Dissertation, University of Kentucky, June, 1997.
- [17] S.D. Gedney, J. A. Roden, "Numerical Stability of Nonorthogonal FDTD Methods", *IEEE Trans. on Antennas and Propagation*, vol 8, no 2, February, 2000.

Computational Electromagnetics and EMC

-- What's Next?

Colin E. Brench
Hewlett-Packard Company
200 Forest St, Marlborough MA 01752
colin.brench@hp.com

As I type this up I must admit to suffering from PC envy. My wife has a new laptop that incorporates a faster CPU and more and faster memory than mine. Over the years my CEM engine has migrated from a cluster of specially build VAX systems in the corner of my office through large servers and now primarily resides with my PC desktop. My laptop that was completely adequate for my needs a few months ago now seems a bit slow, though this is offset by being light in weight, which I do appreciate for traveling.

As computers became more capable I always assumed that the problems I would tackle would expand and always challenge the available resources. This really has not happened; I find myself running models and still have unused RAM. Similarly, the time I have to wait for results does not seem to be too long. Not only have computers improved but the efficiency of the tools I use have improved. So why is EMC modeling still such a difficult problem? – there are no more excuses about insufficient compute power or inadequate tools.

The challenge faced by EMC engineers is largely one due to the stray and parasitic nature of EMC issues. Recent discussions concerning losses on high data rate lines raised the issue of loss through radiation and how much impact it had to the numbers. Looking at the issue from a signal integrity engineer's viewpoint, losses attenuate the wanted signal and contribute to data errors; so all sources of loss are to some extent important. After a rather quick analysis with NEC it became clear that the loss due to radiation was 20dB or more less than other losses in the path. Microwatts rather than milliwatts, this fact put the issue of radiation loss out of view for the mainstream designer engineers. However, these losses are far from insignificant to the EMC engineer where a microwatt or so in the wrong place will cause major headaches.

Consider the EMC problem where high data rate signals are sent from one printed circuit card to another. For the signal integrity engineer there are copper and dielectric losses, discontinuities where signals transition from the source device to etch, from etch to connector back to etch, and then to the final termination. For the EMC engineer the picture may include many more elements. The source device alone may exhibit small loops that can radiate, it may couple to a heat sink or heat spreader on the package, and if not adequately decoupled or vias incorrectly positioned, there may be unwanted currents in the vicinity of the device. Each discontinuity adds a little extra uncertainty into the way the structure could radiate. A final issue that can be missed is the effect of positioning these two boards close to any other conductors. A small loop or plate on the source device might be a terrible antenna but, when placed in close

proximity to the side of an enclosure or the backside of another printed circuit board, radiation may be greatly enhanced. The EMC engineer has a very complex problem that is difficult even to define.

The nature of the EMC problem often means solving the same general source structure a number of times each under different conditions. This often results in numerous, practically identical runs. Now, the computers don't mind this and as stated earlier they are getting faster. The basic fact is that 90% or more of the solution is identical each time – perhaps there is a place for EM modeling tools that allow for elements to be added or moved within the simulation in an intelligent manner such that only the segments that need to change do so. There are more cases like this than might be first thought, interactions between antennas on masts are important studies. Today, with the prevalence of cell phones and many other wireless devices, coupling issues become highly complex. Distance, polarization, and radiation patterns can change moment by moment with other key factors staying constant. These problems are quite different from those faced even ten years ago.

CEM has come a long way; computer technology has developed but also the world has become far more complex. One of the next challenges faced in the continuing creation of better techniques and algorithms may well be an entirely different approach to solving EM problems. An approach that is more general rather than specific, one that looks at the sensitivity of the elements within a structure to external influence as well as those internal to the primary structure – these might be the new techniques of tomorrow. I have some unused RAM and extra CPU cycles, so am ready and anticipating the next innovations.

Important announcement Concerning Security and Access to the Naval Postgraduate School

No access to the Naval Postgraduate School, "NPS" the ACES conference site, will be permitted unless a pre-registration is submitted and confirmed by ACES executive officer, Dr. Dick Adler. If you are planning to attend you should register on-line ASAP and no later than Wednesday March 13, 2003. All pre-registered persons will be included on the access list IF the additional information shown below is added to the registration form or is submitted by some other method.

All persons MUST carry a picture ID (Passport or Drivers License, etc.) and the name on the ID MUST match the name on the access list. Be sure to list all names exactly as they appear on the picture ID and include the name of the agency (company, university, private consultant, etc.) that you represent when you make the request for access.

On-site registration is possible, but will not be allowed unless you get permission from the ACES executive officer to gain access to the guarded gates of NPS. The last date for requesting for permission for the full week of March 23-28 is Thursday March 13, 2003 at 1400 PST (2200 GMT/UTC).

Short Courses will be offered on Thursday Afternoon (27th) and All-Day Friday (28th)

Wives/friends who are attending any of ACES activities with their husbands/friends, will also need to submit their names to be on the list to be permitted to enter.

ACES 2003 Program

The 19th Annual Review of Progress in Applied Computational Electromagnetics Naval Post Graduate School March 24-28, 2003

Symposium Chair: Atef Elsherbeni, Symposium Administrator: Richard Adler,
Short Course Chair: Bruce Archambeault, Exhibits Chair: Andrew Drozd, Publicity Chair: Keith
Lysiak,
Administrative Assistant: Mattiew Inman, Conference Secretaries: Anthea Wilson

Sunday

Room: SP 101A

2:00-6:30 Conference Registration

Monday

Room: SP 101A

8:00-4:30 Conference Registration

Room : GL, Courtyard

7:30-7:55 Continental Breakfast

Room : GL 102

7:55-8:05 ACES Business Meeting Osama Mohamed, ACES President

8:05-8:15 Welcome Atef Elsherbeni, Conference Chair

8:15-10:15 Panel Session – 1

"Challenges in Advanced Mixed-Signal Circuit Simulation and Design"

8:15-8:20 **Introduction:**

Dr. John Rockway, Space and Naval Warfare Systems Command

Speakers:

8:20-8:35 **"CAD Strategies for Advanced Mixed-Signal System and Circuit Design"**

Dr. Peter Petre, HRL Laboratories, Malibu, CA

8:35-8:50 **"Fast Electromagnetic Simulation Techniques Applicable for Mixed-Signal Circuits"**

Prof. Stephen Gedney, University of Kentucky, Lexington, KY

8:50-9:05 **"Advanced Reduced Order Modeling Techniques"**

Prof. Madhavan Swaminathan, Georgia Institute of Technology, Atlanta, GA

9:05-9:20 **"Fast Parasitic Extraction Methods"**

Prof. Jacob White, MIT, Cambridge, MA

9:20-9:35 **"Fast Broadband Electromagnetic-Circuit Solvers for RF and Parasitic Simulation of Systems on Chip"**

Prof. Vikram Jandhyala, University of Washington, Seattle, WA

9:35-9:50 **"Electromagnetically Accurate Modeling of On-Chip Interconnects & Integrated Passives"**
Prof. Andreas Cangellaris, University of Illinois, Urbana, IL

9:50-10:15 Discussion

10:15-10:30 Break (Refreshments at GL, Courtyard)

10:30-12:30 Panel Session – 2

10:30- 10:40 **"Ship Propulsion System Utilizing Superconducting Components"**
Dr. Swarn S. Kalsi, American Superconductor Corporation

10:40-11:00 **"Ship Electrical System Architecture"**
Dr. Swarn S. Kalsi, American Superconductor Corporation

11:00-11:20 **"Superconducting motors and generators for ship propulsion"**
Dr. Bruce Gamble, American Superconductor Corporation

11:20-11:40 **"Transient Modeling of Magnetoelastic Problems in Electric Machinery"**
Prof. Osama Mohammed, Florida International University,
Mr. T.E. Calvert, ONR-Arlington, VA
Mr. L. Peterson, ONR-Arlington, VA
Mr. R. McConnell, NSWCCD-Philadelphia, PA

11:40-12:00 **"Dynamical Nature of Shipboard Electric Power Systems"**
Prof. John V. Amy Jr., MIT

12:00-12:20 **"CAPS Simulation as a Tool in Superconductivity Research"**
Dr. David Goodson, Syntek Technologies
Dr. Cyril F. Krolick, Syntek Technologies

12:20-12:30 Discussion

12:30-1:30 Lunch

Room: GL 102

1:30-3:45 Advanced Computational Techniques for System Design Session 1

Session Organizer: Dr. Ross Speciale

Session Chairs: Dr. Ross Speciale and Prof. Weng Cho Chew

1:30-1:50 "Broad-Band Fast Computational Electromagnetics Algorithm -- MFIPWA"
Lijun Jiang and Weng Cho Chew

1:50-2:10 "Three-Dimensional Material Optimization for Printed Antenna Bandwidth Enhancements"
Gullu Kiziltas, John L. Volakis, and Noboru Kikuchi

2:10-2:30 "A Novel Numerical Approach for the Analysis of 2D MEMS-Based Variable Capacitors with Arbitrary Motions"
Michiko Kuroda, Noriyuki Miura, and Manos M. Tentzeris

2:30-2:50 "Modelling of Surface Feature Scattering Through a Coherent Subtraction Process"
George R. Simpson and William D Wood

2:50-3:05 Break (Refreshments at GL, Courtyard)

3:05-3:25 "From Component to System Simulation"
Thomas Weiland, Irina Munteanu, and Martin Timm

3:25-3:45 "Error Convergence Process of the Multipole Expansion"
Shinichiro Ohnuki and Weng Cho Chew

Room : IN 130

1:30-3:45 Scattering by Complex Objects Session 1

Session Organizer: Prof. Michael Hamid

Session Chairs: Prof. Michael Hamid and Prof. Hashim A. Yousif

1:30-1:50 "The Mueller Matrix for the Scattering of Light by an Elliptical Cylinder"
Hashim A. Yousif

1:50-2:10 "Bistatic Cross Section of an Array of Dielectric Spheres Each Covered with a Dielectric Shell"
Mousa I. Hussein, Abdul-Kader Hamid, and Michael Hamid

2:10-2:30 "Radiation Characteristics of an Infinite Axially Slotted Elliptical Antenna Partly Embedded in a Ground Plane"
Mousa I. Hussein and A-K Hamid

2:30-2:50 "Estimation of Target Orientation from Scattering Data"
Ali Kabiri, Nima Sarshar, and Kasra Barkeshli

2:50-3:05 Break (Refreshments at GL, Courtyard)

3:05-3:25 "Electromagnetic Scattering from an Multilayered Domain via an Integral Equation Approach"
F. Seydou

3:25-3:45 "Profile reconstruction in Multilayered Media"
F. Seydou

Room: IN 122

1:30-4:05 Recent Antenna Applications Session 1

Session Organizer: Prof. Samir Mahmoud

Session Chairs: Prof. Samir Mahmoud and Prof. Allen Glisson

1:30-1:50 "Wideband and Dual-Band Loaded Monopole Dielectric Resonator Antenna"
Swee Huat Ong, Ahmed A. Kishk, and Allen W. Glisson

1:50-2:10 "On the Significance of Current Vector Alignment in Lowering the Resonant Frequency of Fractal and Small Wire Antennas"
Steven R. Best and Jarrett D. Morrow

2:10-2:30 "Study of Reduced Size Circular Microstrip Patch Antenna with Two-Pin Loading. "
Samir F. Mahmoud

2:50-3:05 Break (Refreshments at GL, Courtyard)

3:05-3:25 "Multi-Slot Antenna for Radar Systems"
Cuthbert M. Allen, Abdelnasser A. Eldek, Atef Elsherbeni, and Charles E. Smith

3:25-3:45 "Modeling, Synthesis and Broadband Matching of a Panel Crossed-Dipole Antenna for FM Broadcasting Applications"
Mehdi Hosseini and Keyvan Forooghi

3:45-4:05 "Numerical Characterization of Cavity-Backed Aperture-Coupled Antenna Problem using Hybrid Finite Element Method (FEM) / Method of Moment (MoM) technique"
Donghoon Chun and Kazem Sabet

Room: SP 101A

3:00-5:00 **Poster Session 1**

Session Chair: Prof. M. Hamid

"New Small Size 3 dB 0°/180° Microstrip Coupler Configurations"

Ashraf Mohra, Hoda Baghdady, Abdel Fattah Sheta, and Samir F. Mahmoud

"A Survey of the Eigenvalues of Pyramidal Waveguides"

Michael Hamid and A. K. Hamid

"Mueller Matrix Elements for Subsurface Sensing Applications of Targets Buried Beneath 2-D Randomly Rough Ground"

Magda El-Shenawee

"Multimode Hybrid Junctions"

M. Hamid

"Where Does the Radiation Come From?"

Steve R. Inge

Room: HH, La Novia Terrace

6:30-8:00 **Conference Reception**

Tuesday

Room: SP 101A

8:00-4:30 **Conference Registration**

Room : GL, Courtyard

7:30-8:30 **Continental Breakfast**

Room: GL 102

8:30-9:30 **Plenary Session 1**

"The Marvels of Electromagnetic Band Gap (EBG) Structures"

Prof. Yahya Rahmat-Samii, UCLA, CA

9:30-9:45 **Break (Refreshments at GL, Courtyard)**

9:45-11:45 **Plenary Session 2**

"Industry Applications of Numerical Modeling Tools to EMC and Signal Integrity Problems"

Session Moderator:

9:45-9:55 Prof. Todd Hubing - University of Missouri-Rolla

Speakers:

9:5-10:20 **"Computational EM for High Speed Computer Design: Challenges, Successes and Future Directions"**

Dr. Bruce Archambeault, IBM, Research Triangle Park, NC

10:20-10:45 **"Numerical EM Modeling Tools at Sanmina"**

Dr. Franz Gisin, Sanmina Corporation

10:45-11:10 **"Useful Numerical Simulation Tools for EMC and SI at the Printed Circuit Board and System Levels"**

Dr. Cheung-Wei Lam, Apple Computer

11:10-11:35 "Getting Useful EMC and SI Results from Numerical EM Modeling Tools"

Dr. Larry Smith, Sun Microsystems

11:45-12:00 Break

12:00-12:30 Invited Speaker 1

"Maxwell Without Mathematics"

Mr. Alan Nott, Antuition Enterprises

12:30-1:30 Lunch

Room: IN 267

1:30-4:25 FDTD Methods and Applications

Session 1

Session Organizer: Dr. John H. Beggs

Session Chairs: Dr. John H. Beggs and Prof. Christopher Trueman

1:30-1:50 "Z-diagonalized Planewave/FD Approach for Analyzing TE Polarized Waves in 2D Photonic Crystals"
Karri VARIS and Alireza Baghai-Wadji

1:50-2:10 "Numerical Solution of Time-dependent Maxwell's Equations in Spherical Coordinates"
Eugene Kashdan and Eli Turkel

2:10-2:30 "Application of a High Accuracy Nonstandard Finite Difference Time Domain Method in the Analysis of Subwavelength Optical Gratings"
Saswatee Banerjee, James B.Cole, and Toyohiko Yatagai

2:30-2:50 "A Fast Graphical User Interface (GUI) Based FD-TD Algorithm for Simulation of EMF Interaction with Biological Media "
Sachin Singh, Sevaiyan Balaguru, Sarita Kapoor, Suketu Bhatt, and B. P. Kumar

2:50-3:05 Break (Refreshment at GL, Courtyard)

3:05-3:25 "Numerical Dispersion in the Alternate-Direction-Implicit Finite-Difference Time-Domain Method"
Guilin Sun and Christopher W Trueman

3:25-3:45 "FDTD Model of Electrically Thick Material Coatings Based on a Higher-Order Surface Impedance Boundary Condition"
Mikko Kärkkäinen

3:45-4:05 "Broadband Modeling of Waveguide Antennas by a Combined FDTD and Modal-N2F Method"
Gaetano Marrocco and Matteo Ciattaglia

4:25-4:30 Break

4:30-5:50 Finite Element Method and Applications

Session 1

Session Organizer: Prof. Leo Kempel

Session Chairs: Prof. Leo Kempel and Dr. Matthys Botha

4:30-4:50 "Subdividing Distorted Prisms into Tetrahedra"
Leo Kempel, Jeffery Meese, and Stephen Schneider

4:50-5:10 "Comparison Between Two a posteriori Error Indicators for Adaptive Microwave FE Analysis"
Matthys M. Botha and David B. Davidson

5:10-5:30 "Finite Element Time Domain Method Using Laguerre Polynomials"
Young-seek Chung, Tapan K. Sarkar, Sergio L. Romano, and Magdalena Salazar Palma

5:30-5:50 "Using Mixed Elements with the Finite Element-Boundary Integral Technique"
Jeffery Meese and Leo Kempel

Room: IN 122

1:30-4:25 Electromagnetic Modeling by WIPL-D Code

Session 1

Session Organizer: Prof. Branko Kolundzija

Session Chairs: Prof. Branko Kolundzija and Prof. Tapan K. Sarkar

- 1:30-1:50 "Is it Diffraction of Electromagnetic Waves or Gravitation?"
Seongman Jang, Tapan K. Sarkar, and Branko Kolundzija
- 1:50-2:10 "Assessing the Effect of Finite Conductivity on the Performance of Microstrip-Fed Patch Antennas"
James W. Stewart, William D Wood, and Michael Harvey
- 2:10-2:30 "Parallel Scene Generation – Why Parallelize WIPL-DP?"
Ralph L. Kohler, Jr., Alan George, and Tapan Sarkar
- 2:30-2:50 "Single-Fed Circularly Polarized Dielectric Resonator Antenna"
Ahmed A. Kishk

2:50-3:05 Break (Refreshment at GL, Courtyard)

- 3:05-3:25 "WIPL Code Validation for Metallic Structures"
Antonije R. Djordjević, Branko M. Kolundzija, Alenka G. Zajic, Marija M. Nikolic, Toma H. Stirovic, and Aleksandra S. Stekovic
- 3:25-3:45 "WIPL-D Compared to Other EM Codes for the Analysis of Printed Antennas"
Carlos A. Fernandes and Custódio O. Peixeiro
- 3:45-4:05 "Broadband Analysis in WIPL-D Using the Cauchy Approach"
Raviraj Adve
- 4:05-4:25 "Numerical Analysis of Inverted-F Antenna on Side of Small Rectangular Conducting Plate in Vicinity of B5-sized Conducting Plate"
Mitsuo Taguchi, Yoshifumi Yanagisako, and Kazumasa Tanaka

4:25-4:30 Break

4:30-5:50 Time Domain Numerical Modeling Beyond FDTD

Session 1

Session Organizer: Prof. Pascal Leuchtman

Session Chair: Prof. Pascal Leuchtman

- 4:30-4:50 "Boundary Conditions Simulation in a FDTD/FVTD Hybrid Code"
Pierre Bonnet
- 4:50-5:10 "Finite-Volume Time-Domain Modeling of Antennas"
Christophe Fumeaux, Dirk Baumann, Pascal Leuchtman, and Rüdiger Vahldieck
- 5:10-5:30 "Triangular Grids: A Review of Waveguide Analysis with Classical FIT and Some Reflections on Yee-like FIT- and FEM-Schemes"
Ursula van Rienen
- 5:30-5:50 "Errors in FDTD, FIT and FVTD"
Pascal Leuchtman and Ruediger Vahldieck

Room: IN 265

1:30-4:25 Advances in Integral Equation Techniques

Session 1

Session Organizer: Prof. Raed Shubair

Session Chairs: Prof. Raed Shubair and Prof. Alireza B-Wadji

- 1:30-1:50 "Efficient Computation of Sommerfeld Integrals"
Surendra Singh and Ritu Singh
- 1:50-2:10 "Analysis of Vertical Dipoles Above a Semi-Infinite Ground Using The Induced EMF Method and Simulated Image Technique"
R. M. Shubair
- 2:10-2:30 "Universal Functions in Computational Electromagnetics"
Alireza Baghai-Wadji
- 2:30-2:50 "High-Order Integral Equation Solution Based On a Hybrid Volume/Surface Formulation"
Stephen D. Gedney and Caicheng Lu
- 2:50-3:05** Break (Refreshment at GL, Courtyard)
- 3:05-3:25 "Solution of Vertical Antennas in Contiguous Dielectric Half-Spaces Using MPIE Formulation and Simulated Image Green's Functions"
R. M. Shubair
- 3:25-3:45 "On the Discretization of Fredholm Integral Equations of First Kind Using Compactly Supported Wavelets"
Robert Kolm and Alireza Baghai-Wadji
- 3:45-4:05 "Robust Preconditioning Techniques for Electromagnetic Wave Scattering Problems"
Jun Zhang, Jeonghwa Lee, and Cai-Cheng Lu
- 4:05-4:25 "Analysis of PEC Objects in Layered Media Using Higher-Order Hierarchical Basis Functions"
Oleksiy S. Kim, Erik Joergensen, Peter Meincke, and Olav Breinbjerg

4:25-4:30 Break

4:30-5:10 Wavelets in Electromagnetics

Session 1

Session Organizer: Prof. Nathan Ida

Session Chairs: Prof. Nathan Ida and Prof. Richard Gordon

- 4:30-4:50 "Analysis of Scattering Problems by MOM with Intervallic Wavelets and Operators"
Sami Barmada and Marco Raugi
- 4:50-5:10 "Generation and Use of Two-Dimensional Wavelet-Like Basis Functions"
W. Elliott Hutchcraft and Richard K. Gordon

Room: GL 102

1:30-4:25 Hybrid and Coupled Time Domain Solution Methods

Session 1

Session Organizer: Prof. Wolfgang J.R. Hoefer

Session Chairs: Prof. Wolfgang J.R. Hoefer and Dr. Poman So

- 1:30-1:50 "Reduced Order Modeling in TLM"
Dzianis Lukashevich, Andreas Cangellaris, and Peter Russer
- 1:50-2:10 "Simulation of Scattering Problems in Time Domain Using a Hybrid FDTD-UTD Formulation"
Anastassios Skarlatos, Rolf Schuhmann, and Thomas Weiland

2:10-2:30 "Generalized and Numerically Robust Singularity Correction in TLM Models of Electromagnetic Fields"
Huilian Du, Poman So, and Wolfgang Hoefer

2:30-2:50 "A Hybrid Time Domain Method To Calculate Electromagnetic Induction Scattering From Targets with Arbitrary Skin Depths"
C. D. Moss, K. O'Neill, T. M. Grzegorzcykf and J. A. Kong

2:50-3:05 Break (Refreshment at GL, Courtyard)

3:05-3:25 "The Use of Surface Impedance Boundary Conditions in Time Domain Problems: Numerical and Experimental Validation"
Sami Barmada, Luca Di Rienzo, Nathan Ida, and Sergey Yuferev

3:25-3:45 "Intracell Modeling of Metal/Dielectric Interfaces for EBG/MEMS RF Structures Using the Multiresolution Time-Domain Method"
Nathan Bushyager and Manos Tentzeris

3:45-4:05 "A Hybrid FDTD and ADI-FDTD Scheme for Efficient RF/Microwave Structure Simulation"
Iftikhar Ahmed and Zhizhang Chen

4:05-4:25 "Finite Difference Time Domain Modeling of General Dispersive Bi-isotropic Media."
Ana Grande, Ismael Barba, Jose Represa, Ana C. L. Cabeceira, Poman P.M. So, and Wolfgang J. R. Hoefer

4:25-4:30 Break

4:30-5:50 Hybrid Techniques in Computational Electromagnetics Session 1

Session Organizer: Dr. Kazem F. Sabet

Session Chairs: Dr. Kazem F. Sabet and Prof. Ercument Arvas

4:30-4:50 "Accelerating Computations with a MoM-Based Computer Program using a Model Based Parameter Estimation Algorithm"
Markus Schick and Friedirch M. Landstorfer

4:50-5:10 "Generalized Network Formulation of Electromagnetic Fields -- Tableau Analysis of Waveguide Discontinuities"
Tian Jan Ong, M. Fujii, M. Mongiardo, and P. Russer

5:10-5:30 "Use of Model-Based Parameter Estimation in Electromagnetic Scattering Problems of a Conducting Body of Revolution"
Hyunwung Son, Joseph R. Mautz, and Ercument Arvas

5:30-5:50 "A Decompose-Solve-Recompose (DSR) Technique For Large Phased Array Analysis"
K. Y. Sze, K. F. Sabet, and D. Chun

6:00-8:30 ACES Board of Directors Meeting

Wednesday

Room: SP 101A

8:00-4:30 Conference Registration

Room : GL, Courtyard

7:30-8:00 Continental Breakfast

Room: GL 102

8:00-9:00 Plenary Session 1

"EM Modeling of Surfaces with STOP or GO Characteristics - Artificial Magnetic Conductors and Soft and Hard Surfaces"

Prof. Per-Simon Kildal, Chalmers University of Technology and Prof. Ahmed Kishk, University of Mississippi

9:00-9:10 Break

9:10-10:10 Invited Talk 1

"Envelope-Finite Element Techniques for Microwave Component and Antenna Design"

Prof. Tatsuo Itoh, UCLA and Dr. Yuanxun Wang, UCLA

10:10-10:20 Break (Refreshment at GL, Courtyard)

10:20-11:20 Invited Talk 2

"Solution to the General Helmholtz Equation Starting From Laplace Equation"

Prof. Tapan K. Sarkar, Syracuse University

11:20-11:30 Break

11:30-12:30 Invited Talk 3

"Integration of Different Numerical Algorithms for the Electromagnetic Modeling of Complex Geometries"

Prof. A.S. Omar, University of Magdeburg

12:30-1:30 Lunch

Room: IN 265

1:30-3:30 **Advanced Computational Techniques for System Design**

Session 2

Session Organizer: Dr. Ross Speciale

Session Chairs: Dr. Ross Speciale

1:30-1:50 "Accurate Wide-band De-embedding of Port Discontinuities in Full-wave Models of Integrated Circuits"

Vladimir Okhmatovski, Jason Morsey, and Andreas Cangellaris

1:50-2:10 "Efficient Hybrid MM/FE/MoM Analysis of Horn and Slot Arrays"

Prof. Dr. Fritz Arndt, V. Catina, A. Enneking, I. Rullhusen, and J. Brandt

2:10-2:30 "A "Cycle-Harvesting" Framework for Problems in Computational Electromagnetics"

Christopher B. Smith

2:30-2:50 "Performance Analysis of MoM Patch Antenna Simulations – RWG Basis Functions"

Shashank Kulkarni, Anuja Apte, and Sergey Makarov

- 2:50-3:10 "A Uniaxial Time-Domain Wave Potential Analysis of the Electromagnetic Field in Nonuniform Media"
Natalia K. Nikolova
- 3:10-3:30 "Computer Simulation of Scattering Parameter Measurements"
Dr. Ross A. Speciale

Room: GL 102

1:30-2:50 Modeling Tools for EMC and Signal Integrity Problems Session 1
Session Chair: Dr. Bruce Archambeault

- 1:30-1:50 "Full-Wave Analysis of Transmission Line Structures in Damascene Technology"
Dzianis Lukashevich and Petter Russer
- 1:50-2:10 "Description of the Magnetic Field Distribution in a Non-linear Breaker Relay"
Jean Clovis, Njeumeni Siango, Brigit Neuhaus, Eva Vargaf, and Adalbert Beyer
- 2:10-2:30 "Application of Prolate Spheroid Solutions in Simulation of EMI Scattering with Realistic Sensors and Objects"
Keli Sun, Ko'Neill, I. Shamatava, and F. Shubitidze

Room: IN 122

1:30-2:50 FDTD Methods and Applications Session 2
Session Organizer: Dr. John H. Beggs
Session Chairs: Dr. John H. Beggs and Dr. James B. Cole

- 1:30-1:50 "Design of Slot Antennas and Arrays Using the FDTD Technique and a Parallel Supercomputer"
Manabu Omiya, Kosuke Munakata, and Takashi Hikage
- 1:50-2:10 "A New FDTD Solution Method Without The Time Variable"
Tapan K. Sarkar, Young-seek Chung, and Baek Ho Jung
- 2:10-2:30 "High Accuracy FDTD Algorithm for the Conducting Maxwell's Equations Using a Nonstandard Finite Difference Model"
James B. Cole and Saswatee Banerjee
- 2:30-2:50 "FDTD Models of Small Microwave Devices"
Qing-Xin Chu and Xiao-Juan Hu

Room: IN 267

1:30-3:10 Hybrid Techniques in Computational Electromagnetics Session 2
Session Organizer: Dr. Kazem F .Sabet
Session Chair: Dr. Kazem F .Sabet

- 1:30-1:50 "Fast Modeling and Design of HF Loop Antennas on Aircraft by a Combined FDTD and MTL Method"
Piero Tognolatti and Gaetano Marrocco
- 1:50-2:10 "A Combined MAS-TSA Algorithm for Broadband Electromagnetic Induction Problems"
Fridon Shubitidze, Ko'Neill, K. Sun, I. Shamatava, and K. O. Paulsn
- 2:10-2:30 "A Hybrid MoM/FDTD Technique for the Modeling of Multi-antenna Systems on Vehicular Platforms for Wireless Communication Systems"
Werner Thiel and Kazem Sabet

2:30-2:50 "Coupling of Electromagnetic Time-Domain Simulators with DSP/Multigridding Techniques for the Adaptive Modeling of Multilayer Wireless Packaging Structures"
Jong Hoon Lee, E.T.K. Dalton, N. Bushyager, M. Kunze, and W. Heinrich, M.M. Tentzeris

2:50-3:10 "A Hybrid Nonlinear Antenna Analysis Technique"
Eray Yasan and Kazem F. Sabet

Room: HH, Ballroom

1:30-5:00 Vendor Exhibits

Room: HH, Ballroom

2:00-5:00 Wine & Cheese Tasting

Room: HH, Ballroom

2:00-5:00 Posters Session 2

Session Chair: Dr. Reinaldo Perez

"An XML Schema for NEC Input Files"
Daniel D Reuster, Glen L. Harris, Mary L. Fricke, Tat Fung, and Jeffrey T. Hoppe

"A Novel Dirichlet-Neumann Random-Walk Algorithm for Electromagnetic Analysis of IC Interconnects Beyond Quarter-Wavelength Length Scales"
Kausik Chatterjee and Yannick L. Le Coz

"A View of Avionics Design of Spacecraft, Past, Present and Future"
Reinaldo Perez

"Dielectric Polarizability of a Homogeneous Cube"
Ari Sihvola, Pasi Yla-Oijala, Seppo Jarvenpaa, and Juha Avelin

"Field Theoretical Investigations on Dielectric Image Line Isolators in I-Line Technique"
D. Koether, P. Waldow, B. Neuhaus, D. Schreurs, and A. Beyer

"Numerical Modeling of Electromagnetic Fields in Strongly Heterogeneous Anisotropic Media"
P. Jorna and P.M. van den Berg

"Interaction Between Highly Conducting and Permeable Metallic Objects in the EMI Frequency Range"
Fridon Shubitidze, KoNeill, K. Sun, and I. Shamatava

"Electromagnetic Modelling of Helmholtz Coils "
Ashley Bocking

"Computation of SAR in Cell Culture Flasks Exposed to 900 MHz GSM Type Signals in a Modified TEM Cell"
Dr Robert L McIntosh, Raymond J McKenzie, Steve Iskra, Amico Carratelli, and Paul Standaert

"Evaluation and Comparative Analysis of Radio-Wave Propagation Model Predictions and Measurements"
Nicholas DeMinco and Paul M. McKenna

"Slotted Waveguide Transitions for Spatial Power Combining"
Chris W. Hicks, Alexander B. Yakovlev, and Michael B. Steer

"Scattering of a Scalar Plane Wave from a Circularly Symmetric Random Dirichlet Surface"
T. A. Leskova, A. A. Maradudin, E. R. Mendez, and S. Silverman

"Design and Simulation of Microwave Filters for Improving Out-of-Band Characteristics"
Kouji Wada, Tomohide Kamiyama, Yoshiyuki Aihara, and Osamu Hashimoto

"An Improved Arbitrary Resolution MRTD Method"
Qunsheng Cao and Kumar K. Tamma

"Multiresolution Time Domain for Studies of Planar Stratified Media"
Qunsheng Cao and Kumar K. Tamma

"Inclusion of Flaking Effects Inside a Pressed Layer Structure in the Electromechanical Analysis with the Aid of Static Condensation and Floating Potentials"
Christian Grabner and Erich Schmidt

"Antenna Design and Radiation Pattern Visualization"
Atef Z. Elsherbeni, Matthew J. Inman, and R. Christopher-Lee Riley

"Capacity Estimation of HF Ionospheric Channel"
Abderrazak Abdaoui, Claude Goutelard, Han Vu-thien, and Ammar Bouallegue

"Fast Converging Graded Meshes for Bodies of Revolution with Tip Singularities"
Kueichien Hill and Tri Van

Room: HH, Ballroom

2:00-5:00 Computer Modeling and Simulation

Session Organizer: Dr. Andrew Drozd

Session Chair: Dr. Andrew Drozd

"High Accuracy FDTD Simulation and Visualization of Electromagnetic Propagation and Scattering on a Laptop"
James B. Cole

"A Method for Building CEM Models of Complex Platforms"
Gerald J. Burke, Nathan J. Champagne, and Robert M. Sharpe

"System-Level EMC Antenna Coupling Analysis for Large, Complex Structure Topologies Using a Multi-Fidelity Modeling and Simulation Approach"
Andrew L. Drozd and Irina P. Kasperovich

"Using FDTD for EMC Applications"
Bruce Archambeault

"Comprehensive and Practical Electromagnetic Simulations Using FEKO" by
C. J. Reddy

"CEM Code Validation Using Thermal Imaging Techniques"
John Norgard

"Antenna Modeling and Analysis Using WIPL-D"
Saad Tabet

"Degradation of EMI Shielding in the Presence of Extraneous Conductors"
Colin Brench

EMPiCASSO: An Advanced Design Tool for Multilayer Printed Microwave Circuits and Antennas"
Kazem Sabet

Room: HH, Ballroom
6:30 No Host Bar

7:30 Awards Banquet

Thursday

Room: SP 101A

8:00-11:00 Conference Registration

Room : GL, Courtyard

7:30-8:00 Continental Breakfast

Room: IN 122

8:00-9:40 EMC Design Session 1

Session Organizer: Dr. Bruce Archambeault

Session Chairs: Dr. Bruce Archambeault and Dr. Andrew L. Drozd

8:00-8:20 "Effect of Distance between Noise Source and Decoupling Capacitor on the EMI Performance of Power and Ground-Reference Planes"
Bruce Archambeault, Sam Connor, and Juan Wang

8:20-8:40 "A Novel EMC Testing Technique based on Time Domain Methods"
Florian Krug, Tobias Hermann, and Peter Russer

8:40-9:00 "Analysis of Antenna-Coupled EMI For Large Resonant Structures Using Hybrid Multi-Resolution Modeling"
Andrew L. Drozd, Irina P. Kasperovich, Clifford E. Carroll Jr., and Sharon C. Hall

9:00-9:20 "The Effects of PCB Split Reference Planes on High Speed Signals: Analysis and Mitigation"
J. Alan Roden , Bruce Archambeault, and Ruthie Lyle

9:40-10:00 Break (Refreshment at GL, Courtyard)

10:00-11:00 Time Domain Numerical Modeling Beyond FDTD Session 2

Session Organizer: Prof. Pascal Leuchtman

Session Chairs: Prof. Pascal Leuchtman and Prof. J. B. Cole

10:00-10:20 "Efficient High-Spatial-Order FDTD Analysis of 3D Optical Ring Resonator Filters"
Masafumi Fujii, Wolfgang Freude, and Peter Russer

10:20-10:40 "Grid Construction and Boundary Condition Implementation for the Isotropic Vector Field Decomposition Methodology"
J.F. Nystrom

10:40-11:00 "Parametric Model Generation Algorithm for Planar Microwave Structures based on Full-Wave analysis and Design of Experiment"
Mahmoud Al--Ahmad, Fabio Coccetti, Manos Tentzeris, and Peter Russer

Room: GL 102

8:00-10:20 Japanese Research in Electromagnetic Field Computations Session 1

Session Organizer: Prof. Yasushi Kanai

Session Chair: Prof. Yasushi Kanai

8:00-8:20 "Optimization Analysis in an Induction Heating Problem using GA on a Parallel Computer"
Takeshi Iwashita, Tasuku Kirikoshi, and Masaaki Shimasaki

- 8:20-8:40 "Electromagnetic Field Analysis of Inductors with Various Lamination Method for High Frequency Circuits"
T. Tsukamoto, K. Torigoe, M. Hasu, M. Mizumoto, H. Saeki, and Y. Kanai
- 8:40-9:00 "Application of a Fast Multigrid Solver for High Frequency Electromagnetic Simulation"
David Dibben and Takashi Yamada
- 9:00-9:20 "Convergence of Multigrid Finite Element Method in Eddy Current Analysis"
Kota Watanabe, Hajime Igarashi, and Toshihisa Honma
- 9:20-9:40 "Spectra of Finite Element Matrix for Magnetostatic and Quasi-static Electromagnetic Fields"
Hajime Igarashi and Toshihisa Honma

9:40-10:00 Break (Refreshment at GL, Courtyard)

- 10:00-10:20 "Analytical Study on Change of Temperature and Absorption Characteristics of Single-layer Radiowave Absorber to Irradiation Electric Power"
Masanori KATO, Osamu Hashimoto, Takayuki Nakamura, and Kouji WADA
- 10:20-10:40 "Estimation of Complex Permittivity Using Rectangular Waveguide with Flange at 10GHz"
Kouji Shibata, Osamu Hashimoto, and Kouji Wada

10:40-11:00 Break

11:00-11:40 Electromagnetic Nondestructive Testing

Session Organizer: Prof. Nathan Ida

Session Chairs: Prof. Nathan Ida and Prof. Sami Barmada

- 11:00-11:20 "Simulation of Non Contact Ultrasound NDT Methods via Electromagnetic Modelling"
Sami Barmada and Marco Raugi
- 11:20-11:40 "Transmission Line Matrix Model for Microwave Scanning Microscopy"
Razvan Ciocan and Nathan Ida

Room: IN 322

8:00-9:40 Partial Differential Equations Techniques

Session 1

Session Organizer: Prof. Richard K. Gordon

Session Chairs: Prof. Richard K. Gordon and Dr. Vicente Rodriguez

- 8:00-8:20 "Complementary Basis Functions and the Vector Magnetic Potential"
William A. Davis, and K. Sitapati
- 8:20-8:40 "A Study of the Effect of Placing Microwave Pyramidal Absorber on Top of Ferrite Tile Absorber on the Performance of the Ferrite Absorption"
Vicente Rodriguez
- 8:40-9:00 "Design of a New Type of Absorber for EMC Chambers Using the Finite Elements Technique and Ray Tracing Methods."
Vicente Rodriguez
- 9:00-9:20 "A Novel 2-Level IE-SVD Algorithm to Model Large Microstrip Antenna Arrays"
Kezhong Zhao and Jin-Fa Lee
- 9:20-9:40 "T-elements for 3-D Electromagnetic Problems"
Yuriy Shlepnev

9:40-10:00 Break (Refreshment at GL, Courtyard)

10:00-12:00 Practical Applications of Method of Moments Modeling

Session 1

Session Organizer: Dr. Keith Lysiak

Session Chair: Dr. Keith Lysiak

- 10:00-10:20 "Modeling the Antenna Configuration of a Digital Very-High Frequency (VHF) Direction Finding System"
Michael E. McKaughan, Keith C. Gross, and Richard J. Hartnett
- 10:20-10:40 "Modeling Guidelines for the Computation of Electrode Grounding Resistance Using NEC"
J. Patrick Donohoe
- 10:40-11:00 "Model Validity Insights From Inter-Code Comparisons and Graphics Displays"
Stanley J. Kubina, Christopher W. Trueman, David Gaudine, and Thuy T. Tran
- 11:00-11:20 "USCG 270' Cutter - NVIS Study"
Kevin Cybert, Jim Potter, Richard Mead, and Michael E. McKaughan
- 11:20-11:40 "MH-53J/M Pave Low Helicopter, Shunt-Type HF Towel Bar Antenna Rotor Modulation Effects"
Jim Potter, Kevin Cybert, Terry Vogler, and Ricard Mead
- 11:40-12:00 "Numerical Study of Coupling between Coagulators and Electrodes of Cardiac Pacemakers under Consideration of the Human Body"
Markus Schick and Friedrich M. Landstorfer

Room: IN 321

8:30-11:30 **IEEE P1597 CEM Standards Committee Meeting**

12:30-1:30 Lunch

Short Courses

Thursday

1:30-5:30 Short Courses (Afternoon)

Room: GL 118

"E3EXPERT, A Multi-Fidelity Computer Modeling and Simulation Tool for the EMI/C Analysis of Large, Complex Systems", Dr. Andy Drozd

Room: GL 129

"Introduction to Computational Simulation Techniques", Dr. Bruce Archambeault

Room: GL 130

"Wavelets in Electromagnetics", Prof. Nathan Ida and Prof. Sami Barmada

Room: GL 203

"The FDTD Technique for EM Applications", Prof. Atef Elsherbeni and Prof. Allen Glisson

2:50-3:05 Break (Refreshment at GL, Courtyard)

Friday

Room : GL, Courtyard

7:30-8:30 Continental Breakfast at GL, Courtyard

10:15-10:30 Break (Refreshment at GL, Courtyard)

12:30-1:30 Lunch (on your own)

2:50-3:05 Break (Refreshment at GL, Courtyard)

8:30-5:30 Short Course (Full Day)

Room: GL 129

"Time Domain EM Simulation with TLM" , Prof. Wolfgang J.R. Hoefler

Room: GL 130

"Recent Advances in Finite Element Method for Computational Electromagnetics" , Prof. Leo Kempel and Prof. Jian-Ming Jin

8:30-12:30 Short Courses (Morning)

Room: GL 203

"Workshop on Antenna Analysis and Design Using The FDTD Technique", Prof. Atef Elsherbeni and Prof. Allen Glisson

Room: GL 118

"Basic Modeling with WIPL-D", Prof. Tapan Sakar and Dr. Branko Kolundzija

1:30-5:30 Short Courses (Afternoon)

Room: GL 118

"An Accessible Introduction to Fast Techniques in Computational Electromagnetics", Dr. A. R. Baghai-Wadji

Room: GL 203

"Workshop on Advanced Modeling with WIPL-D", Prof. Tapan Sakar and Dr. Branko Kolundzija

Title: Wavelets in Electromagnetics

Instructors: Prof. Nathan Ida and Prof. Sami Barmada

Program

Part I Theory and Background

- Introduction to the basic theory of wavelets.
- The Continuous Wavelet Transform
- The concept of multiresolution
- Wavelet analysis - emphasis on the discrete time approach.
- Algorithmic aspects of the discrete time wavelet transform
 - Mallat algorithm
 - Implementation with filter banks
 - Design issues.
- Some applications of wavelets
 - compression
 - de-noising
 - numerical solution of PDEs

By emphasizing the properties one can expect from wavelet methods, their advantages and limitations in diverse fields of application will be shown. This should enable the participants to develop a practical understanding and know-how of the wavelet techniques.

Part II Applications

- Application of the wavelet transform to computational electromagnetics.

Multiresolution techniques based on wavelets have demonstrated their capability to reduce computation time and computer memory requirements in the modeling of electromagnetic structures; the use of wavelets also provides a natural approach to adaptive refinement of the computational domain in those regions of space where the electromagnetic fields and their derivatives require improved accuracy.

The purpose of this part of the tutorial is to provide insight into the wavelet framework and to show how it can be an efficient tool for numerical modeling.

In particular, wavelet based techniques will be discussed for the solution of electromagnetics problems formulated by both differential and integral equations, pointing out the advantages and drawbacks they provide, in contrast to the more traditional numerical methods.

Title: Introduction to Computational Simulation Techniques

Instructor: Dr. Bruce Archambeault

The world of computational electromagnetics has become more important than ever before due to the higher speed electronics in lower cost packages. There is a new set of tools available to the engineer, which allows a more accurate estimation of the electromagnetic effects of a system before that system is built. The old rules-of-thumb cannot be relied upon to ensure success.

This course provides a complete assessment of the various modeling techniques available today. An introduction to the Method of Moments (MoM), the Finite Difference Time Domain (FDTD) technique, the Finite Element Method (FEM), the Partial Element Equivalent Circuit (PEEC) technique and the Transmission Line Matrix (TLM) method will be presented.

**Title: Basic Electromagnetic Modeling using the WIPL-D Code
(<http://wipl-d.com>)
(Morning session)**

Instructors: Branko Kolundzija, University of Belgrade and Tapan Sarkar, Syracuse University

Background: The objective of this course is to present the integral equation formulation for electromagnetic scattering from lossy composite material bodies (both dielectric and magnetic) for analysis of various electromagnetic structures including antennas, scattering and modeling of RF devices. The application will be demonstrated using the commercially available code WIPL-D (structures composed of *Wires*, *PLates* and *Dielectric* or finite lossy material bodies). Attendees of this course will receive a demo version of this code. Please bring your computer with you to the course so that you can run some examples that are of interest to you.

The following materials will be covered:

- Theoretical background (field equations particularly representing the integral form, geometrical modeling, approximation of currents, Galerkin method).
- Description of WIPL-D entities, menus, commands and toolbars.
- Basic steps in using WIPL-D: problem definition, editing input data, running the analysis, inspection and checking the input data, printing, and exporting of results (in the form of tables and 2D and 3D graphs).
- Examples of electromagnetic modeling (using all the basic steps):
 1. metallic structures
 2. wire structures (single wire, single and multiple wire junctions, generators, plane waves)
 3. plate structures (single plate, single and multiple plate junctions)
 4. composite wire and plate structures (simple and combined wire-to-plate junction)
 5. dielectric and/or magnetic structures (homogenous, inhomogeneous, multi-layered, with and without losses)
 6. composite metallic and dielectric structures (multiple metallic and dielectric junction, coated plate, wire protruding dielectric surface, plate protruding dielectric surface)
 7. loadings (distributed and concentrated, skin-effect losses)

Title: Advanced Electromagnetic Modeling by WIPL-D Code (Afternoon Session)

Instructors: Branko Kolundzija, University of Belgrade and Tapan Sarkar, Syracuse University

- Using symmetry (plane and rotational) for analysis of various structures.
- Efficient modeling by Custom codes (symbolic dimensioning, objects, manipulations, import).
- Improving (checking) the quality and speed of the solution (integration accuracy, approximation of currents, matrix inversion, power balance)
- Advanced modeling of wire structure (end effects, feed area, coaxial line excitation, plate model)
- Modeling of microstrip structures on finite lossy material (dielectric/magnetic) substrates (single and double "edging", finite thickness metalization, finite ground plane, "imaging")
- Easy creation of structures by using a mouse, creation of grids and patterns.
- S-parameters de-embedding technique for numerically analyzed microwave circuits.
- Analysis of antennas above real ground.

Title: Time Domain EM Simulation with TLM (Full day)

Instructor: Prof. Wolfgang J.R. Hoefer

Abstract:

This Workshop will empower participants to tackle electromagnetic field problems using Electromagnetic Field Simulation Tools that yield dynamic field solutions in space and time. Background information suitable for understanding the operating principles and basic features of such tools will be provided. Typical field problems arising in analog microwave and high-speed digital circuits, antennas, cross talk, signal integrity, and rf/microwave heating will be solved to demonstrate its wide range of powerful problem-solving capabilities. Simulation examples will be demonstrated using TLM simulator MEFiSTo-3D Pro by Faustus Scientific Corporation.

Presentation Outline

- 1 Introduction
 - 1.1 Historical and Scientific Background
 - 1.2 Time Domain Modeling Principles
- 2 How does a Time Domain Simulator work?
 - 2.1 The Nature of Time Domain Algorithms
 - 2.2 The Structure of a Time Domain Simulator
 - 2.3 Input and Output Features
- Refreshment Break
- 3 Two- and Three-Dimensional Time Domain Modeling
 - 3.1 2D/3D Structure Geometrical Editor
 - 3.2 Space and Time Discretization
 - 3.3 Excitation and Parameter Extraction
 - 3.4 Field Display and Animation
- Lunch Break
- 4 Two- and Three-Dimensional Time Domain Modeling
 - 4.1 Accuracy, Errors and Their Reduction
 - 4.2 2D and 3D Simulation Examples
- Refreshment Break
- 5 Advanced Modeling Techniques
 - 5.1 Radiation in Frequency and Time Domain
 - 5.2 Dispersive and Absorbing Boundaries
 - 5.3 The SPICE-EM hybrid modeling
 - 5.4 Structure Synthesis by Monochromatic Injection
 - 5.5 Advanced Simulation Examples
- Discussion and Closure

Title: E3EXPERT, A Multi-Fidelity Computer Modeling and Simulation Tool for the EMI/C Analysis of Large, Complex Systems

Instructor: Andrew L. Drozd

Description:

This workshop/short course will provide an overview of a new computer modeling and simulation tool developed for the Air Force Research Laboratory which is used to analyze the EMI/C properties of large, complex systems. The tool leverages sophisticated visualization utilities, expert system software technologies, and graphical pre/post processing tools to facilitate CEM modeling and simulation tasks. The tool, called E3EXPERT, can be used to model diverse multi-spectral EM environments and co-site or intersystem interactions involving air and space vehicles, and ground-based systems. E3EXPERT can be used to predict EM interference and antenna jamming, and can specify interference cancellation requirements for co-located mobile wireless communications (including spread spectrum systems) and on/off-board sensors (e.g., high power radars). E3EXPERT provides a capability to compute coupling involving RF communications, network, and multi-spectral surveillance systems as part of RF battlespace information warfare simulations. RF battlespace scenarios are imported as "CAD" models comprised of satellite or aerial imagery combined with system platform CAD descriptions, which are then converted into CEM models. The tool provides for multi-fidelity simulation to analyze complex EM systems and scenarios in a coarse, conservative manner using a discrete system-level modeling approach and then applying more refined methods to the problem using hybrid MoM/UTD/FD codes. This technique is used to identify worst-case problem areas involving many EM radiators and then selectively analyze them in a high-fidelity manner to verify coupling margins. The code can be readily extended to include other CEM modeling tools and methods within its framework.

Title :Recent Advances in Finite Element Method for Computational Electromagnetics

Instructors:

Jian-Ming Jin, Center for Computational Electromagnetics, Department of Electrical and Computer Engineering, University of Illinois, Urbana, Illinois 61801-2991

Leo Kempel, Fraunhofer Center for Coating and Laser Applications, Department of Electrical and Computer Engineering, Michigan State University, East Lansing, Michigan 48824-1226

Course Outline:

During the past decade, significant advances have been made in the finite element method for computational electromagnetics. As a result, large and complex problems of scattering, antenna, and microwave circuit, devices, and cavities can be analyzed accurately and efficiently using the finite element method. Problems involving millions of unknowns have been handled on workstations and devices consisting of inhomogeneous anisotropic material have been simulated successfully. The major advances include: (1) the development of higher-order vector finite elements, which make it possible to obtain highly accurate and efficient solutions of vector wave equations; (2) the development of perfectly matched layers as an absorbing boundary condition; (3) the development of hybrid techniques that combine the finite element and asymptotic methods for the analysis of large and complex problems that were unsolvable in the past; (4) the development of fast integral solvers, such as the fast multipole method, and their integration with the finite element method; and finally (5) the development of the finite element method in time domain for transient analysis. The objective of this full-day short course is to summarize these advances and demonstrate the increased capabilities of the finite element methods to solve complex computational electromagnetics problems.

Topics will include: (1) introduction to the finite element method for electromagnetic analysis; (2) absorbing boundary conditions and perfectly matched layers; (3) adaptive ABC and hybrid finite element-fast boundary integral method; (4) novel hybridization of the finite element and boundary integral methods and a highly effective preconditioner; (5) fast finite element analysis of deep-cavity scattering; (6) fast finite element analysis of microwave devices; (7) higher-order vector finite elements for higher-order accuracy; (8) asymptotic waveform evaluation for broadband calculations; and (9) time-domain finite element analysis. Many numerical examples will be presented to demonstrate the finite element analysis of scattering, antennas as well as microwave devices and cavities.

The textbook is *The Finite Element Method in Electromagnetics, Second Edition*, by Jian-Ming Jin (John Wiley, NY, 2002).

Title: An Accessible Introduction to Fast Techniques in Computational Electromagnetics

Instructor: A. R. Baghai-Wadji Vienna University of Technology, Accelerated Computational Technology Group alireza.baghai-wadji@tuwien.ac.at

Based on illustrative examples the standard-, the fast- and the accelerated techniques in applied computational electromagnetics will be explained. The finite difference-, the conservative finite difference-, the finite element-, and the finite integral methods will be briefly reviewed. Our focus, however, will be on the multipole-, the multilevel multipole-, the multigrid-, and the wavelets-based analysis methods, and, even in much greater detail, the instructor's Fast-MoM.

We start with standard methods which will be introduced by carefully designed examples. The chosen examples will also serve to define the involved terms and notions, to identify the methods' shortcomings, and to demonstrate the urgent need for high performance computing techniques. The examples include problems in the electrostatic- and magnetostatic applications, the EM scattering on perfectly conducting objects with arbitrary shapes, the EM scattering on dielectric bodies, antenna radiation problems, RF-MEMS, EM cross-talk, electronic packaging, and photonic crystals.

In order to design fast techniques it is first necessary to have an adequate understanding of the underlying philosophy. The second part of our discussion is devoted to this end. First we develop concepts and tools to measure the complexity of computations, and then we discuss four fast algorithms for calculating (i) the product of integers, (ii) the multiplication of matrices, (iii) the discrete Fourier transform of signals, and (iv) the discrete convolution integrals. The course attendees will be then in a position to appreciate several novel and intriguing fast algorithms in the wavelet theory and, more generally, in the multiresolution analysis. This part of our presentation will be communicated entirely by diagrams, charts, and networks and, therefore, it will be most easily accessible to EM engineers.

In the third and final part of our discussion, we start with the multipole-, the multilevel multipole-, and the multigrid techniques, and then delve into the Fast-MoM. The analysis technique Fast-MoM uses moments of the Green's functions and their derivatives rather in a sophisticated manner and generates functions which are universal. The attribute *universal* is meant in the sense that these functions do not depend on the operating frequency, problems' geometrical features, and material parameters. The universal functions are, in addition, astonishingly smooth and, therefore, digitally easy to process. After introducing and constructing several universal functions, their smoothness property will be explained. We will present three alternative techniques for the construction of Green's functions and develop a library of universal functions for the applications mentioned above. Thereby, wavelets will be used not only to create universal

functions but also to store them. The formulations and computations will be explained in Matlab.

The FDTD Technique For EM Applications

Dr. Atef Z. Elsherbeni atef@olemiss.edu
Dr. Allen W. Glisson aglisson@olemiss.edu

This course will provide an overview of the finite difference time domain technique (FDTD) as applied in the electromagnetic and microwave arena.

Course Outline:

- Basic formulation of time domain techniques
 - Maxwell's equations in Cartesian coordinates
- Difference approximations and Yee algorithm
- Total vs. scattered field formulation
- Numerical stability and dispersion
- Types of sources and waveforms
- Absorbing boundary conditions
- Thin wire approximation
- Near to far field transformation
- Modeling of lumped elements
- Non-uniform grid and sub-cell FDTD formulations
 - Applications (microstrip antennas, crosstalk analysis in digital circuits, coplanar waveguide analysis, biological effects of hand held communication antennas)

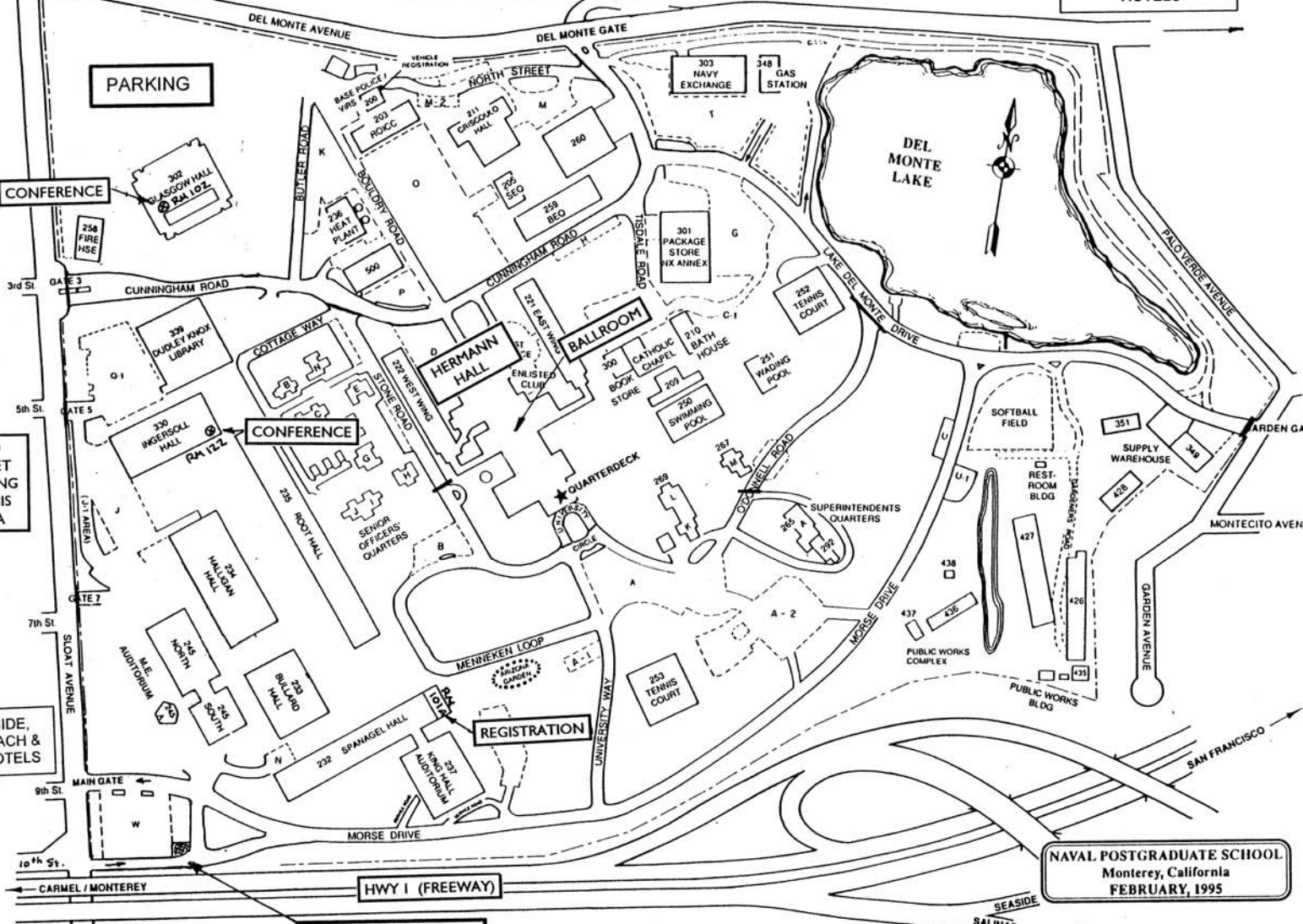
Workshop on Antenna Analysis and Design Using The FDTD Technique

Dr. Atef Z. Elsherbeni atef@olemiss.edu
Dr. Allen W. Glisson aglisson@olemiss.edu

This workshop will start with demonstrations of 1D, 2D and 3D FDTD codes, followed by detailed examples for the analysis of printed microstrip and aperture antennas excited by either a microstrip transmission line or a coplanar waveguide feed. Attendee will be trained on using a 3D code for the analysis and design of printed antennas, coplanar waveguide structures, and radiation from thin wire structures. The 3D code is developed using Matlab release 13 running on PCs and consisting of many files that fits on a single floppy. Some of these files will be distributed in regular Matlab m-files format, and the others will be in the Matlab p-coded format. No imposed limitations on the distributed version of this 3D code, other than the memory size limitation of the machine that will be used to execute the code. Other 2D and 1D executable codes will be available for distribution if requested.

ACES CONFERENCE

TO H.I. EXPRESS & EMBASSY SUITES HOTELS



NO STREET PARKING IN THIS AREA

TO FIRESIDE, STAGECOACH & HILTON HOTELS

NAVAL POSTGRADUATE SCHOOL
Monterey, California
FEBRUARY, 1995

MAIN ENTRANCE

HYATT REGENCY

TO AIRPORT

APPLIED COMPUTATIONAL ELECTROMAGNETICS SOCIETY
RICHARD W. ADLER, EXECUTIVE OFFICER
ECE DEPARTMENT, CODE ECAB, 833 DYER ROAD, ROOM 437
NAVAL POSTGRADUATE SCHOOL, MONTEREY, CA 93943-5121,
PHONE: 831-646-1111 FAX: 831-649-0300
EMAIL: RWA@ATTGLOBAL.NET

Please print

LAST NAME	FIRST NAME	MIDDLE INITIAL
COMPANY/ORGANIZATION/UNIVERSITY	DEPARTMENT / MAIL STATION	
MAILING ADDRESS WHERE PUBS MAY BE MAILED		
CITY	PROVINCE/STATE	COUNTRY
		ZIP/POSTAL CODE
TELEPHONE	FAX	AMATEUR RADIO CALL SIGN
		E-MAIL ADDRESS

	NEW MEMBERSHIP RATES (EFFECTIVE JANUARY 2003)			
	BASIC	INTERMEDIATE	EXPANDED	INSTITUTIONAL
WORLD AREA	Journal & Newsletter Access via Website & Annual (Nov) Searchable CD Rom of Proceedings of March Conference & Searchable CD ROM of year's Journals	BASIC, plus CD ROM of March Journal (Mar) & CD ROM of July Journal (Jul)	BASIC, plus Unbound Paper Copies of Journals (Mar, Jul, Nov)	BASIC, plus Bound Paper Copies of Journals (Mar, Jul, Nov)
US, CANADA and MEXICO	\$35. USD	\$55. USD	\$90. USD	\$125. USD
ALL OTHER AREAS	\$35. USD	\$55. USD	\$110. USD	\$125. USD

FULL-TIME STUDENT/RETIRED/UNEMPLOYED: BASIC RATE IS \$20.00 USD FOR ALL COUNTRIES

Non-USA participants: Prices are in U.S. dollars. All currencies must be converted to U.S. dollars payable by banks with U.S. affiliates. (1) Bank Checks must have U.S. address of bank; Checks are payable to "ACES", (2) U.S./International Money Order drawn in U.S. funds, payable in U.S. \$\$, (3) Credit Cards: Visa, MasterCard, Amex and Discover.

CREDIT CARD USERS

PRINT CARD HOLDER NAME: _____

CREDIT CARD HOLDER SIGNATURE: _____

CREDIT CARD HOLDER ADDRESS: _____

ADDRESS, CONT: _____

CREDIT CARD ACCOUNT #: _____

CARD EXP. DATE: _____

2003

ADVERTISING RATES		
	FEE	PRINTED SIZE
Full page	\$200	7.5" × 10.0"
1/2 page	\$100	7.5" × 4.7" or 3.5" × 10.0"
1/4 page	\$50	3.5" × 4.7"
<p>All ads must be camera ready copy.</p> <p>Ad deadlines are same as Newsletter copy deadlines.</p> <p>Place ads with Ray Perez, Newsletter Editor, Martin Marietta Astronautics, MS 58700, PO Box 179, Denver, CO 80201, USA. The editor reserves the right to reject ads.</p>		

DEADLINE FOR THE SUBMISSION OF ARTICLES	
Issue	Copy Deadline
March	February 1
July	June 1
November	October 1

For the **ACES NEWSLETTER**, send copy to Bruce Archambeault in the following formats:

1. A PDF copy.
2. A MS Word (ver. 97 or higher) copy. If any software other than WORD has been used, contact the Managing Editor, Richard W. Adler **before** submitting a diskette, CD-R or electronic file.